https://ntrs.nasa.gov/search.jsp?R=19700002183 2020-03-23T21:04:35+00:00Z

NASA TECHNICAL REPORT

NASA TR R-291

C.1

TECH LIBRARY KAFB, NM
0068337

LOAN COPY
AFWL (WLIL)
KIRTLAND AFB, N

NASA TR R-291

THE TEMPERATURE DISTRIBUTION IN THE SOLAR CHROMOSPHERE

by Stuart D. Jordan

Goddard Space Flight Center
Greenbelt, Md.

NATIONAL AERONAUTICS AND SPACE ADMINISTRATION • WASHINGTON, D. C. • NOVEMBER 1969

TECH LIBRARY KAFB, NM
0068337

THE TEMPERATURE DISTRIBUTION IN THE SOLAR CHROMOSPHERE

By Stuart D. Jordan

Goddard Space Flight Center
Greenbelt, Md.

NATIONAL AERONAUTICS AND SPACE ADMINISTRATION

For sale by the Clearinghouse for Federal Scientific and Technical Information
Springfield, Virginia 22151 – Price $3.00

ABSTRACT

A new approximate method is developed for calculating the temperature distribution in an atmosphere where local mechanical-energy dissipation is balanced by local net radiative loss in one or more spectral lines for which the atmosphere is optically thick. The method uncouples the equations of radiative transfer for the individual spectral lines from the energy-conservation equation and from each other. This permits a solution of each individual transfer equation for the radiation field in each line. These results, used in the energy-conservation equation, yield the temperature distribution if the optical depth ratio of the spectral lines at each point is known. The method is applied to selected strong resonance lines in the solar chromosphere.

CONTENTS

THE TEMPERATURE DISTRIBUTION IN THE SOLAR CHROMOSPHERE

by
Stuart D. Jordan*
Goddard Space Flight Center

Chapter I

INTRODUCTION

A fundamental problem in solar physics is to understand the origin of the high temperatures in the outermost region of the solar atmosphere. Assuming only radiative transfer of energy in this region, we should expect no temperature minimum above which temperature increases with height. In fact, however, Edlen (1943) has shown that the outermost region, the corona, has a temperature on the order of 10^6 °K, which is at least two orders of magnitude above the minimum temperature.

In seeking sources of energy to explain the temperature rise, we can look outside the solar atmosphere as well as beneath it. We shall see that no satisfactory sources have been found outside the sun. Thomas (1948a) suggested that spicules might heat the corona if they were supersonic jets, but current estimates of ambient gas temperatures for most of the region through which spicules move require that spicules be subsonic.

The only mechanical source that has proved promising to date is granulation, as first suggested by Biermann (1946, 1948) and, independently, by Schwarzschild (1948). They suggested that the granules are a manifestation of turbulent convection; this could generate acoustic waves that would build up into shock waves as they propagate out into the chromosphere and corona. This transformation of acoustic waves into shock waves was deemed reasonable because there is a rapid decrease of mass density with height in the chromosphere-corona region, where they proposed the shock dissipation should take place. Rough estimates of the energy available for shock dissipation do agree in order of magnitude with rough estimates of the radiative energy loss from the chromosphere-corona, although (as we shall see) estimates of the available mechanical energy and of the radiation losses could both be in error by as much as an order of magnitude.

Much work has since been done on the problem of what wave modes are generated by the convection zone, how they propagate, and by what mechanism their energy is dissipated into the atmosphere. We shall review this work in Chapter II and, after considering various wave modes

*Solar Physics Branch, Laboratory for Space Sciences.

and dissipation mechanisms, we shall argue in favor of shock dissipation of acoustic waves as the most likely heating mechanism in the chromosphere (to which the calculations of this report are restricted).

Having decided upon the most likely dissipation mechanism, we then consider by what means the dissipated energy is redistributed through the atmosphere and eventually lost from the atmosphere in radiation. For most of the chromospheric region studied in this report, conduction proves to be negligible. Thus, we shall treat only shock-wave heating and radiative redistribution and cooling. By ignoring the transient phenomena associated with the passage of a shock wave through a region and the subsequent radiative relaxation, and instead working with time-averaged quantities for an atmosphere in a statistically steady state, we can use the following local energy-balance condition:

$$E_{in} = E_{out} , \tag{1}$$

where (in line with convention) E_{in} is the dissipated mechanical energy, and E_{out} is the net radiative loss. The problem is to derive functional forms for E_{in} and E_{out}. If this can be done, the temperature distribution in the atmosphere can then be calculated from Equation 1. The main object of this entire study is to exhibit a new approximate method for determining the functional form of E_{out} in a mechanically heated (i.e., nonradiative equilibrium) atmosphere, so that the temperature distribution in the atmosphere can be calculated.

The term E_{in} can be obtained from shock-wave theory for the calculations reported here. The term E_{out} is a function of the radiation fields and associated source functions for various spectral lines and continua. In general, these quantities can be derived only from equations of transfer for the various lines and continua.

What we need is an approximate method to uncouple the equations of radiative transfer from Equation 1 and from each other, so that we can solve the separate transfer equations independently and use the results in the equation, which can then be solved at various heights in the atmosphere to give the temperature distribution. Such an approximate, iterative method is given in Chapter III. The so-called non-LTE or general approach to radiative-transfer problems provides the basis for everything we shall do. Two relevant references which will be used throughout are *Physics of the Solar Chromosphere* by Thomas and Athay (1961) and *Some Aspects of Non-Equilibrium Thermodynamics in the Presence of a Radiation Field* by Thomas (1965). Hereafter, we shall refer to the above by PSC and NETPRF, respectively. All of the non-LTE work used in the report will be derived in detail, following the notation of NETPRF.

Chapter II
THE SOLAR ATMOSPHERE

A. The Classical Problem of a Stellar Atmosphere

To construct a model for any stellar atmosphere, including the sun, we must make some physical assumptions in order to obtain a number of equations equal to the number of unknown quantities. More precisely, we must first specify what quantities we need to describe the atmospheric gaseous ensemble, and then introduce the number of physical assumptions that will let us derive these quantities from observational data. We call that set of parameters required to describe the physical state of the gas a "complete set." By physical state of the gas, we mean the populations of all internal atomic or molecular energy levels and all kinetic degrees of freedom for all individual particles, as well as the photon distribution, in terms of energy and direction. These physical-state parameters must be known at every point in the gas. Our problem is to derive this complete set of parameters from the observational data, which we call the "observational set." Since the observational set will not, in general, be sufficient to give the complete set, we must introduce physical assumptions to supplement our observations. We discuss several physical assumptions which astronomers often use, and evaluate these assumptions for the solar atmosphere.

Assumptions commonly used in constructing atmospheric models are local thermodynamic equilibrium, radiative equilibrium, and hydrostatic equilibrium. Hereafter we shall refer to them as LTE, RE, and HE, respectively. We define them and discuss their applicability.

LTE, as we shall use it here, means that in each small volume element of gas all the well known thermodynamic-equilibrium distribution functions are valid at some local temperature. In particular, the Maxwell, Boltzmann, and Saha equations describe the energy state of the matter gas; the Planck function describes the energy state of the photon gas. Local temperature is the only parameter required to describe the energy state of a small gas element; a complete set of parameters to describe the physical state would be temperature, density, and chemical composition.

LTE differs from thermodynamic equilibrium TE in that temperature gradients are permitted in LTE, as long as the energy fluxes resulting from the gradients are too small to disturb the local energy distributions given by the TE distribution functions evaluated at the local temperature. Obviously, a star cannot be a strict thermodynamic equilibrium enclosure, since a TE enclosure is defined as a system isolated from its surroundings by an adiabatic wall through which no fluxes are permitted, and a star must lose energy to surrounding space or we could not see it. Thus, the LTE assumption has been proposed as the simplest assumption we could use (subject to verification) to describe conditions in part of the atmosphere.

There is one region of any atmosphere where LTE cannot be valid, i. e., the outer region, which itself produces negligible radiation but through which passes all the radiation that escapes the star. In LTE as defined, the radiation field must be isotropic—a condition obviously violated in the above example. To provide a less restrictive assumption (which we shall see is usually still to restrictive) for handling these regions where the radiation field is anisotropic, some astronomers have introduced the assumption LTE-R. This means that the TE distribution functions for the matter are assumed to apply at some local temperature, but that the radiation field is not assumed to be either isotropic or equal to a Planck function at that temperature. We must obtain the radiation field by solving the equation of radiative transfer for intensity I_ν, where the restriction of LTE-R on the matter distribution functions requires that

$$S_\nu = B_\nu (T_e) , \qquad \underline{\text{LTE-R}} , \tag{2}$$

where S_ν is the source function, and $B_\nu (T_e)$ is the Planck function, T_e being the local value of the electron kinetic temperature, which is the temperature we shall use throughout this report.

Note: Not all authors mean the same thing by LTE. For example, Aller (1963) uses it to denote what we mean by LTE-R. To avoid confusion, the reader is urged to keep in mind the definitions in this section.

Radiative equilibrium, RE, is the second commonly used assumption we consider here; this is defined by the statement that the net integrated flux

$$F \equiv \int_0^\infty F_\nu \, d\nu$$

remains constant with depth in the atmosphere, F_ν being the monochromatic flux given by

$$F_\nu \equiv 2\pi \int_{-1}^{1} I_\nu (\mu) \mu \, d\mu , \tag{3}$$

where $\mu = \cos\theta$ and θ is the angle between an outward normal to the atmosphere's surface and the direction of the radiation intensity $I_\nu(\mu)$. Assumption RE obviously implies that

$$\frac{dF}{dh} = 0 , \qquad \underline{\text{RE}} , \tag{4}$$

where h is the depth parameter. If an atmosphere is "in RE" then, in the absence of local, nonradiative sources of energy, the radiation field carries a constant fraction of the total energy transported through the atmosphere. In the absence of convective or conductive energy transfer, this in thrn means that the radiation field carries all the energy transported through the atmosphere.

Hydrostatic equilibrium, HE, is the third commonly used assumption we consider. This means that all velocity fields are thermal, unless the pressure, P, used in the following equation for HE includes the turbulent pressure caused by small-scale isotropic turbulence, in which case this too can be treated under the HE assumption. Any large-scale mass motions and all motions resulting in a net mass transport across any arbitrarily oriented surface in the atmosphere represent departures from HE. Where HE applies, we can use the equation

$$\frac{dP}{dh} = -\rho g , \qquad \underline{\text{HE}} , \tag{5}$$

where P is the sum of the gas and radiation pressure at a point, ρ is the mass density, and g is the acceleration caused by gravity.

Consider, in turn, the applicability of LTE-R, RE, and HE to the solar atmosphere. Insofar as these assumptions apply, they simplify our problem of deriving the temperature distribution. Where they do not apply, we must introduce less restrictive assumptions that can be justified.

Before evaluating these assumptions, let us clarify what we mean by photosphere, chromosphere, and corona—subregions of the solar atmosphere we shall refer to constantly. We define the photosphere as that region of the sun we can observe anywhere in the visible spectrum lying below the following zero point for height, measured positive outward in a radial direction: $h = 0$ is that depth in the solar atmosphere at which the radial optical depth at $\lambda = 5000$ Å is 1.0×10^{-3}. This value corresponds to the zero point on the chromospheric height scale used in Chapter 6 of PSC. The chromosphere and corona, defined in terms of the radiation characteristic of each, must necessarily lie above this $h = 0$ surface.

We are now ready to evaluate the assumptions of LTE-R, RE, and HE. The first question we should pose is: At what depth in the solar atmosphere does the source function equal the Planck function so that LTE-R is valid? In NETPRF it is shown that for "collision-dominated" lines an approximate measure of the optical depth above which the source function differs from the Planck function is ϵ^{-1}, where ϵ can be considered the ratio of collisional deexcitation to radiative deexcitation (ϵ is defined more precisely by Equation 27). Thus, for those lines for which $\epsilon << 1$, the optical depth above which $S_\nu \neq B_\nu(T_e)$ will be large compared with unity. We shall see that $\epsilon \simeq 10^4$ is a resonable value for several strong spectral lines treated in this report. So the optical depth at frequency ν_0, corresponding to the center of these lines above which LTE-R is invalid, is $\tau_0 \simeq 10^4$. For these lines, only for $\tau_0 >> 10^4$ can we be sure that LTE-R applies. On the other hand, we shall see that $S_\nu \simeq B_\nu(T_e)$ is a good approximation for the solar continuum source function in the photosphere. Each spectral frequency regime must be tested independently for the validity of LTE-R. Where LTE-R is invalid, a more general expression for the source function than $S_\nu = B_\nu(T_e)$ must be used.

Assumption RE provides a photospheric temperature distribution close to the empirically determined one we adopt, but RE is certainly violated in the chromosphere and corona where the presence of nonradiative energy sources is necessary to maintain the high temperatures. Thus,

Equation 4 is not valid for these regions. What we need for the temperature calculation there is an analogue of Equation 4 for the case of departure from RE caused by the nonradiative heating mechanism. To derive this, we start with the transfer equation for a plane parallel atmosphere,

$$\mu \frac{dI_\nu}{d\tau_\nu} = I_\nu - S_\nu , \tag{6}$$

with the usual notation, as given in Kourganoff (1963). Source function S_ν is a composite of line source function S_ℓ and continuum source function S_c. Introducing r_ν:

$$r_\nu \equiv \frac{d\tau_c}{d\tau_\ell} , \tag{7}$$

where the subscripts c and ℓ refer to continuum and line, we can write composite source function S_ν as

$$S_\nu = \frac{S_\ell + r_\nu S_c}{1 + r_\nu} . \tag{8}$$

Substituting Equation 8 in Equation 6, multiplying both sides by $d\tau_\nu/dh$, operating on both sides with

$$\iint \cdots \, d\mu \, d\nu ,$$

and recalling the definition of monochromatic flux, Equation 3, we obtain

$$\frac{dF}{dh} = 4\pi \left[\sum_j^N \int (J_\nu - S_\ell)_j \frac{d\tau_{\ell j}}{dh} \, d\nu + \int (J_\nu - S_c) \frac{d\tau_c}{dh} \, d\nu \right] , \tag{9}$$

where the sum extends over all N lines which are important energy sinks in the region where we apply Equation 9. We shall transform equation 9 into a more convenient form for our calculations after discussing non-LTE theory.

We assume HE is our calculations, which extend from $h = 0$ to $h \sim 1250$ km. In the region lying above $h \sim 1250$ km, this assumption is invalid, owing to spicules. It is possible that HE is never a good assumption for any region of the solar atmosphere. This question is complex and we shall defer a more detailed discussion to section E.

Our general procedure, then, will be to develop an approximate method for calculating the chromospheric temperature distribution for a gas in which HE is assumed but departures from RE and, when important, LTE-R are taken into account.

Another assumption we shall make is spherical symmetry. Obviously, this assumption is invalid in the upper chromosphere where the spicules are observed. We must consider atmospheric inhomogeneities in greater detail in the photosphere and lower chromosphere to see if we can assume spherical symmetry there. We do this in Section E. Finally, the thickness dR of the atmospheric region we shall treat is very small compared to the radius R of the Sun; this justifies the plane parallel atmosphere approximation, which will be made throughout.

B. The Photosphere and the Temperature Minimum

The photosphere has a two-fold importance for our chromospheric energy balance problem. We shall see later in this chapter that, in the lower (deeper) region of the photosphere, the gas is convectively unstable and the associated turbulent motions provide the most probable source of mechanical energy for heating the chromosphere. Also, the bulk of the solar radiation field in the continuum originates in the photosphere, and it is this background continuum that will be important for the source functions of certain types of spectral lines. This section is devoted to a brief discussion of this continuum radiation field and the associated temperature distribution in the photosphere. We are particularly interested in the temperature distribution in the outer region of the photosphere and in the lowest part of the chromosphere. In this region, the temperature goes through a minimum, whose position and value we want to know as accurately as possible.

The most notable feature of the photosphere is the continuous radiation of the Sun. The Sun's high surface gravity produces a rapid density increase in the photosphere. This produces a rapid increase in both the volume emission and absorption coefficients, restricting the emitting region to depths above $h \simeq -400$ km on our scale of heights. We can estimate the total power output of the photosphere by measuring the radiant energy from the Sun at a position on Earth. All values reported in Minnaert (1953) lie at or below 2.00 cal cm^{-2} min^{-1}, which corresponds to a net emergent flux of 6.50×10^{10} erg cm^{-2} sec^{-1}. We shall see that this is at least three orders of magnitude larger than current estimates of radiant energy losses from the chromosphere and corona.

Of even more interest to us is the spectral distribution of continuous radiation. Early work by Abbot (1920) used light from the entire solar disk and this gave the true monochromatic intensity. Later work by Peyturaux (1951) used light only from the center of the disk, thus giving the radiation intensity along the normal. We compare the two, using a reduction factor derived by Minnaert (1953) who tabulates the results. We have graphed these data in Figure 1, along with black-body radiation fields at 6500°K and 5800°K. The curves demonstrate that the solar continuum radiation approximates very well a black-body or thermodynamic equilibrium radiation field at the given temperatures.

Photographs of high spatial resolution taken in white light reveal a significant intensity fluctuation, with a scale for the brighter features of the order of 1000 km. These bright features are, of course, the granules, which will be discussed in Section E. The values for the emergent intensities discussed so far are averages, including radiation from the granules and the material between them.

The temperature distribution in the photosphere has been obtained theoretically and empirically. The most elementary theoretical temperature distribution that reasonably fits empirical distributions in the solar case is the grey-body distribution, given by

$$T_e^4 = \frac{3}{4} T_{eff}^4 \left[\tau + q(\tau)\right] , \tag{10}$$

where $q(\tau)$ is a complicated function satisfying $1/2 < q < 1.0$ and tabulated in Chandrasekhar (1960), and T_{eff} (the "effective temperature") is defined by

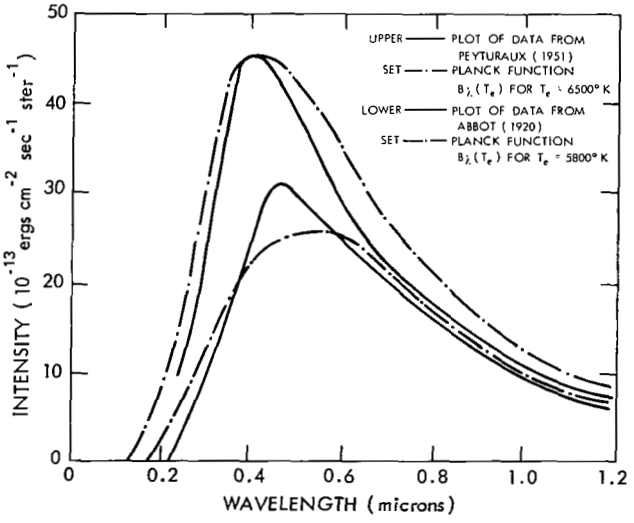

Figure 1—Spectral distribution of solar radiation based on observational data and comparison with Planck function.

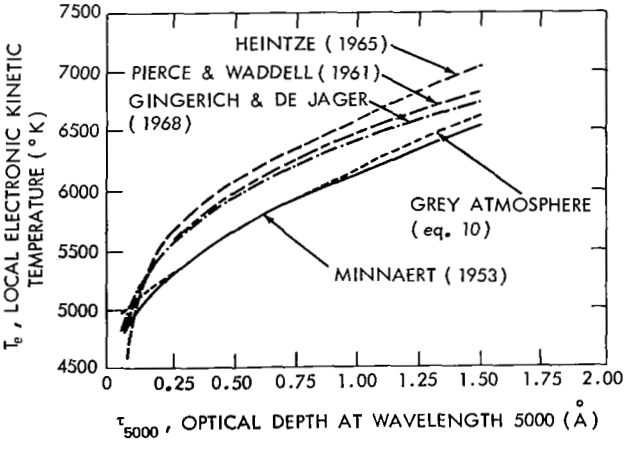

Figure 2—Comparison between observed and grey-body temperature distribution in the photosphere.

$$F = \sigma T_{eff}^4 , \tag{11}$$

where σ is the Stefan-Boltzmann constant. From our value for F of 6.50×10^{10} erg cm^{-2} sec^{-1}, we obtain $T_{eff} = 5825°K$, very close to the value providing a good fit between the Planck function and the observed intensity I_λ in Figure 1. The assumptions underlying grey-body distribution are LTE-R, radiative equilibrium, and a grey absorption coefficient (i.e., one independent of frequency). Figure 2 shows how the grey temperature distribution compares with values from several empirical studies.

The closeness of the fit suggests the assumptions underlying simple grey-body distribution are good ones over most of the photosphere. It is already clear that $B_\nu (T_{eff})$ gives a good representation of the observed solar intensity, so it is not surprising that LTE-R should be a good assumption. As for RE, it is shown in Section E that the deeper layers of the photosphere around $\tau_{5000} = 1$ are convectively unstable, but that above this region RE should apply. The grey-atmosphere assumption also proves reasonable because the H^- negative ion of hydrogen turns out to be the dominant source of continuous absorption; moreover, studies of the H^- absorption coefficient α_ν for both bound-free and free-free transitions show that α_ν has only a very weak frequency

dependence over a frequency band that includes the strongest part of the solar continuum. This dominance of H^- was first suggested by Wildt (1939); the ion was first observed in the laboratory by Branscomb and Smith (1955); a recent reference for calculations of the absorption coefficient α_ν (H^-), which contains reference to previous calculations, is Doughty et al. (1966a, 1966b).

Our discussion of the grey-atmosphere temperature distribution has provided some useful insights into physical conditions in the photosphere, but has been of no help to us in fixing the temperature minimum mentioned before. We can show from Equation 10 that T_e decreases monotonically to a "boundary" value of $T_e(\tau = 0) = 0.8544\ T_{eff}$, so we learn nothing about the solar atmosphere for $\tau << 1.0$ from Equation 10. Can we, perhaps, learn more about the temperature minimum from models based in part on observational data? PSC contains a discussion of two temperature models based on limb-darkening measurements: the Minnaert and the Pierce and Waddell models, which appear in Figure 2. The Pierce and Waddell (1961) model appears the more satisfactory of the two, based on Thomas' criticism in PSC. We add for reference the Heintze (1965) model, which is a slight modification of the Utrecht Reference Photosphere, and the Bilderberg Continuum Atmosphere, which is discussed by Gingerich and de Jager (1968). The temperature curves from these latter two models lie on either side of the Pierce and Waddell curve, which we adopt for our discussion here.

Pierce (1954) concluded that limb-darkening measurements in the continuum for $\mu \leq 0.2$ are not very reliable for temperature determinations. Accordingly, the Pierce and Waddell limb darkening measurements end at about this value of μ. However Dunn (1959) analyzed observations near the solar limb in the continuum at λ 6600 Å, carrying his limb darkening measurements $I_\nu(0,\mu)/I_\nu(0,1)$ right out to $\mu = 0$. His data for $\mu \leq 0.2$ are more reliable than those of previous investigators because he uses a narrow-band interference-filter to reduce the scattered light, thus reducing the uncertainty $\Delta I_\nu(0,\mu)$ in $I_\nu(0,\mu)$. Dunn's results out to $\mu \simeq 0.03$ fall very close to an extension of the Pierce and Waddell data curve. Thomas in PSC concludes from these two studies that we can have the following $T_e(\tau_{5000})$ for $\tau_{5000} < 0.2$:

τ_{5000}	0.1	0.05	~0.02
T_e	5200 ± 50°	4900 ± 100°	~4750

We accept these values out to $\tau_{5000} = 0.02$.

We now wish to proceed outward to those regions of the atmosphere where limb-darkening data are of no avail. We begin by discussing the line-blanketing effect, to estimate roughly the gross effects of the Fraunhofer lines on the temperature distribution in this region where $\tau_{5000} < 0.02$. We ask for the effect of line blanketing on the so-called "boundary" temperature.

The gross effects on the boundary temperature (or temperature minimum, for our purpose) give us our first glimpse of the importance of non-LTE effects on the solar atmosphere. First, we recall that for LTE-R, $S_\ell = B_\nu(T_e)$. We now anticipate a result of the next section, and state

that for many spectral lines the source function S_ℓ can be written as

$$S_\ell = \frac{\int J_\nu \phi_\nu \, d\nu + \epsilon B_\nu (T_e)}{1 + \epsilon} , \tag{12}$$

where ϵ is effectively the ratio of collisional to radiative de-excitation. In NETPRF, Thomas shows that, if we write the volume absorption coefficient as

$$K_\nu = K_c + K_\ell + \sigma_c , \tag{13}$$

where K_c, K_ℓ, σ_c are absorption coefficients for true continuous absorption, line absorption, and scattering, respectively, we can rewrite the transfer equation in a form that yields, (when we operate on both sides with $\int \cdots d\mu \, d\nu$ and apply the condition of radiative equilibrium of Equation 4) the following two equations for T_e :

$$\int K_c B_\nu (T_e) \, d\nu = \int K_c J_\nu \, d\nu - \sum_j^N K_j \left[B_{\nu j} (T_e) - \int J_\nu \phi_\nu \, d\nu \right] , \tag{14}$$

for the case where S_ℓ is given by Equation 2, and

$$\int K_c B_\nu (T_e) \, d\nu = \int K_c J_\nu \, d\nu - \sum_j^N K_j \left[B_{\nu j} (T_e) - \int J_\nu \phi_\nu \, d\nu \right] \frac{\epsilon_j}{1 + \epsilon_j} , \tag{15}$$

for the case where S_ℓ is given by Equation 12. The summation is over the number of lines in the spectrum. Equations 14 and 15 illustrate the difference between the LTE-R case and the non-LTE case of Equation 12 for spectral lines. The only difference in form is the inclusion of the factor $\epsilon_j / (1 + \epsilon_j)$ which multiplies the second term on the right in the non-LTE case. We have already noted that for many lines in the solar atmosphere $\epsilon_j << 1$. Thus, the effect of these lines in lowering the temperature is less than in the LTE-R case, and we would expect the temperature minimum to have a higher value than if we assumed $S_\ell = B_\nu (T_e)$ as in LTE-R. The larger value of the first term on the right in the non-LTE case, due to less absorption by the lines (physically, the scattering term $\int J_\nu \phi_\nu \, d\nu$ predominates over $\epsilon B_\nu (T_e)$ in Equation 12), also raises the temperature. However, a detailed calculation is required to determine the extent of this effect, because the change in the expression $B_{\nu j} (T_e) - \int J_\nu \phi_\nu \, d\nu$ may reduce the difference between the two cases.

What we need is a reasonable estimate of the temperature. In PSC, Thomas argues for a value not lower than 4750°K, occurring in the interval $10^{-3} \leq \tau_5 \leq 10^{-2}$, with the possibility of a somewhat

lower value at a slightly smaller τ_5. He bases this conclusion on the previously mentioned work of Dunn and his own model for the chromospheric region $0 \leq h$ (km) ≤ 1300 which we shall describe in Section D.

A slightly lower value for the minimum temperature is obtained by Curtis (1965) from an analysis of the sodium D lines. The analysis is based on limb-darkening data on the sodium D lines collected earlier by Waddell (1962). Following a suggestion by Jefferies, Curtis assumes that the line source function S_ℓ is equal at a given physical depth for the two components D_1 and D_2 of the sodium doublet and estimates the value and location of the minimum temperature. The derived temperature distribution reaches a minimum of about 4600°K at $\tau_{5000} = 10^{-2}$ and retains this value out to $\tau_{5000} = 10^{-4}$. This result is not inconsistent with the above-mentioned conclusions of Thomas and is also very close to the temperature distribution of the previously mentioned Bilderberg Continuum Atmosphere in the range $10^{-2} \geq \tau_{5000} \geq 10^{-4}$. We shall adopt the value $T_e = 4600°$ for our temperature at $h = 0$, which lies in the above optical depth range. Unfortunately we cannot say with certainty that we have not overestimated the minimum temperature. For example, Athay and Skumanich (1968) conclude from their analysis of the CaII K line that a minimum temperature of $\leq 4200°$K is required to match their computed K_1 profiles with observations. We hope that this discrepancy will be cleared up soon.

Now, let us discuss the chromosphere and corona to see what physical conditions exist there and what temperature models for these regions have so far been derived. It would be advisable to set down beforehand the basic ideas and relations of non-LTE theory, which will be used in discussing the outer atmosphere and in the derivation of the equations for the chromospheric temperature calculation.

C. Non-LTE Theory for Solar Spectral Lines

First, let us emphasize that non-LTE does not mean we are forcing the source function to depart from the Planck function. Instead, it means that we assume the more general condition of a statistically steady state and derive a source function which, under the special conditions for LTE-R, will equal the Planck function. We shall follow NETPRF quite closely, but necessarily be much more brief.

The non-LTE theory grew from an attempt to express the source function for spectral lines formed in an atmosphere where simple estimates readily show that collisional processes do not control the internal, atomic-energy level populations. This is certainly the case in the atmospheres of the Sun and most stars. The radiation field which, therefore, plays an important if not dominant role in fixing local energy-level populations must be considered. This radiation field is produced in regions of the gas where excitation conditions are usually not the same as conditions where we want to know the source function. Through its radiation field, the source function depends on a range of excitation conditions—not just those conditions at the point in question.

To develop a more general expression for the source function under these conditions, we must assume a more general physical condition to exist locally than LTR-R. We presuppose a

statistically steady state (abbreviated SSS), given by

$$\frac{dn_k}{dt} = 0 , \qquad \underline{SSS} , \tag{16}$$

where n_k is the number density of a given chemical species in the k-th energy level. The non-LTE theory based on Equation 16 applies at each instant of time only when the time for a transient perturbation is long compared with the time for a SSS to be established. It may be objected that a shock-heated gas does not generally satisfy these conditions. However, in this study, we are concerned only with time-averaged quantities. We ignore how the gas relaxes after a shock wave passes through it, and how a chromosphere-corona develops out of an atmosphere in radiative equilibrium after a source of mechanical energy dissipation in the atmosphere has been "turned on."

We proceed to derive the source function for a spectral line in an atmosphere in a SSS, following NETPRF. Thomas shows that the source function for a transition between an upper-level U and a lower-level L can be written in the following general form:

$$S_\nu = \frac{j_\nu}{\phi_\nu} \frac{2h\nu^3}{c^2} \left(\frac{g_U n_L}{g_L n_U} - \frac{\psi_\nu}{\phi_\nu} \right)^{-1} , \tag{17}$$

where j_ν, ϕ_ν, and ψ_ν are called "profile coefficients" for spontaneous emission, absorption, and stimulated emission, respectively; g_U and g_L are statistical weights for levels U and L, respectively; and the other symbols have their usual meaning. The profile coefficients are normalized, so their integral over ν and solid angle is 4π. If $\phi_\nu = \psi_\nu$, the above reduces to an expression written more compactly as

$$S_\nu = \frac{j_\nu}{\phi_\nu} B_\nu (T_{ex}) , \tag{18}$$

where

$$B_\nu (T_{ex}) = \frac{2h\nu^3}{c^2} \left(\frac{g_U n_L}{g_L n_U} - 1 \right)^{-1} . \tag{19}$$

The advantage of Equation 18 as a form for the source function is that it separates S_ν into two factors, giving the frequency dependence of S_ν on frequency and the occupation numbers, respectively. In LTE-R,

$$\frac{g_U n_L}{g_L n_U} = \exp\left\{ \frac{h\nu}{kT_e} \right\} ,$$

so $T_{ex} \to T_e$ or $B_\nu (T_{ex}) \to B_\nu (T_e)$, as must occur for the non-LTE theory to be valid.

The factor j_ν/ϕ_ν is evaluated by Thomas (1957) for the central core of resonance lines on the assumption that chromospheric conditions apply. He concludes that the profile of the absorption coefficient is Doppler out to some three Doppler half-widths from line center, and that the ratio j_ν/ϕ_ν equals 4 at the most, over the same Doppler core. Since the number of absorbers for the Doppler (Gaussian) line profile varies as $\exp\left\{-\left(\Delta\nu/\Delta\nu_D\right)^2\right\}$ (where $\Delta\nu_D$ is the Doppler frequency half-width) $\Delta\nu/\Delta\nu_D = 3$ corresponds to a variation in the absorption coefficient of $e^9 \simeq 10^4$ over the Doppler core of the line. Since our chromospheric temperature calculations of Chapter IV will require source functions for three resonance lines (Ly α, and the resonance doublets of CaII and MgII), all of which have their cores formed in the chromosphere, we conclude that Thomas' conclusion on j_ν/ϕ_ν applies; furthermore, we ignore frequency dependence altogether by estimating

$$S_\nu \simeq B_\nu\left(T_{ex}\right) . \tag{20}$$

It is easy to derive a general expression for $B_\nu\left(T_{ex}\right)$; See Appendix A. Our starting point is Equation 16, expressing the statistically steady state. Following Thomas in NETPRF, we introduce a "net rate bracket" notation for treating the net rates of various processes. If P - R refers to the net rate of process P (R is the reverse process), then for P (radiative; U, L) we define the net radiative bracket $(NRB)_{UL}$ as

$$P(\text{rad; U, L}) - R(\text{rad; L, U}) = n_U A_{UL} (NRB)_{LU} . \tag{21}$$

Likewise we define the net collisional bracket $(NCB)_{LU}$ as

$$P(\text{col; L, U}) - R(\text{col; U, L}) = n_L C_{LU} (NCB)_{LU} . \tag{22}$$

In Equations 21 and 22 A_{UL} is the Einstein coefficient for spontaneous emission, and C_{LU} is the inelastic collision rate, which we assume for collisional excitation by free electrons is given by

$$C_{LU} = n_e \int_{v_{LU}}^{\infty} \sigma_{LU} f_e(v)\, v\, dv , \qquad v_{LU} = \left(2\chi_{LU}/m\right)^{1/2} , \tag{23}$$

where n_e is the electron density, σ_{LU} is the inelastic-collision cross section for these collisions, $f_e(v)$ is the electron-velocity distribution function (which we assume is Maxwellian) and v_{LU} is the minimum velocity for collisional excitation obtained from $1/2\, mv_{LU}^2 = \chi_{LU}$, where $\chi_{LU} = \chi_L - \chi_U$ is the difference in ionization potentials between levels L and U.

Using the net brackets defined by Equations 21 and 22, we can write a completely general expression for the equation of statistically steady state (Equation 16). For a level k, this

expression becomes

$$\sum_{\ell>k} n_\ell A_{\ell k} (NRB)_{\ell k} + \sum_{j<k} n_j C_{jk} (NCB)_{jk} + \int_{\nu_k}^{\infty} A_{\kappa k} n_k n_e (NRB)_{\kappa k} d\kappa \cdots$$

$$= n_k \left\{ \sum_{j<k} A_{kj} (NRB)_{kj} + \sum_{\ell>k} C_{k\ell} (NCB)_{k\ell} \right\} . \quad (24)$$

Subscript κ refers to states in the continuum; n_i is the ion density. According to convention, we include collisional processes that have an upper level in the continuum in the last term of Equation 24. To obtain the desired expression for $B_\nu (T_{ex})$, we write Equation 24 for levels U and L of the transition. We solve these two equations for n_U/n_L, then substitute this expression for n_U/n_L in Equation 19, thus arriving at the desired expression for $B_\nu (T_{ex})$ given below. (Refer to Appendix A for details.) The result is

$$B_\nu (T_{ex}) = \frac{\int J_\nu \phi_\nu d\nu + \epsilon B_\nu (T_e) + \eta B^*}{1 + \epsilon + \eta} , \quad (25)$$

where

$$J_\nu = \frac{1}{2} \int_{-1}^{1} I_\nu (\mu) d\mu , \quad (26)$$

$$\epsilon = \frac{C_{UL}}{A_{UL}} \left[1 - e^{-h\nu/kT_e} \right] , \quad (27)$$

$$\eta = \frac{g_L}{g_U} \frac{\delta_1}{A_{UL}} \frac{F_U}{F_L + F_U} \left[\frac{F_L}{F_U} \frac{g_U}{g_L} \frac{\delta_3}{\delta_1} - 1 \right] , \quad (28)$$

$$\eta B^* = \frac{2h\nu^3}{c^2} \frac{g_L}{g_U} \frac{\delta_1}{A_{UL}} \frac{F_U}{F_L + F_U} . \quad (29)$$

Quantities δ_1, δ_3, F_L, and F_U have not yet been introduced; Appendix A gives their detailed functional forms. Here, to save space, we merely state what they represent physically. These four quantities equal zero, if we consider our atom to be made up of only two levels, U and L. In

this case, $B_\nu\ (T_{ex})$ becomes

$$B_\nu\ (T_{ex}) = \frac{\int J_\nu\, \phi_\nu\, d\nu + \epsilon B_\nu\ (T_e)}{1 + \epsilon}, \qquad (30)$$

where collisions and the radiation field in the line itself control $B_\nu\ (T_{ex})$. In general, δ_1, δ_3, F_L, and F_U express the dependence of $B_\nu\ (T_{ex})$ on collisional and radiative processes that couple U and L to levels other than U and L. In particular, we see from Appendix A that δ_1 represents terms that depopulate L through all levels except U, δ_3 represents terms that depopulate U through all levels except L, F_L represents terms that populate L through all levels except U, and F_U represents terms that populate U through all levels except L.

When we use $B_\nu(T_{ex})$ in Chapters III and IV, we find that the line source function of Equation 30 is probably often a good approximation; in all other cases, we consider the dependence of δ_1, δ_3, F_L, and F_U on the continuum only. Here, we work with only two level atoms, or with atoms approximated by two levels plus a continuum. When these simplified treatments are not justified, we must use Equation 25, including as many additional levels as are needed.

Now it is evident why LTE-R is a poor assumption for strong chromospheric lines of the sort we shall treat in the energy-balance problem. In the two-level atom source function (Equation 30), $B_\nu(T_{ex}) \rightarrow B_\nu(T_e)$ only if $\int J_\nu\, \phi_\nu\, d\nu \rightarrow B_\nu(T_e)$, or if $\epsilon >> 1$ and $\epsilon B_\nu(T_e) >> \int J_\nu\, \phi_\nu\, d\nu$. We noted in Section A that, for the lines of interest here, $\epsilon \simeq 10^{-4}$. The second alternative above is ruled out immediately. To see from what depth in the atmosphere the radiation field escapes at the outer "boundary" $\tau_0 = 0$, and hence how far the influence of the boundary penetrates to producing an anistropy in I_ν, negating $\int J_\nu\, \phi_\nu d\nu \simeq B_\nu(T_e)$, we use the following fact: ϵ^{-1} provides a rough measure of the optical thickness of a region through which a photon will move, once it is created and before it is destroyed. Above optical depth ϵ^{-1} the radiation field is anisotropic, as there are not enough sources lying above the point in question to provide an inward directed I_ν^- to equal the outward directed I_ν^+.

Thus, for $\tau_0 < 10^4$ for the lines involved in our final calculations, LTE-R is certainly invalid. A rough criterion for LTE-R then becomes: $\epsilon\tau_0 >> 1$. A more rigorous development in NETPRF yields the same result, as well as a very lengthy criticism of the misuse of the LTE-R assumption.

Earlier in this section, we mentioned that we would want source functions for Lyα and the resonance doublets of CaII and MgII. We shall also find Hα an important chromospheric line, though we shall not solve a transfer equation for it. Jefferies and Thomas (1959) offer some interesting general results on Hα and ionized metal lines; Morton and Widing (1961) make a detailed study of Lyα. A summary of the relevant findings of these authors appears in NETPRF. More detailed studies of these lines have recently been made, but they do not affect these general comments.

In an effort to find the proper form of the source function for different types of lines, the general source function of Equation 25 can be written in several different ways, each corresponding

to different physical mechanisms of line formation. Jefferies and Thomas considered the following two possibilities:

$$B_\nu (T_{ex}) = \frac{\int J_\nu \phi_\nu \, d\nu + \epsilon B_\nu (T_e)}{1 + \epsilon} , \tag{31}$$

$$B_\nu (T_{ex}) = \frac{\int J_\nu \phi_\nu \, d\nu + \eta B^*}{1 + \eta} , \tag{32}$$

where η and ηB^* are given below. Equations 30 and 31 are identical in form and represent the two-level atom. We call $\int J_\nu \phi_\nu d\nu$ the "storage term," as it represents scattering which neither enhances nor depletes the radiation field in the line. We call $\epsilon B_\nu (T_e)$ a "source term," along with ηB^* in Equation 32. We call ϵ in Equation 31 and η in Equation 32 "sink terms." The source terms enhance the radiation field in the line, while the sink terms inhibit the build-up of this radiation field by representing direct (ϵ) and indirect (η) ways of populating the lower level at the expense of the upper without producing line radiation. Note that Jefferies and Thomas chose source functions whose source and sink terms are collision-dominated in the case of Equation 31, and dominated by radiation fields in the free-bound continua coupled to the upper and lower levels of the line transition in Equation 32. We can see this for the latter case, if we take Equations 28 and 29 for η and ηB^*, ignore all levels except U and L of the line and the continuum, and consider only radiative transitions between the continuum and U and L. We obtain for η and B^*:

$$\eta = (\text{atomic parameters}) \cdot \frac{W_{\kappa 1} e^{-Y_1}}{Y_1} \cdot \left(e^{Y_1 - Y_2} - 1\right), \tag{33}$$

$$B^* = \frac{2h\nu^3}{c^2} \left(e^{Y_1 - Y_2} - 1\right)^{-1} , \tag{34}$$

where $W_{\kappa 1}$ is the dilution factor for the Lyman continuum, $Y_k \equiv \chi_k / kT_{rk}$, and T_{rk} is a radiation temperature for the mean radiation field in the $\kappa \rightarrow k$ free-bound continuum such that $J_\nu (\kappa \rightarrow k) \simeq B_\nu (T_{rk})$. The atomic parameters, in general, vary from line to line.

The important conclusion of the Jefferies and Thomas study is that there is an apparent one-to-one correspondence between type of source function, or mechanism of line formation, and type of emitter, or class of line-forming ions in the solar atmosphere. Using source functions given by Equations 31 and 32 to solve the transfer equation for representative models of the chromosphere, they obtain line profiles typical of ionized metals from Equation 31 and line profiles typical of

neutral metals and the Balmer lines from Equation 32. The ionized metals' source functions are called "collision-dominated," and the neutral metals' and Balmer lines' source functions are called "photoionization-dominated," after the dominant source and sink terms. The line shape of the two types appears is Figure 3.

The Morton and Widing study considers Ly α, which is a strong emission line with a central reversal 35 percent below the intensity maxima on either side. Evaluating ϵ, $B_\nu(T_e)$, η, and B^* from Equations 27, 33, and 34, Morton and Widing find that $\epsilon B_\nu(T_e) >> \eta B^*$ and $\eta >> \epsilon$. Thus, for Ly α, which becomes a line of the "mixed type" of source function,

$$B_\nu(T_{ex}) = \frac{\int J_\nu \phi_\nu \, d\nu + \epsilon B_\nu(T_e)}{1 + \eta} . \qquad (35)$$

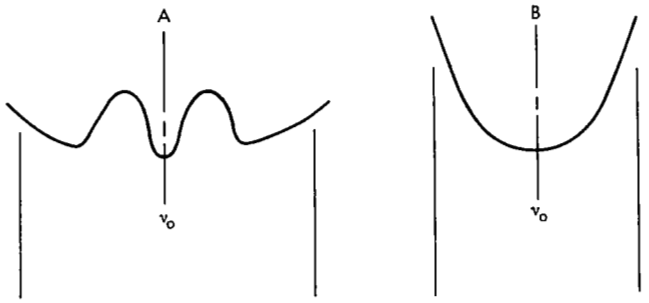

Figure 3—Line profiles in cores of (A) collision-dominated lines and (B) photoionization-dominated lines—asymmetrics ignored.

Equations 31, 32, and 35, to the first approximation source functions for three types of solar lines, cover all interesting possibilities. Although we need detailed studies of individual lines (for which good observed profiles are required) to specify more completely the details of the line-formation mechanism, this rough scheme for classifying solar lines will serve for our preliminary calculations.

There are two more points to be made, before leaving the subject of the source function. The ionized metal lines and Lyα have source functions for which the source terms exhibit a first-order dependence on the local electron temperature T_e. This is not true of the Balmer lines or the neutral metal lines. This will be of some importance to our discussion of the energy balance in Chapter IV. Also, the T_e-dependence of the first named lines demonstrates the existence of a temperature rise in the chromosphere, discussed in detail by Jefferies and Thomas (1959, 1960).

The final matter we wish to consider is a convenient form for the net brackets defined by Equations 21 and 22. Here we follow NETPRF exactly. We can write Equation 21 in the form

$$P(\text{rad; } U,L) - R(\text{rad; } L,U) = n_U A_{UL} + n_U B_{UL} \int J_\nu \phi_\nu \, d\nu - n_L B_{LU} \int J_\nu \phi_\nu \, d\nu , \qquad (36)$$

where B_{UL} and B_{LU} are the Einstein coefficients for stimulated emission and absorption, respectively, and the other symbols have been defined. Combining Equations 21 and 36, we obtain

$$(NRB)_{UL} = \left[1 - \frac{n_L B_{LU}}{n_U A_{UL}} \int J_\nu \phi_\nu \, d\nu - \frac{B_{UL}}{A_{UL}} \int J_\nu \phi_\nu \, d\nu \right]_{UL} . \qquad (37)$$

Now let us assume that $\phi_\nu = \psi_\nu$, as we did to derive Equation 19 for $B_\nu\,(T_{ex})$; and then, after using the relations for the Einstein coefficients,

$$\frac{A_{UL}}{B_{UL}} = \frac{2h\nu^3}{c^2}\,,\quad g_L B_{LU} = g_U B_{UL}\,, \tag{38}$$

let us combine Equations 19 and 37. Then we obtain

$$(NRB)_{UL} = \left[1 - \frac{\int J_\nu\,\phi_\nu\,d\nu}{B_\nu\,(T_{ex})}\right]_{UL}\,. \tag{39}$$

To obtain a simple expression for $(NCB)_{LU}$, we proceed in a similar way. We can write Equation 22 as

$$P(col;\ L, U) - R(col;\ U, L) = n_L C_{LU} - n_U C_{UL}\,, \tag{40}$$

where the notation is obvious. Equations 40 and 22 give

$$(NCB)_{LU} = \left[1 - \frac{n_U C_{UL}}{n_L C_{LU}}\right]_{LU}\,, \tag{41}$$

which can be written as

$$(NCB)_{LU} = \left[1 - \frac{b_U}{b_L}\,\frac{g_U}{g_L}\,\frac{C_{UL}}{C_{LU}}\,e^{-\chi_{LU}}\right]_{LU}\,, \tag{42}$$

where we use the Boltzmann equation for the ratio $(n_U/n_L)^*$ in LTE, the * indicating LTE, and introduce so-called "departure co-efficients" b_k, defined by the LTE Saha equation

$$n_k = \left[\left(\frac{2\pi h^2}{m_e\,kT_e}\right)^{3/2} n_e n_i\,\frac{g_k}{2U_i}\,e^{\chi_k/kTe}\right] b_k\,, \tag{43}$$

which is equivalent to

$$b_k = \frac{n_k}{n_k^*}\,, \tag{44}$$

since the quantity in square brackets in Equation 43 is the LTE value of n_k at local values of n_e, n_i, T_e. Also $X_{LU} \equiv \chi_{LU}/kT_e$, and, in the Saha equation, U_i is the partition function for the ion. Other symbols should be self-evident. Now, in LTE,

$$n_L^* C_{LU}^* = n_U^* C_{UL}^* \rightarrow C_{LU}^* \frac{g_U}{g_L} e^{-X_{LU}} , \tag{43a}$$

as $(NCB)_{LU} = 0$ from detailed balance and $b_U = b_L = 1$. Remembering that we assume a Maxwellian velocity distribution for electrons, and noting that C_{UL} and C_{LU} then assume their LTE values, we obtain

$$(NCB)_{LU} = \left[1 - \frac{b_U}{b_L}\right] . \tag{44a}$$

This is the desired expression for $(NCB)_{LU}$.

Equation 39 for the $(NRB)_{UL}$ appears in the energy-conservation equation we shall solve for our final chromospheric temperature distribution. Equation 41 for the $(NCB)_{LU}$ appears in the expression we derive for the apportionment of mechanical energy among all spectral lines formed in the same region of the atmosphere.

Now let us consider current models for the chromosphere and corona—especially the chromosphere. We shall find that the detailed model of the low chromosphere described in Section D is based on studies of emission in line-free regions of the continuum. Thus, at first we need not use everything developed in this section, but we must still use the general principle of a SSS contained in Equation 24. We shall find that significant departures from LTE-R do occur in the low chromosphere.

D. Solar Chromosphere and Corona

In Section A, we defined the top of the photosphere by the surface which lies at normal optical depth 1.0×10^{-3} at λ 5000 Å. This defines the base of the chromosphere and the zero point for our vertical height scale, measuring positive upward. The chromosphere and corona comprise the entire region lying above $h = 0$; hereafter we refer to this composite region as the "outer solar atmosphere." The chromosphere and corona are usually defined by the types of emission characteristic of each (van de Hulst, 1953). In general, then, we describe as chromospheric the "flash" spectrum seen at the limb in eclipse. This spectrum consists of emission lines of hydrogen, neutral metals, singly ionized metals, neutral helium, and ionized helium. There is also a background continuum of the H^- ion and the lower free-bound continua of hydrogen. Much of the continuum is scattered radiation. A more detailed consideration of chromospheric lines and the question of how much of the continuum emerging from the chromosphere is scattered photospheric radiation will appear in Chapter IV.

There is some question about the origin of certain lines from ions of ionization stages intermediate between chromospheric values (neutral, singly ionized metals) and coronal values (same metals - Ca, Fe - many times ionized). For example, strong lines of CIV, λ1548, and OVI, λ1038, and λ1032, are seen in emission in UV disk spectra (Detwiler et al., 1961). We shall not attempt to identify these lines as either chromospheric or coronal. Their existence does illustrate a vexing problem, however: the nature of the transition region between the chromosphere and corona.

The corona is characterized by emission lines of highly ionized metals, superimposed on a background of partially polarized continuum radiation. The corona has a mean density several orders of magnitude lower than the chromosphere. As a result, the net energy losses from the corona, estimated in Chapter IV, fall about two orders of magnitude below our net-loss estimates for the chromosphere. Also, the chromosphere's location just in and beyond the temperature minimum gives it a basic role in the energy-balance problem, since the source of mechanical energy seems to lie in the subphotospheric convection zone. We shall restrict our calculations to the chromosphere in this report, subject to some uncertainty as to where the boundary between chromosphere and corona lies.

A general feature of chromospheric emission lines discussed in PSC is that their intensity scale height is much larger than the pressure-density scale height $H = \mathcal{R}T_e/\mu g$ (where $\mathcal{R} = 8.31 \times 10^7$ ergs°K^{-1} mole^{-1} is the gas constant, and μ is the mean molecular weight) for an isothermal atmosphere, evaluated at our minimum temperature $T_e = 4600$°K. This strongly suggests an outwardly increasing temperature and possible departures from LTE-R, both of which we find in the chromosphere. An increase in temperature will increase the local pressure-density scale height. The exact role of the non-LTE effects will become apparent only after a detailed study of each emitting ion.

The model we shall adopt to begin our calculations for the first 1300 km above our zero point is the model derived in chapter 6 of PSC. Table 1 gives the quantities derived for this model. We choose this model, based on data obtained at the 1952 Khartoum eclipse expedition, because the method of analysis is highly self-consistent. We cannot accept those earlier models, typified by the one given by van de Hulst (1953), which neglect all non-LTE effects in their analysis. The Utrecht Reference Photosphere (Heintze et al., 1964) of the photosphere and low chromosphere extends out only to $h \simeq 230$ km on our height scale, and the Bilderberg Continuum Atmosphere (Gingerich and de Jager, 1968) ignores the conflicting results from line-profile analysis. Thus, for our calculations based largely on features of the chromospheric line spectrum, the PSC model of the region $0 \leq h \leq 1300$ km seems best.

The PSC model for $0 \leq h \leq 1300$ km, a region we shall hereafter call the "low chromosphere," is obtained from data in the optical continuum. The choice of continuum data is prompted, in part, by a desire to treat that spectral region where strong self-absorption plays a negligible role. A thin atmosphere analysis, where a SSS assumption in the form of Equation 24 takes account of non-LTE effects, is all that is required. No transfer equation need be solved, as all relevant radiation fields are known, except for the radiation field in the Lyman continuum discussed below.

Table 1

Model of Low Chromosphere from Chapter 6, PSC, Using Tables 6-9 and 6-10. (Subscripts 1 and 2 refer to levels in atomic hydrogen.)

h (km)	T_e(°K)	n_1 (cm^{-3})	$10^{-11} n_e$ (cm^{-3})	$10^{-5} n_{H^-}$ (cm^{-3})	$10^{-5} n_2$ (cm^{-3})	$b_1 \simeq b_2$	τ rad λ5000	$\tau_{Ly\,\alpha}$
0	5050	3.78(15)	6.36	38.8			1×10^{-3}	
100	5250	1.60(15)	5.05	11.5			4×10^{-4}	
200	5460	6.99(14)	4.65	4.10			2×10^{-4}	
300	5680	3.15(14)	4.58	1.62			6×10^{-5}	
400	5910	1.46(14)	4.63	0.670			3×10^{-5}	
500	6150	6.95(13)	4.72	0.290		3.4	1×10^{-5}	
750	6650	1.21(13)	4.04		9.98	6.1		1×10^{7}
850	6840	6.28(12)	3.69		8.38			
950	7040	3.19(12)	3.38		7.02			
1000	7150	2.27(12)	3.24		6.44	12.6		2×10^{6}
1100	7400	1.10(12)	2.97		5.42			
1200	7700	5.05(11)	2.75		4.61			3×10^{5}
1250	7901	3.19(11)	2.65		4.28			2×10^{5}
1300	8310	1.71(11)	2.60		-			7×10^{4}

The model is based on observed continuum radiation at λ3646, which is the head of the Balmer continuum, and at λ4700. Rayleigh scattering due to neutral hydrogen is taken into account; also Thompson scattering, free-bound and free-free scattering of H^-, free-bound transitions in the Balmer continuum at λ3646 and in the Paschen continuum at λ4700, and free-free transitions of hydrogen at λ4700. The observations give two equations in four unknowns: n_e, T_e, n_H, and n_p. An assumed hydrogen/metals ratio for $h \leq 500$ km or the assumption $n_e = n_p$ for $h > 500$ km adds a third relation. For the region $h > 500$, an expression based on the SSS relation (Equation 24) for $b_1 (n_e, T_e)$, defined by Equation 43, provides a fourth equation. The $b_1(n_e, T_e)$ relation is derived assuming detailed balance in the Lyman continuum, and a correction scheme is introduced to allow for some departure from detailed balance. Spherical symmetry is assumed.

Actual construction of the model is complicated and involves selecting good data points to provide boundary conditions to start the integration, as well as invoking other relations to supplement estimates made in regions where the data are considered unreliable. For example, hydrostatic equilibrium is assumed, to get the results for $h \geq 750$ km. The data below 500 km are not reliable, and begin to enter the region where self-absorption is not negligible as we approach the limb. Thomas notes that in the range $0 \leq h \leq 500$ km the T_e values of the model are an upper limit, which is reassuring in view of the great discrepancy between the T_e ($h = 0$) of this model and our adopted minimum temperature of Section B.

What are the conditions beyond the low chromosphere? Hiei (1963) concludes that spicules extend at least as far down as $h = 1500$ km, and there is evidence that they may extend down farther (House, 1961). The region $1300 \leq h \leq 1500$ km is certainly unknown territory, and the situation is little better from $h \geq 1500$ km until the corona is reached. The unanswered questions include:

What is the state of the gas in spicules?

What is the state of the gas in the interspicular material?

What fraction of the surface area at a given height h is covered by spicules?

How far does the corona penetrate into the interspicular material, if it penetrates at all?

There is no universally accepted answer to any of these questions.

In Chapter V of PSC, Athay considers some general stability arguments which he uses, along with an analysis of emission in the region $h \geq 1500$ km, to produce a model for this region. A stability criterion is obtained by requiring that an increase in energy input dE_{in} must cause an increased energy output dE_{out} along with the associated initial rise in temperature, such that

$$\frac{dE_{out}}{dT_e} \geq \frac{dE_{in}}{dT_e} \quad . \tag{45}$$

Thus, at any point in the atmosphere, we require an increase in net radiative losses to counter a small temperature increase, and vice versa, or the atmosphere is unstable. Consider a point in the atmpsphere where T_e has reached a value at which there are no efficient radiators to provide the necessary E_{out} to satisfy inequality 45. In the presence of an E_{in}, the atmosphere will not be stable at this T_e. Obviously, the atmosphere temperature will rise until, through some process such as ionization, a new efficient radiator will be produced and condition 45 can be fulfilled again. The atmosphere will be stable at the new T_e. The process is presumably repeated at each stage of stable equilibrium, as the temperature increases as height increases until the efficient radiator becomes inefficient, at which point the atmosphere finds a new stable equilibrium at a higher temperature. The process stops when E_{in} is exhausted, presumably somewhere in the solar corona. Beyond that point the process might be thought to reverse as T_e decreases with height, but other complications enter and we wish to consider only the upper chromospheric regions.

An idealization of an atmosphere, viewed from this simple stability viewpoint, would be a succession of temperature "plateaus" connected by infinite temperature gradients. In reality, conduction arising from these infinite temperature gradients and radiative energy redistribution between and within the plateaus should smooth out the temperature curve, but the gross feature of very shallow rises connected by steep rises will presumably remain. As Athay argues in PSC, there is evidence from spectral data that this is true for the outer solar atmosphere.

Athay notes that if observed stages of ionization of common elements are plotted against corresponding ionization potentials, there are gaps in which no stages of ionization of certain common

elements are observed in the solar atmosphere, even though a corresponding stage of ionization should be expected on chemical-composition grounds alone. The inference is clear: the ion we expected to observe is not present over a significant height range. The most direct explanation, in the light of our comments above, is that very little atmosphere gas is at the temperature at which we expect to find the ion (considering non-LTE effects, of course). This temperature lies on one of the steep rises of the temperature curve. The reason is that not enough of the ion is present to provide a sufficiently strong radiator to satisfy inequality 45, so instead of forming a plateau at T_e (ion), T_e continues to rise.

On the basis of these considerations, and after studying emission from hydrogen, HeI, and HeII, including the Lyman continuum of hydrogen and HeII, Athay concludes that the hydrogen emission comes from the spicules, and the helium emission from the interspicular gas, in the region $h \geq 1500$ km. However, conditions at the top of the spicular component are found to blend with those of the interspicular matter, suggesting a rapid temperature rise near the top of the spicules.

We shall not digress to show how Athay constructed a model for the chromospheric region $1500 \leq h \leq 4000$ km. We only note that his results show a strong dependence on the values of electron density n_e used in these regions, and the uncertainty in n_e may be as high as an order of magnitude. Table 2 gives the resulting model of this region $1500 \leq h \leq 4000$ km, which we shall call the "upper chromosphere." We see that he calculates the fractional area covered by the cold component (spicules), and also the n_e and T_e values for both components.

Table 3 gives the fractional areas covered by both cold and hot components, from Table 2. This can be used to construct a temperature model for a spherically symmetrical atmosphere whose excitation conditions lie between those of the cold and hot components. We can use such a rough temperature distribution to begin our calculations.

To construct this temperature model, we assume pressure equilibrium between the hot and cold components. Thus, for $P_c = P_h$, we define R:

$$R \equiv \frac{n_c}{n_h} = \frac{T_{eh}}{T_{ec}} , \tag{46}$$

Table 2

Model of Upper Chromosphere from Chapter 7 of PSC where a_c = Percent of Surface at h Covered by Cold Component.

h(km)	a_c	$\log_{10} n_{ec}$	$\log_{10} n_{eh}$	T_{ec}	T_{rh}
1500	4-20	11.9-12.4	11.1-11.4	7500	50000
2000	4-8	11.4-12.4	11.0-11.3	9000	50000
3000	0-4	11.6-11.9	10.8-10.8	10000	50000
4000	<60	10.6-11.3	<11.0	50000	>50000

Table 3

Estimates of a_c, a_h Based on Table 2.

h(km)	a_c	a_h
1500	20	80
2000	8	92
3000	4	96
4000	0.1	99.9

where n_c and n_h are particle densities for the two regions. We now form our "weighted temperature" T_{ew} in the following manner:

$$A_c = \frac{a_c R}{a_c R + a_h} , \tag{47}$$

$$A_h = 1 - A_c , \tag{48}$$

$$T_{ew} = A_c T_{ec} + A_h T_{eh} , \tag{49}$$

where the fractional areas a_c and a_h appear in Table 2, and T_{ew} in Table 4.

Table 4

Weighted Temperature T_{ew} for Upper Chromosphere Based on Table 3 and Equations (46) - (49).

h(km)	R	A_c	A_h	T_{ew}
1500	6.67	0.625	0.375	23,440
2000	5.55	0.328	0.672	36,550
3000	5.00	0.173	0.827	42,130
4000	>5	0	1	>50,000

It is appropriate now to consider some of the shortcomings of Athay's upper-chromosphere model. Athay knew that it predicted much higher intensities of radio emission (due to free-free electron transitions in a proton field) than are actually observed. To remove this discrepancy, he made a complicated alternation, in PSC. A more radical suggestion was made by Zirin and his co-workers (Zirin and Dietz, 1963; Zirin and Howard, 1966; Zirin, 1966): that the interspicular region is coronal gas, and all the helium emission hitherto ascribed to this interspicular gas, as well as the radio emission and hydrogen emission, actually arises in spicules. While there is some additional evidence for coronal excitation in the upper chromosphere, no quantitative treatment of this problem has so far appeared. We are left with no satisfactory model of this region, and terminate our calculations in Chapter IV at h = 1250 km.

Regardless of what model for this region finally emerges, electron thermal conduction is certain to play an important role somewhere in the transition region between the chromosphere and corona. We do not consider a mechanical flux of energy down from the corona due to conduction in the spherically symmetric model we construct, as this conduction is demonstrably negligible over the greater part of the region covered by our calculations.

This completes the background material dealing with radiation-matter-interaction aspects of the solar atmosphere. Now we shall consider macroscopic velocity fields and possible mechanical energy sources for heating the outer atmosphere. Sections E and F are devoted to these subjects.

E. Velocity Fields and Inhomogeneities

So far, we have not questioned our assumptions of HE and spherical symmetry in the chromosphere in the light of ambient velocity fields and inhomogeneities. Also, observed velocity fields may provide indirect support for the energy-generation mechanism and the mode of energy transport discussed in the next section. The suggestion for acoustic-wave generation, propagation, and shock dissipation at least must agree with these fields. This section is devoted to the observational study of velocity fields and inhomogeneities in the solar atmosphere. Some current theoretical interpretations of these observations will be discussed in the next section, together with the actual mechanical heating of the atmosphere.

Photospheric granulation is the first phenomenon we consider. Granulation is an aggregate of cells which are brighter than their surroundings when seen in continuum radiation and appear roughly circular near the center of the solar disk. Since optical depth unity occurs somewhere around $h = -350$ km in the continuum at $\lambda = 5000$ Å, depending on the photospheric model (Minnaert, 1953), this is the region of the photosphere where we see disk granulation. A detailed study of granulation has been made both by Bahng and Schwarzschild (1962) and by Edmonds (1961). Both studies are based on observations obtained from a balloon-borne telescope launched under Schwarzschild's direction (Project Stratoscope). In spite of differences in their interpretations, both studies agree that disk granulation represents elements with diameters ranging from a few hundred to 1800 km, a mean lifetime of six to nine minutes, and a mean temperature excess of several hundred degrees above the intergranular matter.

The best current account of the nature of disk granules is given by Böhm-Vitense (1958) and Biermann, et al., (1959); their quantitative calculations support what had already been conjectured: that disk granules are a manifestation of convection at the top of the Sun's subphotospheric convection zone. Indeed, they are thought to be the convective elements in the observable region of the convection zone. That the innermost region of the observable photosphere is convectively unstable has long been known, from applying the familiar Schwarzschild stability criterion to the region's temperature gradient. A simple application of Prandtl mixing length theory of turbulent convection to this convectively unstable region permits us to examine granulation data to see if the granules could be convective elements. This approach was developed by Vitense (1953). Using her equations and assuming a mixing length equal to the local density scale height, we estimate

$$\text{typical diameter} = \text{scale height} = 200 \text{ km},$$

$$\begin{aligned} &\Delta T < 1000^\circ K, && \Delta T \text{ is temperature excess,} \\ &t \simeq 5 \text{ minutes}, && t \text{ is mean time,} \end{aligned} \qquad (50)$$

which are not in exact agreement with the observations but come close enough to provide some support for the convection hypothesis.

If the bright granules are convective elements, they should be rising, as they are at a higher temperature than the surrounding gas and therefore less dense, presuming that the two are in pressure equilibrium. Evidence indirectly confirming this is offered by Evans and Michard (1962b), who find that 70 percent of the bright continuum features they observe are associated with violet shifts in several weak spectral lines. This evidence is of marginal value, however, because the correlation is low and because the continuum and lines refer to different heights in the photosphere.

The granules observed near the limb of the disk are higher in the photosphere than those observed near the center. Whitney (1963) suggests that limb granulation may be evidence of acoustic waves in the upper photosphere.

Next, consider the determinations of upper photospheric and chromospheric velocity fields made by Evans and Michard (1962a, 1962b, 1962c) based on an extensive series of observations at the Sacramento Peak Observatory. From measurements of the Doppler shifts in a large number of spectral lines—which extend far in the direction of the spectrograph slit and appear "wiggly" in the photographs—the authors derive a r.m.s. value for what is called the "random turbulent velocity" ξ. Then they assume that the stronger lines are formed farther out in the atmosphere, and conclude from their observations that ξ is increasing with height over the region where all the lines are formed.

To see the relevance of these observations for this study, we must inquire just how isotropic is the velocity field ξ. Where it is highly isotropic, there is turbulence that can generate acoustic waves. Where, on the other hand, the velocities are predominantly radial and not too large, these radial motions may be quite consistent with the picture evolved in the next section, where acoustic waves with a net flux vertically upward pass through an atmosphere which, to a first approximation, is in hydrostatic equilibrium. The evidence of Evans and Michard is not conclusive, but it does support the view that the velocity field ξ is *not* isotropic. Center-to-limb observations of each line for $\mu \leq 0.6$ yield decreasing values of ξ. When we consider that ξ is thought to increase with height, as already mentioned, the only explanation, other than one based on instrumental-seeing problems, is that the horizontal component of velocity is less than the vertical component. The evidence is weakened by the authors' belief that atmospheric seeing effects may, in fact, produce these observations and thus render the above conclusion invalid. Nevertheless, these observations provide the best available clue to the extent of photospheric-low chromospheric turbulence; their evidence is against isotropic turbulence in this region. Table 5 gives the results of the Evans and Michard study.

Unfortunately, the question of turbulence has not been settled, as the work of Holweger (1967) shows. He concludes, after an analysis of many weak lines, that the horizontal-velocity component exceeds the vertical one and that the micro-turbulent velocity ξ decreases with increasing height in the photosphere, contrary to Evans and Michard.

An interesting feature of the solar atmosphere, regarding wave propagation, is the oscillatory vertical velocity field near the temperature minimum. The heights in the atmosphere at which these oscillations are observed are inferred from depth-of-formation estimates of the spectral lines

Table 5

Center-to-Limb Variation of ξ (km sec^{-1}) from Evans and Michard (1962a).

First Set: Tangential Slit					
Line	μ				Roland Intensity
	1.00	0.64	0.38	0.16	
MgI 5172.700	0.61	0.46	0.34	0.25	20
FeI 5171.612	0.39	0.40	0.34	0.24	6
TiI 5173.751	0.31	0.43	0.30	0.25	2
NiI 5168.665	0.31	0.41	0.34	0.20	1
FeI 5170.770	0.35	0.34	0.27	0.26	0

Second Set: Radial Slit					
Line	μ				Roland Intensity
	1.00	0.60	0.46	0.30	
MgI 5183.621	0.47	0.35	0.41	0.29	30
MgI 5172.700	0.43	0.37	0.39	0.19	20
FeI 5171.612	0.32	0.29	0.38	0.20	6
TiI 5173.751	0.32	0.35	0.46	0.27	2

Line	μ					Roland Intensity
	1.00	0.76	0.65	0.52	0.29	
FeI 5324.193	0.37	0.34	0.37	0.26	0.26	7

studied. The papers by Evans and Michard (1962c), Leighton, et al. (1962), and Noyes and Leighton (1963) are all detailed studies of this phenomenon. A summary of the salient results of both shows the following: 1) There is a periodic, quasisinusoidal variation of vertical velocities in medium-strength lines with periods from 200 to 300 seconds that tend to decrease with increasing line strength, i.e., with increasing height in the atmosphere. In addition, the r.m.s. velocity amplitudes increase with line strength, i.e., with height. The velocity amplitudes are always less that 1.0 km sec^{-1}. 2) Further support for the velocity-field variations comes from intensity fluctuations in the cores of medium-strength lines, with a period roughly the same as for the velocity field and decreasing with increasing line strength. 3) The observed oscillations disappear as one scans the disk from center to limb, indicating that the oscillatory velocity field is largely normal to the solar surface.

The next section takes up the theoretical interpretation of the above three types of observations; their interpretation in terms of various kinds of wave propagation will be particularly direct. We wish to relate some of these observations to our previous considerations on isotropic turbulence.

There is evidence that the non-thermal velocity fields studies by Evans and Michard are anisotropic. Further observation of oscillatory Doppler shifts and brightness fluctuations in the cores of medium-strength lines led Evans and Michard (1962c) to remark, "A sizable fraction of the kinetic energy is contained in the distinctly organized non-turbulent motions of many unrelated small elements." What fraction of the kinetic energy of the photospheric velocity field is tied up in isotropic turbulence is still an open question, but some kind of non-thermal anisotropic motion does seem to be coupled to and lying above the disk granulation. That there might be more nearly isotropic turbulence in the deeper layers of the photosphere is suggested by the results of Evans and Michard (1962a) which show that the ξ derived from the weaker lines actually increases when μ changes from 1.00 to about 0.6. Adding the deduced oscillatory velocity field to the upper part of the region gives a picture of the photosphere-low chromosphere we refer to in the next section in discussing the generation and propagation of various wave modes through this region.

On a much larger scale than the granulation is the recently discovered "supergranulation network," reported by Leighton, Noyes, and Simon (1962). This is a system of large cells easily seen in the Ca λ6103 line. They are approximately circular near the center of the disk, have a mean diameter of 1.6×10^4 km, horizontal motion of matter from center to rim with a mean velocity of 0.5 km/sec, cell lifetime in the range 10^4 - 10^5 sec (difficult to estimate due to the Earth's rotation), and an average spacing between cell centers of 3.0×10^4 km, giving some 5×10^3 cells over the solar surface. A similarity in appearance was revealed between the cells observed in Ca λ6103 and the solar surface seen in the K_2 central emission component of the CaII K line.

The supergranulation network will not play any direct role in the calculations of this report, not because it is unimportant, but because its role and, hence, its importance in the-chromospheric-energy-balance problem is difficult to evaluate. The supergranulation appears to be a manifestation of convective motion that could originate deep in the convection zone, with material moving essentially upward in the center of the cell and down along the rim. This motion appears to be more ordered than the rather random motions of the granulation, which exhibits horizontal as well as vertical motions. Exactly what coupling might exist between the two, and hence what role the supergranulation may play in mechanical energy generation, is an unsolved problem. However, there is one atmospheric phenomenon with which the supergranulation appears morphologically connected: the spicules, already mentioned in Chapter I and in the discussion of the chromosphere and corona.

Two comprehensive studies of spicules are those by Athay (1959), based on data obtained by Dunn (1956), and Beckers (1968). The reader is referred to PSC, where the Athay study is reported in context with many other earlier studies of spicules. The Beckers article is a review of more recent work and offers a comparison with the older studies. Although a fairly consistent picture has emerged correlating high-resolution K_2 spectroheliograms with Hα bright mottles seen at line center between ± 0.2Å, and some information of a statistical nature has appeared regarding the numbers, rise-times, etc., of spicules, their dynamics are not understood, apart from some qualitative theories discussed in the Beckers review. For this reason we shall not discuss spicules any further here, except to mention that the above correlation between the chromospheric network in K_2 and H α (presumably originating in spicules seen on the disk) also correlates with

the supergranulation network and regions of high chromospheric-magnetic-field strength. Eventually a dynamical theory will have to correlate all these observed phenomena.

We return to the assumptions of HE and spherical symmetry mentioned at the beginning of this section. We shall not explicitly use the HE assumption, but since we rely on the PSC model to start our calculations in this region, and since HE was assumed in constructing the PSC model, we *implicitly* assume HE. The evidence presented here suggests that we need not consider isotropic turbulence in the low chromosphere. However, oscillatory motions do occur in the vicinity of the temperature minimum, with velocity amplitudes always less than 1.0 km sec^{-1}. This contrasts with a thermal velocity for hydrogen of the order of 10 km sec^{-1}. On this basis, we shall ignore the pressure perturbation of the oscillatory velocity and retain the assumption of HE.

There was some evidence in the studies cited that the velocity field would lose its "standing wave" character around the temperature minimum and move outward with increasing velocity. In the next section it is argued that these running waves are acoustic waves in the chromosphere. This indicates that to a first approximation HE applies to the state of the low chromospheric gas, which is perturbed by a progressive sound wave that builds up into a shock wave.

Spherical symmetry is also assumed for the PSC-model low chromosphere. Barring significant penetration of convective elements from the low photosphere into the chromosphere, or significant penetration of spicules below $h = 1300$ km (for which there is no direct, observational evidence), spherical symmetry in the low chromosphere is probably a reasonable assumption. On the other hand, House (1961) concludes from a study of emission in MgI that departures from spherical symmetry must occur somewhere between 500 and 1000 km. This may be correct; the effect would be to produce deviations from the PSC-model low chromosphere we have adopted. However, in the absence of a complete chromospheric model based on possible deviations from spherical symmetry, we shall retain the PSC model for $h \leq 1300$ km, along with the implied assumption of spherical symmetry. For $h \geq 1300$ km, we do not invoke spherical symmetry, which is quite invalid in the upper regions, except in our final calculation for $T_e(h)$, which must be interpreted as some suitable average temperature in this region.

One final idea should be mentioned before we try to tie the observations of this section into our mechanical-energy generation and dissipation model for the next. Bhatnagar, Krook, Menzel, and Thomas (1960) point out that the large extension in space of many stellar atmospheres can be seen as a momentum transfer or an energy transfer. These concepts can apply simultaneously. There could be momentum transfer due to the chromospheric velocity fields, which would push the gas radially outward, and energy transfer due to some effective dissipation mechanism, which would cause extension by producing higher temperatures. Some coupling should exist between the two. Which process is dominant in producing the observed extension of the solar atmosphere? The authors give evidence for energy transfer. A rapid rise of temperature with height would favor energy transfer, and go far toward eliminating the need for isotropic turbulence to explain the widths of many spectral lines. This would also support the picture of anisotropic, preferentially radial, mass motions in the chromosphere, as suggested in this section.

F. Generation and Dissipation of Mechanical Energy

In the introductory statement of the problem it is stated that several sources of energy for heating the outer solar atmosphere have been proposed. We consider these sources in turn, and finally select the most probable. First, we should estimate the total energy required to balance the net radiation losses from the chromosphere and corona. In chapter IV we discuss the estimates that have been made to date; that discussion indicates the need for a flux of 10^7 ergs cm^{-2} sec^{-1} at the temperature inversion. Practically all the radiant energy loss is due to the chromosphere alone.

Hoyle (1949) was the first to calculate how the corona, but not the chromosphere, might be heated by accretion of interstellar particles as the Sun moves through the galaxy. Billings (1966) has reviewed the development of this idea to date; he concludes that, for the corona, the accretion-heating hypothesis is weak though not entirely dead. He points out that no accretion-heating theory proposed can explain the very high-temperature, low-lying, yellow-line regions of the corona and that no provision has yet been made for the efflux of matter due to solar wind. Considering these difficulties and the fact that most of the radiant energy loss occurs in the chromosphere (a fact not considered in the accretion studies and of primary importance to us here), we reject the accretion hypothesis.

Cayrel (1963) suggested the photospheric radiation field as a possible means of raising the temperature in the low chromosphere. He claims that, in an atmosphere in radiative equilibrium which is optically thin in the continuum and is subjected to a strong radiation field (the photosphere), a departure of the continuum source funtion from the Planck Function can produce a temperature in the outer region equal to the effective temperature of the continuum-producing region. Unfortunately, I shall show in my treatment of the H^- problem in Chapter V that this mechanism will not work in the low chromosphere. So the Cayrel treatment must be modified to allow for some mechanical heating. The relevant photoionization reaction is

$$H^- + h\nu \rightarrow H + e \ . \tag{51}$$

As for the dominant collisional reaction, Pagel (1959) showed that estimates by Dalgarno (in a private communication to Pagel) of the reaction rate $k = 3.0 \times 10^{-10} cm^3 sec^{-1}$ for the associative detachment reaction

$$H^- + H \rightarrow H_2 + e \tag{52}$$

would cause reaction 52 to dominate the ionization equilibrium of H^- in the solar atmosphere out to $\tau_{5000} \geq 0.002$. More recent theoretical calculations (Dalgarno, 1967) and laboratory measurements (Schmeltekopf et al., 1967) of the rate constant k for reaction 52 give $k = 1.3 - 1.9 \times 10^{-9}$ cm^3 sec^{-1} for a temperature range of 300 - 8000°K. Thus, Pagel's conclusion remains valid. That is,

the reaction 52 now predominates out to $\tau_{5000} \simeq 0.0003$. Table 1 shows that the collisional reaction predominates out to about 200 km. Beyond 200 km, photoionization may predominate. In Chapter IV we shall consider the role of collisions and photoionization in fixing the temperature.

Solar activity can be ruled out for many reasons, the most obvious being that conditions in the steady-state chromosphere (as here defined) are essentially independent of time on the solar cycle, whereas solar activity is strongly dependent on this time.

We have mentioned that spicules seem an unlikely cause of coronal heating, because of their subsonic speeds and low temperatures. Yet they might play a role in heating the upper chromosphere. From PSC or the Beckers' (1968) study it appears that 30 km sec^{-1} is a typical spicule velocity. Following Thomas (1948a), we note that this velocity exceeds the adiabatic speed of sound for all temperatures below 50,000°K, depending on the ratio of specific heats γ which we use to calculate T_e from the adiabatic sound speed formula $c_s = (\gamma \mathcal{R} T_e / \mu)^{1/2}$, where $\mathcal{R} = 8.31 \times 10^7$ ergs $°K^{-1}$ $mole^{-1}$ is the gas constant and μ is the mean molecular weight and using $c_s = 30$ km sec^{-1}. Thus, even if spicules are not found below $h = 1300$ km, they may play a role in heating the upper chromosphere by the mechanism of shock dissipation. Also, we must remember that spicules may originate at some height below $h = 1300$ km.

If the spicules are supersonic jets, heating the ambient chromospheric gas through shock dissipation, then the problem lends itself to a shock-wave treatment, which will be developed presently. Since the origin and dynamics of spicules are not yet well understood, we shall treat the problem no further from this viewpoint, but merely keep in mind that spicules may play some role at least in upper chromospheric heating. A qualitative theory of spicule formation has been developed by Kuperus and Athay (1967), in which thermal conduction downward through the chromosphere-corona transition region is the source of energy that generates the spicules. Only a detailed study can settle this question.

We must look for mechanical sources lying in or beneath the photosphere. This source must satisfy two conditions: 1) Enough energy must be provided to balance the net radiation losses of the outer atmosphere, already mentioned. 2) We must show how this energy is generated, propagated, and dissipated.

We tentatively identify the energy source with the turbulent motions of the gas at the top of the convection zone. That some kind of turbulent motion are present is supported by observations of granules and by theoretical considerations; both should reveal something as to where these motions occur and as to their nature, isotropic or anisotropic.

Unfortunately, continuum observations have so far not been analyzed to determine a "random turbulent velocity", because resolution has not been sufficient, even in the Project Stratoscope work discussed in the previous section. Thus, in the region where disk granulation is observed at 300 - 400 km below the $h = 0$ surface, many current estimates of the energy generated are based on the assumption that an isotropic turbulent velocity field is present, when this has not been established empirically. On the other hand, inferences of a random turbulent velocity, made from studies of weak spectral lines, invariably refer to higher regions of the photosphere (which

may be important for mechanical-energy generation and which we shall discuss later). At present the center of interest lies in the deeper region; thus we are seeking evidence of random turbulent velocity at levels where $h \simeq -350$ km.

Empirically, only vertical velocities have been inferred for this region. (This type of observation is discussed in Section E.) We assume that there is some kind of turbulence here because of the locally high "Rayleigh number" (a dimensionless parameter defined below). Following Unsold (1955) and Schwarzschild (1959), we note from laboratory experiments that the Rayleigh number has a critical value 10^5 below which, in the range of values 10^3 - 10^5, convective motion in the form of laminar flow in stationary, vertical, hexagonally cross-sectioned Bénard cells occurs and above which some form of non-stationary convection occurs. The Rayleigh number Ra is defined by

$$\mathrm{Ra} = \frac{g\ell^4}{\nu k} \frac{\gamma - 1}{T} \Delta(\nabla T) , \tag{51a}$$

where ℓ is the density scale height across which the density decreases by a factor of e, ν is the kinematic viscosity coefficient, k is the radiative conductivity, and $\Delta(\nabla T)$ is the excess of the temperature gradient over the adiabatic gradient. The other symbols have their usual meaning. Using the same values for these parameters as Schwarzschild (1959), which are

$$T = 8200°\mathrm{K}, \quad \ell = 300 \text{ km} ,$$

$$k = 2 \times 10^{12} \text{ cm}^2 \text{ sec}^{-1}, \quad \nu = 2 \times 10^3 \text{ cm}^2 \text{ sec}^{-1} , \tag{52a}$$

$$\frac{\gamma - 1}{T} \Delta(\nabla T) = \frac{1}{4000} \text{ km}^{-1} ,$$

which gives $\mathrm{Ra} \simeq 10^9$. Thus stationary, laminar convection is ruled out. On the other hand, as Schwarzschild points out, solar granulation does not seem to be a structureless, entirely random (i.e., isotropic) phenomenon. He considers this inconsistent with the very high value of $\mathrm{Ra} \simeq 10^9$, which implies a completely random turbulent motion. Arguing that one should use "turbulent viscosity" in place of kinematic viscosity in Equation 51, he reevaluates Ra, only to find a new value too low for any convective motion at all, much less non-stationary convection. He concludes that the true Rayleigh number should lie slightly above 10^5, because kinematic viscosity should be used in Equation 51 and the "Reynolds number" (see below) has a high value appropriate to turbulent flow. He adds that the turbulence is probably not random, on the grounds that such turbulence would require using turbulent viscosity in Equation 51, which leads to a ridiculously low value of Ra. His final conclusion provides a consistent picture both from observational data and from arguments based on the Rayleigh number.

Although some anisotropy is highly probable, we shall assume here that these motions in the lower region of $h \simeq -350$ km are isotropic.

Further evidence for highly turbulent motions is provided by estimating values for the Reynolds number in this region. The Reynolds number is defined by

$$\mathrm{Re} = \frac{\rho \ell v}{\mu} , \tag{53}$$

where ℓ is a characteristic length (taken to be the order of the density scale height as in Equation 51), v is flow velocity, μ is dynamic viscosity (related to kinematic viscosity ν by $\nu = \mu/\rho$), and ρ the mass density. Minnaert (1953) suggested the following values for these parameters at the top of the convection zone:

$$\begin{aligned} \ell &= 10^3 \text{ km} , & v &= 10^5 \text{ cm sec}^{-1} , \\ \mu &= 10^{-3} \text{ dynes sec cm}^{-2} & \rho &= 10^{-5} \text{ gm cm}^{-3} , \end{aligned} \tag{54}$$

which differ somewhat from the values in Equation 52 but not enough to affect the conclusion below, based on a Reynolds number $\mathrm{Re} \simeq 10^{11}$, which follows from Equations 53 and 54. Minnaert's conclusion is that such a high Reynolds number ensures turbulence at the top of the convection zone, because laboratory experiments show that transition from laminar to turbulent flow occur when $\mathrm{Re} \geq 10^3$. On this basis, we assume that a highly turbulent flow exists at the top of the convection zone.

Before reviewing the theory of acoustic-energy generation by this turbulence, let us reconsider some previous statements. First, the choice of the characteristic length ℓ in Equations 51 and 53 is somewhat arbitrary. In the original laboratory experiments where these two numbers Ra and Re were used, ℓ referred to the thickness of the fluid layer and the radius of a pipe through which the fluid was flowing, respectively (Huang and Struve, 1960). Since the element's (granule's) size, the distance (Prandtl mixing length) through which a typical element moves before losing its identity, and the density scale height at the top of the convection zone are all of the same order of magnitude in the range $10^2 - 10^3$ km, according to theories of this region already considered (Vitense, 1953; Böhm-Vitense, 1958; Biermann, 1959), it is felt that a choice for ℓ in this range is the best we can make; but there is some uncertainty.

Consider the Lighthill (1952) theory for acoustic-power generation applied to an isotropic, homogeneous, turbulent velocity field. It is assumed that all the acoustic energy produced will be radiated away with no feedback into the turbulent velocity field; this is justified as long as the Mach number for the turbulent motions is much less than unity. Theoretical estimates of turbulent velocities (Böhm, 1963), based on convection theories which are admittedly rough approximations and

treat vertical velocity components only, give maximum values of about 2.0 km sec^{-1}. This value is sufficiently small compared to the local velocity of sound in the low photosphere for Lighthill's assumption on the turbulent Mach number to be valid in this region.

Lighthill starts with the basic equations of continuity and motion of fluid dynamics (Courant and Friedrichs, 1948), and derives an expression for density perturbation in a turbulent fluid as a function of the stresses associated with the turbulent velocity field. This expression for density perturbation has the form

$$\rho\,(\underline{r},\,t) - \rho_0 \;=\; DI + QU\,, \tag{55}$$

where DI and QU represent dipole and quadrupole acoustic radiation fields, respectively, because of their formal similarity to the dipole and quadrupole integrals in the expansion of the electromagnetic potential; ρ_0 is the equilibrium density of the gas at point $\underline{r}$. The intensity of sound is

$$I(\underline{r}) \;=\; \frac{c_s^3}{\rho_0}\,\left\langle\left(\rho\,(\underline{r},\,t) - \rho_0\right)^2\right\rangle\,, \tag{56}$$

where $\left\langle\left(\rho(\underline{r},\,t) - \rho_0\right)^2\right\rangle$ is the mean-square fluctuation in ρ and the other symbols have been defined already. The total power output is obtained by integrating the intensity over a large sphere of radius $|\underline{r}|$, which encloses the region of sound generation. Dividing by the volume of the sphere gives the mean power density.

Proudman (1952) performed the integration of the quadrupole term obtained by combining Equations 55 and 56 for the case of isotropic, homogeneous turbulence. Lighthill evaluated the dipole term. Kuperus (1965) compares the results of the two integrations and shows that

$$\frac{P_d}{P_q} \;=\; \phi\, M_t^{-2}\,, \tag{57}$$

where P_d and P_q are the power densities for dipole and quadrupole acoustic radiation, respectively, $M_t = v_t/c_s$ is the Mach number for turbulent motions with v_t the velocity of turbulence, and ϕ is a number, evaluated by Kuperus, weakly dependent on the assumption concerning the correlation function $f(r)$, given by

$$f(r) \;=\; \left\langle v_i\,(\underline{r}_1)\;\cdot\;v_i\,(\underline{r}_2)\right\rangle\,. \tag{58}$$

Here, v_i is the velocity component in the i-th co-ordinate direction, and $\langle v_i(\underline{r}_1) \cdot v_i(\underline{r}_2) \rangle$ is the mean value of $v_i(\underline{r}_1) \cdot v_i(\underline{r}_2)$ subject to the condition $r = |\underline{r}_1 - \underline{r}_2|$. Specific forms for Equation 58 are available for the Heisenberg correlation and the Gaussian correlation of velocities. Kuperus uses Proudman's work to show that a difference by a factor of only 2.86 exists in the choice of ϕ, depending on whether we choose the Heisenberg or Gaussian correlation; he claims that experimental evidence favors the Heisenberg. Evaluating ϕ with the Heisenberg correlation function for $f(r)$, Kuperus concludes that $P_d \simeq 0.18\, P_q$ for $M_t = 0.15$, making the quadrupole term dominant. We tentatively accept this conclusion with one reservation: the assumptions of isotropic turbulence and a Heisenberg velocity correlation have not been verified to date for the lower photosphere. Unno and Kato (1963) have also evaluated the terms of Equation 56, using the Lighthill theory with some modifications. They note the sensitivity of the results to these unverified assumptions, including the possibility that sufficient anisotropy in the turbulent-velocity field might cause the dipole term to be as important as the quadrupole term (Unno, 1964).

Lighthill (1954) supplemented the above calculations by deriving a more general form of Equation 55 which includes the effect of anisotropic convection (this, presumably, "drives" the turbulent motions by agitating the gas at the top of the convection zone) on the total power radiated. He shows that the effect on the quadrupole radiation field is to multiply the QU term of Equation 55 by the fac-$(1 - M_c \cos \delta)^{-3}$, where $M_c = v_c/c_s$ is the Mach number for convective motions with v_c the convective velocity, and δ is the angle between v_c and the direction of sound emission. The intensity due to quadrupole emission must then be multiplied by $(1 - M_c \cos \delta)^{-6}$. This correction is not included in the total mechanical flux estimate we give below, because turbulent velocities are assumed equal to convective velocities as a first approximation. A more detailed study should distinguish between the two and include the effect of the convective motion with a preferred direction. The effect of convective elements that penetrate beyond (above) the radiatively unstable lower photosphere will be discussed later in this section.

Now we can consider some estimates of the net flux of mechanical energy generated by the Lighthill (1952) mechanism in the turbulent, radiatively unstable lower region of the photosphere. The effect of magnetic fields is ignored. The formula Proudman obtains for the acoustic power generated per unit volume by the QU term of Equation 55 is

$$P_q = C \frac{\rho_0 \langle v_t^2 \rangle^{3/2} M_t^5}{L}, \tag{59}$$

where C is a number dependent upon our choice for the velocity correlation $f(\underline{r})$ of Equation 58, is a characteristic length of the turbulent-velocity field, and the other parameters have already been defined. The variation in C is only a factor of 2.86 (as with ϕ of Equation 57), depending on whether we choose the Heisenberg or Gaussian correlation. Again we choose the Heisenberg correlation and, like Proudman, obtain $C = 37.7$.

Kuperus (1965) numerically solves Equation 59 for two different models of the convection zone, to obtain a rough estimate of the mechanical-energy flux generated. We use his estimates here. He chooses $L = 500$ km, which is reasonable in the light of our arguments for choosing a characteristic length ℓ to evaluate the Rayleigh and Reynolds numbers. Thus Equation 59 becomes

$$P_q = 7.55 \times 10^{-7} \rho_0 \langle v_t^2 \rangle^{3/2} M_t^5 , \tag{60}$$

where ρ_0 and v_t are obtained directly from the convection zone models, and $M_t = v_t/c_s = v_t/\sqrt{\gamma RT_e/\mu}$ is calculated from these models, which specify T_e, μ, and γ. The models chosen by Kuperus to calculate P_q are theoretical ones calculated by Biermann et al. (1959) and Heintze et al. (1964). The Biermann model is practically identical with the Vitense (1953) model, mentioned in the last section to establish similarities between observed granules and calculated properties of convective elements. The Heintze (1964) model is called the "Utrecht Reference Photosphere" and is similar to the Heintze (1965) model, for which the temperature distribution is plotted in Figure 2. Isotropic-turbulence velocity v_t is assumed equal convective velocity v_c as a first approximation.

Kuperus assumes that all acoustic power generated will ultimately propagate upward from the convection zone. Since half of the power initially generated will propagate downward, according to the early Lighthill (1952) theory, a reflection is needed to change the direction of those waves that initially propagate downward. Kuperus does not consider what fraction of these downward propagating waves will "bounce off" the denser material below and propagate upward before appreciable attenuation. This omission is probably allowable because 1) some reflection can be expected, 2) the already mentioned correction factor $(1 - M_c \cos \delta)^{-6}$ shows us that more sound will be initially emitted upward than downward for a convective velocity v_c directed predominately upward, and 3) the maximum uncertainty of a factor of 2 implicit in this assumption is no greater than the uncertainties upon which the convection zone models or Equation 60 for the power generation are based.

The calculation of the mechanical energy flux F_m is reduced to an integration of the acoustic power output per unit volume over the thickness of the generating region. Thus, Kuperus numerically solves

$$F_m = \int_{h_1}^{h_2} P_q(h)\, dh , \tag{61}$$

where $P_q(h)$ is obtained from Equation 60, and h_1 and h_2 are derived from the convection zone model chosen. The lower boundary, h_1, occurs where the decrease of M_t (due to v_t decreasing and c_s increasing inward) makes $P_q(h)$ negligible. The upper boundary, h_2, occurs where radiative equilibrium is reestablished in the photosphere as one proceeds outward. The region of appreciable

acoustic-power generation is a thin layer about 100 km thick as shown by a simple estimate based on either model Kuperus used for the upper convection zone.

The results of Kuperus' calculation of the flux F_m, obtained from Equation 61, are as follows: $F_m = 2.9 \times 10^8$ ergs cm^{-2} sec^{-1} from the Biermann model of the convection zone; $F_m = 5 \times 10^7$ and 2.7×10^7 ergs cm^{-2} sec^{-1} from Heintze model, depending on whether upward or downward convective velocities are used, as the Heintze model is an inhomogeneous model with columns of both rising and falling material. Kuperus simplifies the calculation by selecting a mean temperature ~6250° for evaluating F_m. Since T_e does not vary strongly within the 100-km layer where the energy is generated, this simplification is justified.

These three estimates of F_m are all equal to or greater than the various estimates of the net radiative loss from the outer atmosphere, given in Chapter IV. Although there are many uncertainties in the estimates of both quantities, we conclude that there is probably enough mechanical energy generated by the Lighthill (1952) mechanism to balance the net radiative losses of the outer atmosphere.

That magnetic fields in the low photosphere probably do not affect the above results, we see from the following considerations. Kulsrud (1955) evaluated the quadrupole term of Equation 55 for the more general case with a magnetic field. The generated power is enhanced by the turbulence components of the magnetic field. This enhancement is exhibited as a function of the Cowling number S, defined here as the ratio of the turbulent magnetic-energy density to the turbulent kinetic-energy density. We have

$$S_t = \left(\frac{H_t^2}{8\pi}\right) \Big/ \left(\frac{1}{2}\rho_0 v_t^2\right) = \left(\frac{H_t^2}{4\pi\rho_0}\right) \Big/ v_t^2 \ , \tag{62}$$

where S_t is the turbulent Cowling number and H_t is the turbulent magnetic-field strength. For $S_t \leq 0.1$, Kulsrud shows that the magnetic field plays a negligible role. We do not know the value of H_t, but if we assume that it is of the same order as the steady-state, photospheric magnetic-field strength of about 1 gauss (Babcock and Babcock, 1955), we can estimate S_t. Suppose we assume, for the low photosphere,

$$\begin{aligned} v_t &= 1 \text{ km sec}^{-1}, \quad H_t = 1 \text{ gauss}, \\ \rho_0 &= 10^{-7} \text{ gm cm}^{-3} \ . \end{aligned} \tag{63}$$

This gives $S_t \simeq 10^{-4} << 0.1$, well within the limit for neglecting the magnetic field in the quadrupole term of Equation 55. Following the method of Kulsrud, Osterbrock (1961) evaluated the effect of a

steady-state magnetic field on the dipole term of Equation 55. He shows that $H \simeq 10^3$ gauss is required before the corrected dipole term will complete in magnitude with the quadrupole radiation term of Equation 60. Thus, ignoring the effect of magnetic fields on energy generation is justified outside active regions. It is probably not justified in the plage regions, but, since they are solar-cycle dependent and cover a small fraction of the photosphere, we do not consider them here.

This completes our review of possible sources of mechanical energy for heating the outer solar atmosphere, except for a discussion to follow on the not yet well understood effects of penetrative convection. We conclude that acoustic waves generated by a turbulent-velocity field in the low photosphere provide the most likely source in view of current observational data and theoretical models of the photosphere and the underlying convection zone. Now it is necessary to consider how these waves propagate.

The term "acoustic" has so far been used to describe the waves generated. "Pressure" waves (generated in the presence of a gravitational and a magnetic field) would be as valid. The resulting energy flux obtained from the Lighthill theory, when generalized by Kulsrud for magnetic-field effects, is seen to be almost independent of gravity and magnetic fields in the low photosphere. Gravity independence is due to the fact that only the weaker dipole term of Equation 55 is gravity-dependent. We have already advanced arguments for magnetic-field independence. The important point is that even though the generation of these pressure waves is practically independent of solar surface gravity and the photospheric magnetic field, the same might not be true of wave propagation. Therefore, we must examine the problem of the propagation of an infinitesimal disturbance through a compressible plasma with gravity and a magnetic field.

This problem has been studied by Ferraro and Plumpton (1958) for an isothermal atmosphere of infinite electrical conductivity. If we further assume zero viscosity for the solar atmosphere, and orient our co-ordinate system so that $\vec{g}$—a vector terminating at $(0, 0, -g)$—lies along the z-axis, we can start with the basic equations of magnetohydrodynamics (the so-called Navier-Stokes equations with a magnetic-force term) and the adiabatic law and, following Ferraro and Plumpton, derive the wave equation governing the displacement $\underline{r}$ of a particle from its equilibrium position. The equation is

$$\frac{\partial^2 \vec{r}}{\partial t^2} = \left(c_s^2 + c_a^2\right) \vec{\nabla}^2 \vec{r} + (\gamma - 1)\, \vec{g}(\vec{\nabla} \cdot \vec{r}) - \vec{\nabla}(g r_z) + \cdots$$

$$\cdots - \frac{1}{4\pi\rho_0} \left[\vec{H}_0 \left(\vec{H}_0 \cdot \vec{\nabla}\right) \vec{\nabla} \cdot \vec{r} + \left(\vec{H}_0 \cdot \vec{\nabla}\right) \left(\vec{H}_0 \times \vec{\nabla} \times \vec{r}\right)\right] , \qquad (64)$$

where all the old symbols have their usual meanings, the subscript "0" refers to the equilibrium value of the quantity, $c_a = H_0/\sqrt{4\pi\rho_0}$ is the Alfvén speed, and r_z is the z-component of $\vec{r}$.

Equation 64 is rather complicated, but by assuming plane wave solutions of the form

$$(r_x,\ r_y,\ r_z) = \exp\left\{i\left(\omega t + k_x x + k_y y + k_z z\right)\right\}, \tag{65}$$

and substituting these solutions in Equation 64, we obtain the dispersion relation for the dependence of angular frequency ω on wave numbers k_x, k_y, k_z, and on physical conditions in the atmosphere through g, c_s, and c_a. From this dispersion relation we can determine what wave modes are likely in the photosphere and low chromosphere. The dispersion relation is itself quite complicated, but if we assume $\vec{H}_0 = (0, 0, H_0)$ for a vertical magnetic field and let $k_y = 0$ for two-dimensional propagation, we still obtain all the physical behavior of the more general case with simpler mathematical expressions. Consider the following special cases.

Case 1 is one-dimensional propagation, obtained if $k_x = 0$. The dispersion relation then becomes either Equation 66 or 67:

$$\omega^2 - c_a^2 k_z^2 = 0, \qquad \text{Case 1a} \tag{66}$$

Here, our phase velocity $v_p = \omega/k_z = c_a = H_0/\sqrt{4\pi\rho_0}$ is the Alfvén speed. The wave is a transverse wave travelling vertically along the magnetic field. Also possible is

$$\omega^2 - c_s^2 k_z^2 - \gamma g k_z\, i = 0, \qquad \text{Case 1b} \tag{67}$$

This is a sound wave travelling vertically. Solving Equation 67 for k_z,

$$k_z = -\frac{\gamma g}{2c_s^2}\, i \pm \frac{1}{c_s}\left(\omega^2 - \omega_s^2\right)^{1/2},\quad \omega_s = \frac{\gamma g}{2c_s}, \tag{68}$$

Only for $\omega > \omega_s$ will the wave number k_z have a real part. Thus, only for $\omega > \omega_s$ will propagation of a pure sound wave be possible. We shall return to this point later.

Case 2 occurs if $k_x \neq 0$, but $g = 0$. In this case, we neglect gravity, but include magnetic-field effects. The dispersion relation becomes

$$\left(\omega^2 - c_a^2 k_z^2\right)\left[\omega^4 - \left(c_s^2 + c_a^2\right)\left(k_x^2 + k_z^2\right)\omega^2 - c_s^2\, c_a^2\left(k_x^2 + k_z^2\right)\right] = 0, \tag{69}$$

which describes magnetohydrodynamic waves in an isothermal compressible plasma of infinite electrical conductivity. If the first factor in Equation 69 is zero, case 1a occurs. If the second factor is zero, two new types of independent modes occur. These are called the "fast" and the "slow" mode, depending on the choice of the ± sign in the equation for the phase velocity, which is

$$V_p^2 = \frac{1}{2}\left(c_s^2 + c_a^2\right) \pm \frac{1}{2}\left[\left(c_s^2 + c_a^2\right)^2 - 4c_s^2 c_a^2 \cos^2\theta\right]^{1/2} , \qquad (70)$$

where θ is the angle between the wave vector and the z-axis.

Case 3 occurs if we put $c_a = 0$, thus neglecting the magnetic field, but put $g \neq 0$. The dispersion relation becomes

$$\left(\omega^2 - \omega_s^2\right)\frac{\omega^2}{c_s^2} - \omega^2\left(k_x^2 + k_z^2\right) + \omega_g^2 k_x^2 = 0, \quad \omega_g \equiv \frac{(\gamma - 1)^{1/2} g}{c_s} . \qquad (71)$$

Equation 71 yields real k_z only where $\omega > \omega_s$ or $\omega < \omega_g$, assuming that $\omega_s > \omega_g$, which is true in the photosphere. If $\omega < \omega_g$, the waves are called "gravity waves."

We are now ready to discuss wave propagation in the photosphere and low chromosphere in terms of the above. Osterbrock (1961) took Equation 69 and showed that, in both the photosphere and the low-chromosphere outside regions of strong magnetic fields associated with plages, the fast mode is practically a sound mode, in that $c_s^2 >> c_a^2$, which makes the second factor in Equation 69 reduce to the $g = 0$ form of Equation 67 for a pure sound wave. This is evident if we note that $c_s^2 >> c_a^2$ is equivalent to $\gamma \mathfrak{R} T_e/\mu >> H^2/4\pi\rho$. From Table 1, we see that the place in the low chromosphere where this condition is least likely to be met is the higher part, owing to the rapid decrease in density with height. Testing the above condition at $h = 1250$ km, with $\rho \simeq 1.5 \times 10^{-12}$gm cm^{-3} and $T_e \simeq 7500°$K, and assuming $H = 1$ gauss and $\gamma = 5/3$, we obtain $c_a^2/c_s^2 \simeq 0.05$. Thus Osterbrock's contention about the fast mode is surely correct below this height.

Equation 70 with the minus sign shows us that, for $c_s^2 >> c_a^2$, $v_p \rightarrow c_a$, so the slow mode is practically an Alfvén mode. We shall review arguments for the rapid damping of the Alfvén mode in the photosphere presently when we come to study dissipation mechanisms. Here, we use *the result due* to Osterbrock's discovery that the Alfvén mode is so rapidly damped in the photosphere that effectively no flux of mechanical energy passes through the photosphere in the form of Alfvén waves. From this we conclude that the entire flux of energy through the photosphere is in the fast mode or, in effect, sound waves, provided that the effect of gravity is negligible.

Whitaker (1963) argues that the effect of gravity cannot be ignored. Accepting Osterbrock's conclusion that the magnetic-field influence is negligible over most of the solar surface, he argues in favor of gravity waves with the dispersion relation given by Equation 71. Since sound waves of angular frequency $\omega < \omega_s$ cannot propagate outward but are reflected back down into the photosphere

at the temperature minimum where ω_s attains a maximum value, Whitaker argues that some of the energy in sound waves cannot propagate into the chromosphere, where the energy is needed. To show that this is a serious problem, let us evaluate ω_s for conditions around the minimum temperature. Using

$$g = 2.74 \times 10^4 \text{ cm sec}^{-2}, \qquad T_e = 4600°K,$$
$$\gamma = 1.2, \qquad \mu = 1, \tag{72}$$

after Whitaker (whose γ lies between the adiabatic and isothermal values) the second Equation 68 gives $\omega_s = 0.0243 \text{ sec}^{-1}$. This ω_s corresponds to a critical period of $T_s = 259$ sec. We saw in Section E that a characteristic period for the observed photospheric oscillatory velocity field is 300 seconds. We also saw that a typical granule lifetime lay at or slightly above this value. Assuming that these times typify the periods of sound waves in the photosphere (since we lack theoretical calculations of the frequency spectrum of the acoustic waves generated by turbulence), we see that much of the energy in the sound mode may not be able to pass through the temperature-minimum barrier. Thus, we must inquire anew whether sound waves with dispersion relation given by Equation 67 with $g \neq 0$ are still the most likely mode for transmitting energy to the chromosphere, or whether the gravity mode may do this more efficiently.

The gravity mode favored by Whitaker and described by the dispersion relation (Equation 71) also encounters difficulties. These two-dimensional waves cannot propagate outward when $\omega > \omega_g$, where ω_g is given by Equation 71. If we evaluate ω_g for the same conditions (given by 72) for which we evaluated ω_s, we find that $\omega_g = 0.0181 \text{ sec}^{-1}$, corresponding to a critical period for gravity waves of $T_g = 348$ sec. This value lies above the characteristic period of 300 seconds which seems to dominate oscillatory processes in the photosphere. Thus there can be no vertically propagating gravity waves of $T \simeq 300$ sec; the same type of argument used to question the efficiency of sound-wave transmission through the photosphere can be applied to gravity waves. In one respect, the situation is more severe for gravity waves. Whereas the temperature minimum, where ω_s and ω_g are evaluated, offers the greatest resistance to sound-wave propagation, it offers the least resistance to gravity-wave propagation, if we hold γ and g constant and consider the dependence of ω_g on T_e. Thus, the critical frequency ω_g above which gravity waves cannot propagate becomes lower on either side of the temperature minimum, excluding a broader range of frequencies and raising the question whether an appreciable flux of gravity waves generated in the low photosphere could reach the temperature minimum.

The fact that $\omega_s > \omega_g$ raises a further problem. For $\omega_s = 0.0243 \text{ sec}^{-1}$ and $\omega_g = 0.0181 \text{ sec}^{-1}$, the corresponding periods are $T_s = 259$ sec and $T_g = 348$ sec. Thus, periods between T_g and T_s define a range of non-outwardly propagating disturbances. Yet this is the very range of periods that dominate oscillatory processes in the photosphere. What, then, are the actual facts about this range? Moore and Spiegel (1964) suggest that these photospheric velocity-field oscillations are a

direct manifestation of non-propagating, standing waves in the region of the temperature minimum. They further suggest that convective elements, penetrating above the upper boundary of the radiatively unstable region to the $h = 0$ region, may be able to generate these oscillations. Such penetrative convection is to be expected (Moore 1967) from the presence of an inertial term in the equation of motion, which the mixing-length theory used for our convective zone models ignores.

Lighthill (1967) argues that one would expect this penetrative convection to generate gravity waves in the upper photosphere, assuming that these motions can be represented as a highly anisotropic, turbulent-velocity field. Indeed, he estimates that gravity-wave generation in the upper photosphere should be so efficient as to produce as much energy in gravity waves as the isotropic turbulence mechanism produces in acoustic waves in the low photosphere. However, he does not say what fraction of this energy flux can propagate through the temperature-minimum region. Thus, these gravity waves may be standing waves; then, Lighthill's suggestion recalls that of Moore and Spiegel.

Uchida (1967) solved an eigenvalue problem to determine what waves can be trapped in a resonant cavity consisting of the temperature "trough" region around the minimum temperature and bounded on the sides by the "walls" of the supergranulation elements, which are reinforced by strong magnetic fields around the rim. He concludes that a standing-gravity-wave oscillation will result in a horizontal wavelength of 2000 - 3000 km and a period of about 300 sec. This conforms surprisingly well with observations of the oscillatory velocity field described in the last section.

On the evidence presented so far, the general features of gravity waves and oscillatory velocity fields in the solar atmosphere might seem to be understood, suggesting more precise questions such as:

1) What fraction of the mechanical energy generated by the convection zone goes into the gravity modes?

2) What fraction of this energy is available in propagating frequencies to heat the chromosphere?

Unfortunately, the picture may not be so simple. Souffrin (1966) studied the general problem of the response of an atmosphere to an underlying turbulent convection zone. He introduces radiative dissipation and describes the response of an isothermal atmosphere as a function of distance from the convection zone. For the solar photosphere, he concludes that gravity waves are unlikely, as the radiative relaxation time of this region is too short.

It is clear that the related problems of penetrative convection, gravity waves, and oscillatory velocity fields have not yet been solved. So we shall not consider what role gravity waves might play in heating the chromosphere, as it is still not certain that there is a flux of gravity waves into the chromosphere.

In spite of the uncertainty as to how much energy will pass through the temperature minimum in sound waves, they seem the most likely agent for carrying energy from the convection zone to the outer atmosphere. Now we must find a means for the dissipation of this energy.

As already stated, Alfvén waves are so rapidly damped in the photosphere that they become negligible. Osterbrock (1961) defines a damping length ζ as the distance in which the energy flux drops by a factor e. For the damping of Alfvén waves due to electrical conductivity and viscosity, he uses a damping length ζ_1, from van de Hulst (1951),

$$\zeta_1 = \frac{c_a^3}{4\pi^2 \nu^2 \left[\left(c_s^2 / 4\pi\sigma \right) + (\mu/\rho) \right]} , \tag{73}$$

where ν is the wave frequency, σ the electrical conductivity, and μ the kinematic viscosity. For "frictional" damping due to collisions between positive ions and neutral atoms, he uses a damping length ζ_2, from Piddington (1956),

$$\zeta_2 = \frac{c_a}{4\pi^2 \nu^2} \frac{1+\eta}{\eta\tau} , \tag{74}$$

where ν is the wave frequency, η the ratio of the mass density of neutral atoms to the mass density of ions, and τ the mean collision time for an atom to lose its momentum in collisions with ions. The net damping length ζ_0 for Alfvén waves is given by

$$\frac{1}{\zeta_0} = \frac{1}{\zeta_1} + \frac{1}{\zeta_2} . \tag{75}$$

Osterbrock obtains the electrical conductivity for electron collisions with positive ions from Spitzer (1956) and for electron collisions with neutral atoms (of importance in the photosphere) from his own previous work (Osterbrock, 1952). He uses Edmonds' (1957) table of viscosity coefficients, extrapolated from the convection zone through the upper photosphere and low chromosphere, assumes H = 2 gauss outside plage regions, combines this with ρ from Minneart's (1953) model photosphere and the van de Hulst (1953) model chromosphere to obtain $c_a = H/\sqrt{4\pi\rho}$, and takes $\nu = 1.2 \times 10^{-2}$ sec^{-1} for the wave frequency. He finds that $\zeta_1 \ll \zeta_2$ in the photosphere and low chromosphere and that $\zeta_1 \simeq 1.0$ km in this region. For reasons already given, we cannot accept the van de Hulst model chromosphere; however, the damping length $\zeta_0 \simeq \zeta_1$ is so small that Alfvén waves can certainly be ignored in the photosphere, where wave generation occurs. In the chromosphere, the fast-mode hydromagnetic wave (which is essentially a sound wave outside active regions) will be the only survivor among the modes generated in the photosphere with dispersion relation given by Equation 69.

Osterbrock has also estimated damping lengths for sound waves in the photosphere and chromosphere. He adopts a result due to Lehnert (1959), which considers the effects of viscosity, electrical conductivity, and the frictional damping already mentioned. Since the viscous effect is

predominant for sound waves, the damping-length formula Osterbrock uses is

$$\zeta_3 = \frac{3c_s^3 \rho}{16\pi^2 \nu^2 \mu} \tag{76}$$

where ζ_3 is the damping length, and the other symbols have already been defined. Application of Equation 76 to the photosphere and chromosphere readily shows that even viscous dissipation is negligible. We obtain $\zeta_3 \simeq 10^6$ km, using $\nu \simeq 10^{-2}$ sec, the Edmonds' viscosity tables, and the (ρ, T) values from any of the atmospheric models we have mentioned. Thus, sound waves will not be effectively damped in the photosphere or low chromosphere by any of the above, linear, damping mechanisms. We are led to consider shock dissipation of these sound waves.

If shock dissipation of acoustic waves is the mechanism for heating the chromosphere, two questions arise: 1) Under reasonable assumptions for the depth of generation of acoustic waves, will they build up into shock waves over a short enough distance from the generation zone to produce the temperature inversion? 2) Can we express the dissipation of shock waves as a function of local atmospheric parameters so that we can solve the final energy conservation equation for temperature distribution, subject to a successful solution of the radiation-transfer problem?

First, consider how the shock wave builds up. Any finite-amplitude disturbance traveling in a compressible fluid builds up into a shock wave because the velocity of particles in the vicinity of maximum compression (the condensation phase) exceeds that of the particles elsewhere (the rarefaction phase), leading to the familiar saying, "the crest of the wave catches up with the trough" (Courant and Friedrichs, 1948). Using this criterion to define the appearance of a shock wave, Kuperus (1965) estimates that a sound wave travels approximately 500 km in the photosphere before the crest and trough coalesce. Bird (1964c) has obtained numerical solutions of the nonlinear equations of continuity, momentum, and energy for a spherically symmetrical fluid, and obtains a formation distance of the order of 500 km for an isothermal photosphere at $T = 6000°K$.

In view of these results, and recalling that the sound waves for which we give mechanical flux F_m estimates are generated in a region about 100 km thick centered at $h \simeq -350$ km, this implies the existence of fully developed shock waves above $h \simeq 100$ km in the chromosphere. If acoustic waves are also generated by penetrative convection in the upper photosphere, the resulting shock waves would presumably develop higher in the chromosphere. Since T_e does not seem to rise beyond the minimum value until $\tau_{5000} = 10^{-4}$ is reached, according to Curtis (1965), and since $\tau_{5000} = 10^{-4}$ lies at $150 \leq h \leq 250$ km for the models of the low chromosphere discussed, the shock wave first appears predictably, somewhat below the level where the temperature rise is thought to begin.

It is convenient to introduce at this point a new parameter, "shock strength η_s," defined in terms of density "jump" $\rho_m - \rho_0$ across the shock front, where ρ_m is the maximum value assumed by ρ during a cycle and ρ_0 the value of ρ in front of the shock wave:

$$\eta_s = \frac{\rho_m - \rho_0}{\rho_0} , \tag{77}$$

From the Rankine-Hugoniot conditions (Courant and Friedrichs, 1948), it follows that shock strength η_s is related to shock Mach number M_s by

$$\eta_s = \left(\frac{\gamma+1}{\gamma-1}\right)\left(1 + \frac{2}{\gamma-1}\,\frac{1}{M_s^2}\right)^{-1} - 1 . \tag{78}$$

Thus, either η_s or M_s suffice to indicate the shock strength.

To include shock dissipation in our final energy conservation equation, we need an expression giving energy loss per unit volume and time as a function of local conditions in the atmosphere. Bazer and Ericson (1959) derived such an expression for so-called "weak" shock waves, defined here as $\eta_s < 1.0$. They give a general derivation for hydromagnetic shocks; their results are given here, in the notation we shall use consistently hereafter:

$$D = \frac{\gamma}{4\omega}\left(\frac{\gamma+1}{3} + \frac{c_a^2}{c_s^2}\right)\frac{R}{\mu}\rho\, T_e\, \eta_s^3 , \tag{79}$$

where D is the mechanical energy input in ergs cm^{-3} sec^{-1}, $\tilde{\omega}$ is the period for "shocking" the gas ($\tilde{\omega} = f^{-1}$, where f is the frequency with which shock waves pass through the local region), μ is the mean molecular weight, and the other symbols have meanings already given. The above expression is for one-dimensional propagation along a magnetic field; otherwise, the c_a^2/c_s^2 term becomes more complicated. In fact, this second term is important only where magnetic-field effects are important. Since we ignore magnetic field effects (a resonable procedure in the low chromosphere where $c_a^2/c_s^2 << 1.0$), the expression for D that we use is

$$D = \frac{\gamma(\gamma+1)}{12\,\tilde{\omega}}\,\frac{R}{\mu}\rho\, T_e\, \eta_s^3 . \tag{80}$$

Finally, if we choose $\gamma = 5/3$, $\tilde{\omega} = 300$ sec, and $\mu = 1$, we obtain

$$D = 1.025 \times 10^5\, \rho\, T_e\, \eta_s^3 . \tag{81}$$

It might be argued that these values for γ, $\tilde{\omega}$, and μ should be different. For example, γ may vary across the shock wave, particularly where ionization occurs. Also, we have chosen for our constant γ the adiabatic value for a monatomic gas. Weymann (1960) argues that radiative cooling behind the shock front occurs so rapidly above $\tau_{5000} = 1$ that one should there use the isothermal value $\gamma = 1$. If we accept his result, we must consider the variation of γ over a "shocking" cycle.

We do not do this, because 1) the extreme isothermal value $\gamma = 1$ changes Equation 81 by a factor of 2.2 only, and 2) any mean γ we might use in that equation must lie well above the isothermal $\gamma = 1$ to be consistent with the Rankine-Hugoniot condition

$$\frac{\rho_m}{\rho_0} \leq \frac{\gamma + 1}{\gamma - 1} ,$$

and our estimates of

$$\eta_s = \frac{\rho_m - \rho_0}{\rho_0} ,$$

which are tabulated in Table 6 and obey the condition $\eta_s \leq 1$. Rather than conduct a detailed analysis for a resulting mean γ (which will not significantly affect Equation 81), or arbitrarily pick some value $5/3 \geq \gamma \geq 1$, we merely use the adiabatic $\gamma = 5/3$. We justify our choice for $\tilde{\omega}$ and μ on the grounds that they are representative values, averaged over the region we are studying. The error we introduce by ignoring their variations will not strongly affect our final T_e (h).

The estimate of η_s is the weakest point in our development. Neither η_s, nor equivalently, M_s, has yet been directly measured and we have only weak theoretical grounds for estimating it. We shall base our estimates of η_s on the work of Osterbrock (1961), which is the most thorough treatment of this problem available for the low chromosphere. He derives a differential equation for the mechanical flux gradient in the form

$$\frac{dF_m}{dh} = -D(\eta_s) , \tag{82}$$

where $D(\eta_s)$ is the energy input given by Equation 79, with the additional effects of refraction included. He also has an expression for F_m of the form

$$F_m = f(\eta_s) , \tag{83}$$

which includes refraction effects. Assuming an atmospheric model for (ρ, T) and an initial value for η_s (or F_m) at $h = 0$, we can solve equations 82 and 83 for $F_m(h)$ and $\eta_s(h)$. From (ρ, T, η_s), using Equation 79, we obtain $D(h)$.

Osterbrock assumes an initial value for F_m of 3.0×10^7 ergs cm^{-2} sec^{-1} at $h = 0$ (which lies in the mid-range of Kuperus' three estimates given earlier in this section) corresponding to $\eta_s(0)$ is 0.32. Osterbrock uses the van de Hulst (1953) model chromosphere for his (ρ, T). We have rejected this model, as it was based on LTE; indeed, the (ρ, T) variation is quite different

from that of the PSC model we have adopted. While T (h) for PSC is greater than T (h) for van de Hulst, the scale height in the van de Hulst atmosphere is somewhat larger than in the PSC atmosphere, so ρ(h) for van de Hulst is greater than ρ(h) for PSC. When h has increased to 1000 km, the difference in D is an order of magnitude because the density inequality is greater than the temperature one, but the general variation in η_s (h) with height h obtained by Osterbrock is still valid.

We illustrate Osterbrock's η_B(h) for magnetic-field strengths of h = 0.5, 2.0 gauss in Table 6. Our own choice for η_s, also given in Table 6, is guided by the following considerations: 1) η_s should grow from a small value ≥ 0 at h = 0 to some value ≤ 1.0 in the low chromosphere. This initial trend is also predicted by Bird (1964c). 2) Osterbrock admits that there may be some dissipation for η_s less than his minimum value of 0.32 (where he concludes the shock waves are first fully developed). Frisch (1967) concludes that Osterbrock overestimates η_s in these low regions of $h \leq 300$ km. Combining these observations, we conclude that it would be better to choose $\eta_s(0) = 0$ and let η_s grow rapidly with height. 3) The condition $\eta_s(0) < 1.0$ must be fulfilled, or our use of Equation 79 for D becomes invalid.

The calculations of both Osterbrock and Bird support this view. On these bases, we have chosen the following η_s (h):

$$\eta_s = \left(1 - e^{-h/P}\right), \quad P = 400 \text{ km}. \qquad (84)$$

These values appear in Table 6. They exhibit the proper trend and remain within the proper limits. This is as reasonable a choice for η_s as we can make; note, however, that the estimate of η_s is uncertain.

Table 6

Value of Shock Strength Parameter η_s.
(η_B are from Osterbrock, 1961.)

h (km)	η_s	$\eta_B = 0.5$	$\eta_B = 2.0$
0	0	0.32	0.32
250	0.46	0.41	0.43
500	0.71	0.62	0.61
750	0.85	0.71	0.70
1000	0.92	0.78	0.78
1250	0.96	--	--

In the region we call the upper chromosphere, where h > 1300 km, we could assume that $\eta_s \simeq 1$, according to Equation 84 or, in view of the sharp transition between the low chromosphere and upper chromosphere, we could examine the upper part separately. Bird (1964a, 1964b) argues for a constant η_s in this region, and in the upper part of the low chromosphere for that matter. He derives a condition for the gradient dT_e/dh in a spherically symmetrical atmosphere with gravity, starting with the basic hydrodynamic equations and arriving at

$$\frac{d\alpha}{dh} = \frac{\alpha}{4(1+\alpha)}\left(\frac{2g\mu}{RT_e} - \frac{1}{T_e}\frac{dT_e}{dh}\right), \qquad (85)$$

where we have restricted his result to plane parallel atmospheres. ($\alpha \equiv M_s - 1$ is a new measure of the shock strength, and the other symbols have their usual meaning). From Equation 85, Bird argues that, for a negative quantity in square brackets, the large $dT_e/dh > 0$ will cause α to drop

rapidly and make the dissipation also drop, until dT_e/dh has dropped to a value where $d\alpha/dh = 0$. The converse is also true, he notes. Thus, he predicts $d\alpha/dh = 0$ is the criterion for stability; thus α (and hence M_s and η_s) is constant.

Bird's argument is weakened by the fact that his criterion cannot be applied rigorously at a point, but only shows a trend.

To see this, note that assuming $d\alpha/dh = 0$ in Equation 85 gives

$$\frac{dT_e}{dh} = \frac{2g\mu}{R} , \qquad (h \text{ in cm}) \tag{86}$$

For $\mu = 1$ and the solar surface gravity, we obtain $dT/dh \simeq 65°K\ km^{-1}$. This is much too large for the low chromosphere. In fact, for reasonable values of $(T_e, dT_e/dh)$, Equation 85 tells us that $d\alpha/dh > 0$ in the low chromosphere, as we have shown already. For $h \geq 1250$ km, however, the temperature may rise at a rate not appreciably different from $65°K\ km^{-1}$. Thus, in the upper chromosphere, the condition $d\alpha/dh = 0$ may apply.

We shall assume that α is constant for $h \geq 1250$ km. Actually, we have no reliable model for the upper chromosphere, so it would be useful to consider a range of values for η_s. We shall compute models for the upper chromosphere for $\eta_s = 0.5$ and $\eta_s = 1.00$, realizing that as η_s approaches 1.00 the expression for D in Equation 67 becomes questionable.

There is one aspect of the shock-wave heating problem we have completely neglected. This is the tendency of shock waves to travel along so-called "ray" paths which diverge from the vertical direction. Osterbrock used only a linear theory (geometrical acoustics, analogous to geometrical optics) for his estimates and concluded that there would be no energy left for heating the corona because of diffraction. Kuperus, and also Pikel'ner and Livshits (1964), pointed out that inclusion of the nonlinear terms would reduce this diffraction effect and thus permit coronal heating by shock waves generated low in the chromosphere. We are not studying coronal heating in this report; so we shall not consider the details of shock propagation. We consider only one-dimensional propagation.

Finally, there is the importance of electron thermal conduction from the corona to the upper chromosphere. This problem has been studied in detail by de Jager and Kuperus (1961) and Livshits (1964). We shall include a term for conduction in the general energy-conservation equation, derived in Chapter III, but will not include conduction in the calculations, as its effect is demonstrably small except in the outermost part of the chromosphere.

Chapter III

GENERAL METHOD FOR CALCULATING THE TEMPERATURE DISTRIBUTION

It is stated in Chapter I that the aim of this study is to develop a method to solve an energy-conservation equation and several initially coupled transfer equations simultaneously to determine the temperature distribution in the atmosphere. This chapter is concerned with the development of this method.

The final temperature distribution is obtained by solving the energy-conservation equation which we shall now derive. We begin with Equation 9, which expressed departure from RE:

$$\frac{dF}{dh} = 4\pi \left[\sum_{j}^{N} \int (J_\nu - S_\ell)_j \frac{d\tau_{\ell j}}{dh} \, d\nu + \int (J_\nu - S_c) \frac{d\tau_c}{dh} \, d\nu \right] . \tag{9}$$

We desire a different form of expression for the term

$$\sum_{j}^{N} \int (J_\nu - S_\ell)_j \frac{d\tau_{\ell j}}{dh} \, d\nu .$$

Consider $d\tau_\ell$ for the j^{th} line. In NETPRF, t e optical depth τ_ν can be written as

$$d\tau_\nu = - \frac{(h\nu_0)}{4\pi} (n_L B_{LU} \phi_\nu) \left(1 - \frac{n_U B_{UL} \psi_\nu}{n_L B_{LU} \phi_\nu} \right) dh , \tag{87}$$

where the parameters are all defined in Chapter II, Section C. Ignoring stimulated emission and using the relations between the Einstein coefficients given by Equation 38, we obtain

$$d\tau_\nu = - \frac{1}{8\pi} \frac{g_U}{g_L} A_{UL} \lambda_0^2 n_L \phi_\nu \, dh . \tag{88}$$

Now we introduce the definition

$$A_j \equiv \left[\frac{g_U}{g_L} A_{UL} \lambda_0^2 \right]_j , \tag{89}$$

for the j^{th} line. Combining Equations 9, 88, and 89 gives

$$\frac{dF}{dh} = \frac{1}{2} \sum_{j}^{N} \left[A_j \, n_{Lj} \, (NRB)_j \, S_{\ell j} \right] - 4\pi \int (S_c - J_\nu) \frac{d\tau_c}{dh} \, d\nu , \tag{90}$$

where we have also used Equation 39 for $(NRB)_j$, and the approximation Equation 20, $S_\nu \simeq B_\nu\,(T_{ex})$. Equation 90 is the required energy-conservation equation. We must further develop the left-hand side, which is the radiative flux gradient that equals the mechanical dissipation in ergs cm^{-3} sec^{-1}.

First, let us exhibit a general form for the dF/dh term, which includes the effects of shock dissipation in the presence of magnetic fields in one dimension, and of electron thermal conduction. The shock dissipation term is given by Equation 79 of the previous section. The conduction term is given by

$$F_c = - K_c T^{5/2} \frac{dT}{dh} , \tag{91}$$

where a good estimate for K_c, according to Billings (1966), is

$$K_c \simeq 10^{-6} \text{ ergs cm}^{-1} \text{ sec}^{-1} {}^\circ\text{K}^{-7/2} . \tag{92}$$

Thus, a complete expression for the mechanical dissipation term becomes

$$\frac{dF}{dh} = \frac{\gamma}{4\tilde{\omega}} \left[\frac{\gamma+1}{3} + c_a^2/c_s^2\right] \frac{R}{\mu} \rho T_e \eta_s^3 - \frac{dF_c}{dh} , \tag{93}$$

where dF_c/dh is obtained by differentiating Equation 91. In the calculations that follow, we shall ignore both magnetic field effects and conduction, for reasons given in Chapter II. Taking the same values of γ, $\tilde{\omega}$, and μ used to obtain Equation 81, we arrive at our final form of the energy-conservation equation:

$$\frac{dF}{dh} = 1.025 \times 10^5 \rho T_e \eta_s^3 = \frac{1}{2} \sum_j^N \left[A_j n_{Lj} (NRB)_j S_{\ell j}\right] - 4\pi \int (S_c - J_\nu) \frac{d\tau_c}{dh} d\nu . \tag{94}$$

We shall show in the last part of this chapter how the right-hand side of Equation 94 depends on T_e through the line source function S_{ℓ_j}.

Now we can consider the radiation-transfer problem. Suppose that we ignore the last, continuum term on the right-hand side of Equation 94. The resulting equation couples various spectral lines through the mechanical dissipation term which constitutes the left-hand side. We wish to uncouple these lines to solve N independent transfer equations for the N lines important in any given region of the atmosphere. Only if we know how much of the total mechanical dissipation D goes into exciting the upper level of the j^{th} line can we solve an independent transfer equation in that line. We develop an approximation for this purpose.

Let us assume that we can estimate the fraction of the mechanical dissipation D that excites continuum transitions, without solving a transfer problem. This, in effect, eliminates the continuum term on the right-hand side of Equation 94. Calling this fraction Δ_c, and using subscripts ℓ

and c to denote line and continuum, respectively, we have

$$D_\ell = (1 - \Delta_c) D \quad . \tag{95}$$

Equation 94 assumes the form

$$\left(\frac{dF}{dh}\right)_\ell = D_\ell = \frac{1}{2} \sum_j^N \left[A_j \, n_{Lj} \, (NRB)_j \, S_{\ell j}\right] \quad . \tag{96}$$

Let us further assume that we can estimate the fraction of the dissipation D_ℓ that excites transitions in the j^{th} line, without solving a transfer problem for that line; let us call this fraction D_j. For those transitions in which the mechanical energy input equals the net radiative loss, we can write

$$D_j = \frac{A_j \, n_{Lj}}{2} \, (NRB)_j \, S_{\ell j} \quad . \tag{97}$$

Recalling modified Equation 39 for the $(NRB)_j$, we can solve Equation 97 for $S_{\ell j}$ to obtain a very useful expression for the line-source function $S_{\ell j}$ in this special case:

$$S_{\ell j} = \int_j J_\nu \phi_\nu \, d\nu + \frac{2}{A_j} \left(\frac{D_j}{n_{Lj}}\right) \quad . \tag{98}$$

The problem is reduced to deciding if we can use Equation 98 for $S_{\ell j}$ to solve the equation of transfer for the j^{th} line. In particular, is the two-level atom approximation implicit in equating mechanical input and net radiative loss justified? Is there a function for the expression $(2/A_j)(D_j/n_{Lj})$ that we are justified in using because it gives a good representation of $(2/A_j)(D_j/n_{Lj})$ as the latter varies with height, and that permits us to solve the equation of transfer? We expect the two-level atom approximation to offer a good first approximation for strong chromospheric lines of the collision-dominated type discussed in Chapter II. We shall see in Chapter IV, where we calculate the height variation of $(2/A_j)(D_j/n_{Lj})$ for the lines of special interest that a single negative exponential term of the form $C_j \exp\{-\beta_j \tau_{0j}\}$ will provide a good representation for the height range of interest, i.e.,

$$\frac{2}{A_j} \left(\frac{D_j}{n_{Lj}}\right) \simeq C_j \, e^{-\beta_j \tau_{0j}} \quad . \tag{99}$$

Thus, the source function of Equation 98 can be approximated by

$$S_{\ell j} = \int_j J_\nu \phi_\nu \, d\nu + C_j \, e^{-\beta_j \tau_{0j}} \quad . \tag{100}$$

Solving the transfer equation with the line source function of Equation 100 is quite straightforward, provided that one includes the contribution of the continuum source function to obtain a proper boundary condition deep in the atmosphere. A detailed treatment appears in Appendix B. We start with the general source function of Equation 8:

$$S_\nu = \frac{S_\ell + r_\nu S_c}{1 + r_\nu} , \tag{8}$$

where $r_\nu = d\tau_c/d\tau_\ell$ as in Equation 7, and S_ℓ is given by Equation 100. We assume that $S_c = B_\nu(T_e)$ and parameterize it by

$$S_c = S_{1j} \left(1 + A_j e^{-c_j \tau_{0j}}\right) , \tag{101}$$

corresponding to the outwardly increasing chromospheric temperature, where

$$S_{1j} = B_\nu \left[T_e \left(\tau_{0j} = \tau_1\right)\right] ;$$

A_j and c_j are constants for the j^{th} line; and τ_1 is the optical thickness of the region of integration. In this study we can assume that the atmosphere is semi-infinite, i.e., $\tau_1 = \infty$. Equation 101 exhibits temperature-dependence through the exponential term

$$S_{1j} A_j \exp\left\{-c_j \tau_{0j}\right\} .$$

We shall show that this term can be ignored in the final transfer equation. Physically, this is because mechanical dissipation, which enters the equation through the

$$C_j \exp\left\{-\beta_j \tau_{0j}\right\}$$

term, predominates over the influence of the continuum for strong, collision-dominated chromospheric lines except when τ_{0j} is very large.

In Appendix B, we show how to transform transfer Equation 6 into the second-order differential equation

$$\frac{d^2 J_\nu}{d\tau_0^2} = x_\nu^2 \left(J_\nu - S_\nu\right) , \tag{102}$$

where $x_\nu^2 = 3\left(d\tau_\nu/d\tau_0\right)^2$, by using the Eddington approximation. We can solve Equation 102 by the standard method of Gaussian quadrature; then the equation becomes

$$\frac{d^2 J_i}{d\tau_0^2} = x_i^2 \left(J_i - S_i\right) . \tag{103}$$

The frequency division points "i" depend on the line profile and the order of the quadrature. For the Doppler-broadened line cores to which the non-LTE theory of Chapter II applies, the line profile is Gaussian and both the division points and the weighting functions x_i are based on the zeros of Hermite polynomials. These division points and weights can be obtained from Trumpler and Weaver (1953). Table 7 gives x_i for a three-point quadrature which we use for the calculations here.

Defining δ_ν such that

$$\delta_\nu \equiv \left(1 + r_\nu\right)^{-1} , \tag{104}$$

we can write Equation 103 in the form

$$\frac{d^2 J_i}{d\tau_0^2} = x_i^2 \left[J_i - \delta_i \sum_j^n \alpha_j J_j - \delta_i C e^{-\beta\tau_0} - \delta_i r_i S_1 \left(1 + A e^{-c\tau_0}\right) \right] , \tag{105}$$

where we have used Equations 8, 100, and

$$\int J_\nu \phi_\nu \, d\nu = \sum_j^n \alpha_i J_i , \tag{106}$$

and where the subscript j has been dropped, as we are here treating a single line. We obtain the α_i, like the x_i, once we know the line profile. They satisfy the normalization condition

$$\sum_i^n \alpha_i = 1 , \tag{107}$$

and are tabulated for a Gaussian profile and three-point quadrature, along with the x_i in Table 7. We have merely used the values given by Jefferies and Thomas (1960).

We said earlier that

$$C e^{-\beta\tau_0} >> r_i \left(S_1 A\right) e^{-c\tau_0} \tag{108}$$

would be satisfied for the strong lines of the report. If $c \gtrsim \beta$ and $C >> r_i \left(S_1 A\right)$, condition 108 is fulfilled. That $c \simeq \beta$ follows from assuming that the region for large mechanical dissipation in a spectral line is roughly the same as the region where the temperature will rise owing to this dissipation, although the position of the rise might be at the boundaries of this region, according to the temperature plateau arguments discussed in Chapter II, while the mechanical dissipation per unit mass could remain essentially constant throughout. If we examine the values of $\left(C, S_1\right)$ for

the strong lines treated in Chapter IV, and choose the value of A to correspond to a maximum chromospheric T_e of $\lesssim 10^5$ °K, we find that condition 108 is most nearly violated by CaII. For CaII, $C = 4.2 \times 10^{-10}$, $S_1 = 2.5 \times 10^{-6}$, and $A \lesssim 10^2$. If we use $r_0 = 10^{-8}$, which accords with Jefferies and Thomas (1960), we obtain $r_0 S_1 A \lesssim 2.5 \times 10^{-12}$. Thus, $C >> r_0 S_1 A$. However, for r_2 the condition becomes marginal and it is actually violated for r_3. Since r_3 is most directly involved in the equation for J_3 (which, according to Equation 106 and the value of $\alpha_3 = 0.0051116$ plays the least important role in determining $\int J_\nu \phi_\nu \, d\nu$) and since the problem does not even arise for the other lines, we accept approximation 108. Also, we may have overestimated the r_i values for CaII. Athay and Skumanich (1968) consider $r_0 = 10^{-10}$ a better choice.

Equation 105 now becomes

$$\frac{d^2 J_i}{d\tau_0^2} = x_i^2 \left(J_i - \delta_i \sum_j^n \alpha_j J_j - \delta_i C e^{-\beta \tau_0} - \delta_i r_i S_1 \right) , \tag{109}$$

which is the form of the transfer equation we solve. This equation is solved in Appendix B, where the general solution to Equation 109 for a semi-infinite atmosphere is given by

$$J_i = S_1 \left[1 + \delta_i \sum_j^n L_j \left(1 - \frac{k_j^2}{x_i^2} \right)^{-1} e^{-k_j \tau_0} + \left(\frac{Q_i}{S_1} \right) e^{-\beta \tau_0} \right] , \tag{110}$$

where k_j, Q_i, and L_j are given by

$$\sum_i^n \delta_i \alpha_i \left(1 - \frac{k_j^2}{x_i^2} \right)^{-1} = 1 , \tag{111}$$

$$Q_i = \delta_i C \left(1 - \frac{\beta^2}{x_i^2} \right)^{-1} \left[1 - \sum_j^n \delta_j \alpha_j \left(1 - \frac{\beta^2}{x_j^2} \right)^{-1} \right]^{-1} , \tag{112}$$

$$\sum_j^n L_j \left(1 - \frac{k_j}{x_i} \right)^{-1} + \delta_i^{-1} \left[1 + \frac{Q_i}{S_1} \left(1 + \frac{\beta}{x_i} \right) \right] = 0 , \tag{113}$$

respectively. The boundary conditions used to derive the above are $J_i \to S_1$, as $\tau_0 \to \infty$ and $J_i = x_i^{-1} \left(dJ_i / d\tau_0 \right)$ for $\tau_0 = 0$, with the latter obtained from Krook (1955).

Since $\delta_i \simeq 1$ for all "i", we can make the approximation $\delta_i = 1$ in Equations 110, 112, and 113 without significantly affecting the results. However, we cannot do this in Equation 111. If $\delta_i = 1$ is introduced there, Equation 111 cannot be solved for n real, non-zero values for k_j without

violating the condition

$$\sum_{i}^{n} \alpha_i = 1 .$$

Consider Equation 111 further. For the three-point quadrature we adopt here, Equation 111 becomes a cubic in k_j^2, making it sixth order in k_j with $k_j = \pm(k_j^2)^{1/2}$. We can solve this equation for the three positive k_j values appropriate to our values of (α_i, x_i) already discussed, supplemented by calculated values of $\delta_i = (1 + r_i)^{-1}$. Alternatively, we can approximate δ_i in a suitable manner and use values of k_j already available. As this approximation illustrates the very small role of the continuum in the treatment of the strong spectral lines of this report, we discuss it now.

The dependence of k_j on r_i, through $\delta_i = (1 + r_i)^{-1}$, can be determined from Thomas' (1960) work giving the dependence of the k_j on parameter ϵ, which plays the same formal role in the Thomas study as r_i does here. For the three-point quadrature, Thomas' work shows us that k_1 and k_2 are practically independent of ϵ and that $k_3 \simeq 0.1\ \epsilon^{1/2}$. Thus, k_1 and k_2 are practically independent of the r_i values here. If we make the approximation $r_i \to \bar{r}_i$, Table 8 shows that k_1

Table 7

Values of x_i, α_i, and k_j Used in Solving Equation of Transfer.

	Subscripts i, j for Different Quadrature Points.		
	1	2	3
x_i	1.43210	0.29078	0.0069014
α_i	0.817657	0.177232	0.0051116
$k_j(\bar{r}_i = 10^{-6})$	0.664478	0.045328	0.95418×10^{-4}

Table 8

Values for k_j Adopted from Jefferies and Thomas (1960).

	$\bar{r}_i$		
	10^{-4}	10^{-5}	10^{-6}
k_1	0.664575	0.664487	0.664478
k_2	0.045736	0.045365	0.045328
k_3	0.94547×10^{-3}	0.30148×10^{-3}	0.95418×10^{-4}

and k_2 are indeed almost independent of $\bar{r}_i$, and that $k_3 \simeq 0.1\ \bar{r}_i^{1/2}$. Since $r_i \leq 10^{-6}$ for our lines where $i = 1, 2$, and is probably somewhat larger for $i = 3$, we adopt the approximation $r_i \to \bar{r}_i = 10^{-6}$ for our final calculations, and use the k_j directly from Table 8 for $\bar{r}_i = 10^{-6}$.

This completes our outline of how we solve the transfer equation in the semi-infinite atmosphere. In Chapter II, we stated that a rough criterion for LTE-R, where $S_\nu \to B_\nu(T_e)$, is $\epsilon\tau_0 >> 1$. This is also our criterion for τ_0 in applying the semi-infinite-atmosphere treatment where $J_\nu \to B_\nu\left(T_e\left(\tau_0 \to \infty\right)\right) = S_1$ must be satisfied. We justify this by Equation 110 where, for $k_n \lesssim \beta$ and n the order of quadrature, $J_i \to S_1$ when $k_n \tau_0 >> 1$. In NETPRF, Chapter V, Thomas shows that k_n scales somewhere in the range of ϵ through $\epsilon^{3/2}$. If we say $k_n \sim \epsilon$, then a rough criterion for $J_i \to S_1$ becomes $\epsilon\tau_0 >> 1$.

Now it is necessary to determine D_j, the fraction of the mechanical energy D_ℓ of Equation 96 that goes into the j^{th} line transition. We have solved transfer Equation 102 on the assumption that the transfer equations for the individual spectral lines can be solved independently of one another. This is equivalent to saying that D_j can be determined for each line. Noting that $D_j = \Delta_j D_\ell$ defines the fractional part Δ_j of D_ℓ that goes into the j^{th} line, we proceed to develop a way to estimate Δ_j.

Between two levels in an atom designated L and U, the net number N_U of upward transitions due to collisions per unit volume and time is

$$N_U = n_L C_{LU} (NCB)_{LU} , \tag{114}$$

where the net collisional bracket $(NCB)_{LU}$ is given by Equation 41, and C_{LU} is the collision rate, for which we shall use the general formula in NETPRF:

$$C_{LU} = 1.25 \times 10^{-4} n_e T_e^{-1/2} \frac{\chi_H}{(h\nu)_{LU}} \bar{g} f_{LU} e^{-(h\nu)_{LU}/kT_e} . \tag{115}$$

Equation 115 was suggested by Burgess, Seaton, and van Regemorter, and is based largely on work by van Regemorter (1962). The $\bar{g}$ term is a weakly varying dimensionless parameter, whose value for chromospheric conditions is $\simeq 0.2$ for singly ionized metal lines.

We wish to use Equations 114 and 115 to derive an expression for Δ_j. Noting that $D_j = \Delta_j D_\ell$, we can use Equation 114 to write

$$\Delta_j = \frac{N_{Uj} (h\nu)_{LUj}}{\sum_i^N N_{Ui} (h\nu)_{LUi}} = \frac{n_{Lj} C_{LUj} (NCB)_{LUj} (h\nu)_{LUj}}{\sum_i^N n_{Li} C_{LUi} (NCB)_{LUi} (h\nu)_{LUi}} , \tag{116}$$

where we have noted that

$$D_j = N_{Uj} (h\nu)_{LUj}$$

and

$$D_\ell = \sum_i^N D_i$$

for N spectral lines. Equation 116 is perfectly general, so far. Now, substituting the van Regemorter expression of Equation 115 for C_{LU} in Equation 114, we derive

$$\Delta_j = \frac{n_{Lj} \left(\bar{g}\ f_{LU}\right)_j (NCB)_{LUj}\ e^{-(h\nu)_{LUj}/kT_e}}{\sum_i^N n_{Li} \left(\bar{g}\ f_{LU}\right)_i (NCB)_{LUi}\ e^{-(h\nu)_{LUi}/kT_e}} , \tag{117}$$

which is the expression we use for Δ_j and from which we obtain D_j. We shall see in Chapter IV that the T_e-dependence of Δ_j is not strong in those chromospheric regions where Δ_j is not negligible.

The final subject we consider here is the method for calculating the chromospheric temperature distribution. We restrict ourselves to the problem without the continuum. In Chapter IV, we shall see that the H^- continuum dominates the energy balance up to some height $h \simeq 500$ km, and we shall exhibit there a simple method for calculating the temperature distribution in these regions, considering the continuum alone. At present we consider Equations 96 and 97 for the lines only. For the one line of Equation 97, whose source function is given by Equation 98, we can easily calculate the temperature when the line source function S_{Lj} can be written in the form

$$S_{Lj} = \frac{\int_j J_\nu \phi_\nu\, d\nu + \epsilon_j B_{\nu j}(T_e)}{1 + s_j} , \tag{118}$$

where s_j is a general sink term equal to $\epsilon + \eta$, or whichever is predominant. Equation 118 is general enough to include Equations 31 and 35 of Chapter II, and we shall see in Chapter IV that Equation 118 is probably adequate for the lines we shall study in detail.

If we equate the source functions of Equations 98 and 116 and solve for $B_{\nu j}(T_e)$, we obtain

$$B_{\nu j}(T_e) = \frac{1 + s_j}{\epsilon_j} \frac{2}{A_j} \left(\frac{D_j}{n_{Lj}}\right) + \frac{s_j}{\epsilon_j} \left(\int_j J_\nu \phi_\nu\, d\nu\right) . \tag{119}$$

From our solution of the transfer equation, we know

$$\int_j J_\nu \phi_\nu\, d\nu .$$

Thus, we can calculate the $T_e\,(\tau_{0j})$'s, if we know $\tau_{0j}(h)$, which is the same as knowing $n_{Lj}(h)$. Therefore, to apply the method developed here, we can assume the mass density and chemical composition, and either calculate or assume the ionization, in order to derive $n_{Lj}(h)$. This is done in Chapter IV.

Once we have $T_e(h)$ for a region dominated by one line, the calculation is complete when we have a convergent solution; but not if more than one line is important. Then, the problem of consistency between the different $T_e(\tau_{0j}(h))$'s and Equation 96 arises. This problem arises in the region $500 < h < 1250$ km, in Chapter IV.

Chapter IV

APPLICATION OF THE METHOD TO THE SOLAR CHROMOSPHERE

A. Introduction

Preliminary to our calculations, we shall review the current status of radiative-energy loss estimates for the chromosphere, to establish that these estimated losses do not exceed the values for mechanical flux F_m given in Chapter II, Section F. We find that energy-loss estimates to date are unreliable by as much as an order of magnitude, but nevertheless the computed values of F_m in Chapter II are adequate.

Having established this, we shall consider the important question: which collisional processes remove mechanical energy from the system? This can be answered by our deriving net radiative losses for atoms that can be approximated by only two discrete levels. For these cases, the local radiative loss must just balance the local gain in mechanical energy which has no other outlet. The question becomes more complicated if we must consider additional levels or the continuum. This latter case will arise with hydrogen. The result of these energy-loss estimates will be that the H^- ion continuum, Hα, the resonance doublets of CaII and MgII, Lyα, and, for sufficiently high temperatures, Lyα of HeII, should be considered as important energy sinks for the mechanical energy dissipated in the chromosphere.

Given the above energy sinks, we shall proceed to the temperature calculation. We find that our calculation covers three chromospheric regions: one extending from $h = 0$ to $h = 500$ km, a second covering $500 < h \leq 1250$ km, and a third covering the Lyα region. These three regions correspond to the domination of the energy balance by the H^- ion, the ionized metals and Hα, and Lyα, respectively. We shall calculate T_e in each region, using the method of Chapter III for the outer two regions, and developing a different method for the H^--dominated region.

With regard to chemical composition and mass-density distribution we use values comparable to those for the PSC-model low chromosphere. PSC uses the chemical composition given in the first edition of Allen (1955). We shall assume the composition given in the second edition (Allen, 1962), which differs negligibly from values given in the first edition. The 1962 values are reproduced in Table 9. The mass density we assume for the region $0 \leq h \leq 500$ km is given by

$$\rho(h) = \rho(0)\, e^{-h/H_1}, \qquad H_1 = 130 \text{ km}, \tag{120}$$

where we obtain $\rho(0)$ by assuming a mean molecular weight of unity and all hydrogen is assumed to be neutral at $h = 0$, so that $\rho(0) = n_1(0)/N_A = 6.28 \times 10^{-9}$ gm cm^{-3}, where $n_1(0)$ is from Table 1 and N_A is Avogadro's number. For the region $500 < h \leq 1250$ km, we use

$$\rho(h) = \rho(500)\, e^{-h/H_2}, \qquad H_2 = 145 \text{ km}, \tag{121}$$

Table 9

Relative Abundance by Number of Chemical Elements from H through Fe, Based on Allen (1962).

Element	Atomic Number	$\log_{10}$ Relative Abundance
H	1	12.00
He	2	11.16
Li	3	3.0
Be	4	2.4
B	5	2.8
C	6	8.48
N	7	7.96
O	8	8.83
F	9	5.4
Ne	10	8.44
Na	11	6.22
Mg	12	7.46
Al	13	6.28
Si	14	7.47
P	15	5.53
S	16	7.22
Cl	17	5.4
Ar	18	6.62
K	19	4.88
Ca	20	6.22
Sc	21	2.91
Ti	22	4.82
V	23	3.78
Cr	24	5.38
Mn	25	5.10
Fe	26	6.90

Table 10

$\rho(h)$ from Equations 120 and 121 Compared with $\rho(h)$ Obtained from PSC.

h	$\rho(h)$ from 120 and 121 (gms cm^{-3})	$\rho(h)$ from PSC and 122 (gms cm^{-3})
0	6.28×10^{-9}	6.28×10^{-9}
100	2.92 (-9)	2.66 (-9)
200	1.35 (-9)	1.16 (-9)
300	6.27 (-10)	5.23 (-10)
400	2.90 (-10)	2.42 (-10)
500	1.34 (-10)	1.16 (-10)
750	2.26 (-11)	2.08 (-11)
850	1.20 (-11)	1.11 (-11)
950	6.00 (-12)	5.86 (-12)
1000	4.25 (-12)	4.30 (-12)
1100	2.12 (-12)	2.32 (-12)
1200	1.09 (-12)	1.30 (-12)
1250	7.73 (-13)	9.70 (-13)

where $\rho(h)$ is obtained from Equation 120. Equations 120 and 121 give values for $\rho(h)$ for the low chromosphere that compare satisfactorily (see Table 10) with those obtained from the PSC-model chromosphere of Table 1, assuming that

$$\rho(h) = \frac{n_1(h) + n_e(h)}{N_A} . \qquad (122)$$

For $h > 1250$ km, these scale heights are too low, and another representation for $\rho(h)$ is necessary. We return to this when we calculate $T_e(h)$ for $h \geq 1250$ km.

B. Dominant Energy Loss Mechanisms

1. Estimates from Outside Sources

In this section we first review some energy-loss estimates in the existing literature. Partly on the basis of this review, we can then limit the number of loss mechanisms to be studied further.

Osterbrock (1961) provides a rough estimate of the radiative energy loss from the outer solar atmosphere. He assumes that T_e begins to rise at $\tau_{5000} = 0.003$ and estimates that H^- losses are completely dominant in the low chromosphere. His final value for H^- loss varies linearly with the assumed τ_{5000} where the temperature rise begins. Curtis (1965) places this rise at $\tau_{5000} = 0.0001$;

this makes Osterbrock's figure appear a gross over-estimate. A large factor of uncertainty is characteristic of his estimates, which we shall now discuss at greater length.

Although Osterbrock refers to his section on energy loss by the title "Observation Data," he makes what amounts to a *theoretical* estimate of the H^- loss, which proves to be the largest. He derives a formula for the net H^- losses for a gray atmosphere whose temperature distribution is given by Equation 10, where, for the zero-th order approximation, $q(\tau) = 2/3$. By merely expressing the excess of emission over absorption, with the emission produced in LTE, he derives Equation 123, below. His formula for the outward flux due to H^- loss in the low chromosphere is

$$\pi F_+ (H^-) = 4\sigma T_0^3 (\delta T) \tau , \tag{123}$$

where T_0 is the minimum temperature, δT is a mean value for the temperature difference between the minimum temperature and the maximum temperature at the top of the region where the H^- loss dominates chromospheric losses, and τ is the optical thickness of this region. He chooses $T_0 = 4600°K$, $\delta T = 200°K$, and $\tau = 0.003$, and obtains $\pi F_+ (H^-) = 1.5 \times 10^7$ ergs cm^{-2} sec^{-1}. Multiplying by 2, to account for energy radiated back down into the photosphere, he estimates the total H^- loss from the chromosphere to be 3.0×10^7 ergs cm^{-2} sec^{-1}.

There are several uncertainties in $\pi F_+ (H^-)$. The choice of δT and τ could significantly affect the estimate. Also, Osterbrock did not allow for the possibility that the source function for this emission might depart from the Planck function owing to a departure of the b_{H^-} from unity. The uncertainty in τ could decrease $\pi F_+(H^-)$ by more than an order of magnitude. This quantity τ, and δT too, both depend critically on the temperature structure of the low chromosphere and the extent of the low chromosphere over which H^- dominates the net radiative loss. Osterbrock, in choosing the van de Hulst-model chromosphere, bases his estimate on a currently unacceptable model, as we pointed out in Section D of Chapter II.

By choosing a radiation temperature of 6900°K, based on NRL rocket observations reported by Morton and Widing (1961), Osterbrock estimates the Lyman continuum loss at 3×10^2 ergs cm^{-2} sec^{-1}, obtained by simply integrating the Planck function at $T_r = 6900°K$ over the frequency range beyond the Lyman limit. In the higher-lying hydrogen continua, in which the chromosphere is optically thin, he computes the total radiation loss using formulas derived by Parker (1953), based on the work of Menzel (1937), for the emission per unit volume due to the free bound continua of hydrogen; thus,

$$j(\text{Ba, Pa, } \cdots, \text{C}) = 8.94 \times 10^{-23} \frac{n_i n_e}{T_e^{1/2}} , \tag{124}$$

where n_i is the proton number density. Again using the unacceptable van de Hulst model chromosphere, and also noting that

$$\pi F_+ (\text{Ba, Pa, } \cdots, \text{C}) = \frac{1}{2} \int j \, dh , \tag{125}$$

Osterbrock computes the total loss in these hydrogen continua as 5×10^5 ergs cm^{-2} sec^{-1}. The use of the PSC model chromosphere of Chapter II would increase the value of πF_+ (Ba, $\cdots$) by at least an order of magnitude, because the PSC values of (n_i, n_e), given in Table 1 (with $n_i \simeq n_e$ assumed for $h > 500$ km), lie so much higher than the van de Hulst values. This conclusion follows even though T_e (h) lies lower in the van de Hulst model for a given h and the latter model extends over a larger height range. However, there is an even more fundamental objection to using Osterbrock's πF_+ (Ba, $\cdots$). His value is the total loss in these continua. But most of this total loss is probably scattered photospheric light or radiation produced by what, ultimately, has its source in photospheric light that becomes redistributed in frequency. Thus, the net radiative loss to be balanced by mechanical dissipation is much less than if derived from Equation 125 alone.

In treating losses in the chromospheric lines of the hydrogen Balmer and Lyman series, CaII H and K, MgII λ2795, λ2803, and SiII λ1808, λ1816, Osterbrock does rely on observational data. These empirical estimates rely on actual intensity measurements taken of Lyα emission, and emission in the central emission cores of the above mentioned ionized metal lines, as well as emission of Balmer-series lines observed in eclipse. On the basis of the above data, Osterbrock makes the following net loss estimates: 8×10^6 ergs cm^{-2} sec^{-1} from all Balmer lines, 8×10^6 ergs cm^{-2} sec^{-1} from all metal lines, and 2×10^5 ergs cm^{-2} sec^{-1} from Lyα. He examines data available in 1961 on helium emission and the euv spectrum in general, and concludes that helium and other losses are comparatively negligible.

In assuming that the above losses are net radiative losses, Osterbrock implies that the source term in the source functions of these lines is the collision term $\epsilon B_\nu (T_e)$. This is true for Lyα and the ionized metal lines, but certainly not for the Balmer lines, nor for the neutral metal lines (which seem to have been included in his total for all metal lines, although his paper is unclear on this last point). Here again is significant source of error in his loss estimates.

In all fairness to Osterbrock, he required only rough numerical estimates for his work, though his estimated maximum error of a factor of 3 or so in his final net chromospheric loss of 4×10^7 ergs cm^{-2} sec^{-1} is certainly optimistic. Also, his estimates are made for the entire chromosphere, and do not specify where the losses occur locally, which reduces their value. We have discussed Osterbrock's estimates at some length because the literature contains many references to them, and they are extremely uncertain. For example, see the discussion following the Lighthill (1967) article in the Fifth Symposium on Cosmical Gas Dynamics.

Athay (1966) has provided the most recent and comprehensive treatment of net radiative losses from the chromosphere, and we shall now consider his work in some detail. He estimates the net H^- loss from the entire chromosphere in exactly the same way as Osterbrock. Using observational data in choosing reasonable values for δT and τ in Equation 123, and performing the analysis for successive regions of $\Delta h = 100$ km, Athay concludes that the net H^- loss lies between an order of magnitude below the Osterbrock estimate of 3×10^7 ergs cm^{-2} sec^{-1} and a value slightly above this number. Our criticism of Osterbrock's net H^- loss estimate applies equally to Athay's estimates, except that Athay obtains his values from data upon which the PSC-model chromosphere is based.

Athay develops the following method for treating the losses in spectral lines. He combines the condition of statistical equilibrium for level L with an energy-conservation equation to obtain an expression for the net radiative loss in a series having lowest-level L. This is done by starting with transfer Equation 6 and deriving an equivalent form of our energy-conservation Equation 90 for the case of a spectral line series with no continuum. His conservation equation for the radiative flux gradient, or local net radiative loss, in the series is

$$\frac{dF}{dh} = \langle h\nu_{kL} \rangle \sum_{k>L} n_k A_{kL} (NRB)_{kL} , \tag{126}$$

where $\langle h\nu_{kL} \rangle$ is a suitably weighted mean energy for all the levels involved and we follow our regular notation. In particular, $(NRB)_{kL}$ is the net radiative bracket of Equation 39 and A_{kL} is the Einstein coefficient for spontaneous emission. From the condition of statistical equilibrium for level L, the definition of the departure coefficients and the relation among the collision rates C_{LU} and C_{UL} given in Chapter II, Section C, for a Maxwellian electron-velocity distribution, Athay derives the following relation:

$$\sum_{k>L} n_k A_{kL} (NRB)_{kL} = n_L \sum_{k \neq L} C_{Lk} (NCB)_{Lk} + n_L \sum_{i<L} A_{Li} (NRB)_{Li} . \tag{127}$$

Here $(NCB)_{Lk}$ is the net collosional bracket given by Equation 44a. Now suppose that we are dealing with either a resonance series, for which $A_{Li} = 0$, or a subordinate series which is in radiative balance with all lower levels, making $(NRB)_{Li} = 0$. The second term on the right-hand side of Equation 127 is then zero. If we assume, with Athay, that these conditions apply, then substituting Equation 127 in Equation 126 yields

$$\frac{dF}{dh} = \langle h\nu_{kL} \rangle \, n_L \sum_{k \neq L} C_{Lk} (NCB)_{Lk} . \tag{128}$$

This is the equation Athay uses.

He notes that the $(NCB)_{Lk}$'s are generally much larger than the corresponding $(NRB)_{kL}$'s. From a practical point of view, this means that the ratio b_k/b_L need not be known as precisely as the term $\left(\int J_\nu \phi_\nu \, d\nu / S_{kL}\right)$ that appears in $(NRB)_{kL}$, according to Equation 39, where $S_{kL} \simeq B_{\nu_{kL}} (T_{ex})$. Thus, although the b_k's are not, in general, independent of the radiation field, an estimate of the $(NCB)_{Lk}$ based on rough solutions of the transfer equation or even cruder procedures will not be as unreliable as an estimate of the corresponding $(NRB)_{kL}$ if the latter is obtained in an equally rough fashion. He makes use of this property of the $(NCB)_{Lk}$ to estimate losses in various spectral series, using Equation 128 and rough values for the ratios b_k/b_L obtained from various sources.

Table 11

Collisional Excitation and Ionization Rates for Hydrogen with $n_e = 10^{10}$ cm^{-3} Computed by Henze and Reported by Athay (1965b)

Transition	T_e (°K)			
	1×10^4	2.5×10^4	4×10^4	8×10^4
1 - 2	0.0050	5.2	30.0	1.3×10^2
1 - 3	7.0×10^{-5}	0.27	2.2	13.0
1 - 4	1.0×10^{-5}	0.063	0.57	3.7
1 - 5	3.3×10^{-6}	0.025	0.24	1.6
1 - k	6.1×10^{-6}	0.18	2.6	28.0
2 - 3	5.4×10^2	2.5×10^3	3.8×10^3	5.3×10^3
2 - 4	18.0	1.5×10^2	2.7×10^2	4.5×10^2
2 - 5	3.3	35.0	67.0	120.0
2 - k	21.0	3.8×10^2	8.1×10^2	1.6×10^3

For the Lyman and Balmer series of atomic hydrogen, Athay (1965b) uses the results of some collisional excitation-rate calculations by Henze, who in turn used Seaton's (1962) weak-coupling method to evaluate collision rates C_{LU} for several transitions arising on the ground or the first few excited levels of hydrogen. Some of these results are given in Table 11. Judged by the table, the following estimates by Athay seem not unreasonable:

$$C_{12} \gg \sum_{k>2} C_{1k} \ , \tag{129}$$

and:

$$C_{23} \gg \sum_{k>3} C_{2k} \ , \tag{130}$$

where inequality 130 is restricted to $T_e \lesssim 25000$°K. Using inequalities 129 and 130, Equation 128 becomes, for the Lyman series,

$$\frac{dF_{Ly}}{dh} \simeq n_1 C_{12} (NCB)_{12} (h\nu)_{12} \ , \tag{131}$$

and for the Balmer series,

$$\frac{dF_{Ba}}{dh} \simeq n_2 C_{23} (NCB)_{23} (h\nu)_{23} \ , \tag{132}$$

subject to the condition that the $(NCB)_{LU}$'s of Equations 131 and 132 are sufficiently predominant.

Since $(NCB)_{LU} = (1 - b_U/b_L)$, Equation 131 is valid provided that $b_1 >> b_2$, which condition certainly prevails for the upper chromosphere, where Athay assumes the bulk of the net chromospheric loss occurs in the Lyman series. Though he does not justify Equation 131 on theoretical grounds by estimating terms like $n_1 C_{13} (NCB)_{13} (h\nu)_{13}$ at lower heights in the chromosphere where $b_1 \simeq b_2 > b_3$ prevails and where n_1 is considerably larger than in the upper chromosphere, nevertheless the observed predominance of Lyα over the other members of the Lyman series gives some support to his estimate expressed by inequality 129. It is evident from the relevant b_k's that $(NCB)_{23} = (1 - b_3/b_2)$ is the dominant $(NCB)_{LU}$ for the Balmer series. We shall discuss the variation of these b_k's in the chromosphere presently. Equations 131 and 132 state that the net radiative losses in the Lyman and Balmer series of hydrogen are dominated by the corresponding collisional terms for Lyα and Hα, respectively. Whether the net radiative loss actually occurs in that spectral line cannot be determined until a transfer problem is solved.

Athay's conclusion that, for $h \geq 1000$ km, the condition $b_1 >> b_2$ exists, is based on his analysis (Athay, 1965a) of strong resonance lines in which the effect of continuum processes on the net flux in the line is ignored. He shows that for those lines where the further condition $\epsilon >> \eta B^*/B_\nu (T_e)$ is met, one obtains

$$\frac{b_k}{b_j} = \frac{\epsilon}{(NRB)_{kj}} . \tag{133}$$

Using a result due to Avrett and Hummer (1964), which is a refinement of Thomas' (1960) earlier rough estimates of the variation of $(NRB)_{kj}$ with τ_0, and which says that, for Lyα,

$$(NRB)_{kj} \simeq \eta \tag{134}$$

where

$$\tau_0 \simeq 0.1\, \eta^{-1} ,$$

Athay concludes that, at heights above $\tau_0 \simeq 3 \times 10^3$ in Lyα, $b_1 >> b_2$ is valid. This follows from Equations 133 and 134 where one takes $\eta = 3 \times 10^{-5}$, although the ">>" condition becomes marginal below $\tau_0 \simeq 10^2$. Also, since Athay discusses Lyα losses beginning as low as $h = 1000$ km, using the result $b_1 >> b_2$, which gives $(NCB)_{12} \simeq 1$ in Equation 131, he is introducing a contradiction with the PSC model chromosphere of Table 1 which shows $\tau_0 \geq 7 \times 10^4$ in Lyα for all $h < 1300$ km. Thus, it is debatable whether his treatment of the Lyman series losses is valid for $h < 1300$ km. Essentially the same conclusion can be drawn from a study of $b_1, \cdots, b_3$ by Pottasch and Thomas (1959). These authors evaluate the b_k's under the assumption of detailed balance in the Lyman lines, but variable opacity in the Lyman continuum. Using $T_e = 10^4$ °K, $n_e = 10^{11}$, and $T_r = 6000$°K for the Balmer continuum, they obtain a significant increase in b_1 over b_2 in the range $10 \geq \tau_{LyC} \geq 1$. If we examine $\tau_{LyC}(h)$ in the PSC model chromosphere, we find that $10 \geq \tau_{LyC} \geq 1$ in the region around $h = 1300$ km.

Thus, Athay's application of Equation 131 for Lyα with $(NRB)_{21} \simeq 1$ is somewhat unsatisfactory. However, he does not rely on Equation 131 alone for net loss estimates in Lyα, but observes that Hinteregger's (1964) measured flux in Lyα of 2.7×10^5 ergs cm^{-2} sec^{-1} certainly makes Lyα an important source of net energy loss from the chromosphere. Unfortunately, these measurements do not tell us where in the chromosphere the losses occur.

To treat the Balmer series we need b_2 and b_3. Here, Athay states that $(NCB)_{23} \simeq 1$ for the region of interest ($500 < h \leq 1250$ km), which implies that $b_2 >> b_3$ in this region. This is in complete accord with the Pottasch and Thomas study already mentioned. Athay then estimates Balmer series net losses with

$$\frac{dF_{Ba}}{dh} = n_2 C_{23} \langle h\nu_{2k} \rangle , \tag{135}$$

which is essentially Equation 132 with $(NCB)_{23} = 1$. Using the afore-mentioned C_{23} due to Henze and taking values for (T_e, n_e, n_2) from the PSC-model chromosphere, Athay derives the values for the net Balmer series loss—see Table 12. He estimates $\langle h\nu_{2k} \rangle = 4 \times 10^{-12}$ ergs in Equation 135, intermediate between Hα and the Balmer continuum.

Table 12

Computed $(dF_{Ba}/dh)\Delta h$ and Observed Total (Not Net) Losses in Balmer Continuum, Both from Athay (1966).

Δh	$\left(\frac{dF_{Ba}}{dh}\right) \Delta h$ (ergs cm^{-2} sec^{-1})	Total Observed Balmer Continuum Losses
500- 700	6×10^5	1.3×10^6
700- 900	4×10^5	8.3×10^5
900-1100	4×10^5	5.7×10^5
1100-1300	3×10^5	3.6×10^5
1300-1500	1×10^5	2.1×10^5

Table 12 includes Athay's report of the total radiative output in the Balmer continuum observed during the 1952 Khartoum eclipse expedition which provided the data for the PSC-model chromosphere. A comparison of these values with the calculated values of $(dF_{Ba}/dh)\Delta h$ reveals that the calculated net loss in the Balmer lines series is roughly half the total radiation observed in the Balmer continuum. Athay also observes that the total radiation observed in Hα at Khartoum is 4×10^6 ergs cm^{-2} sec^{-1}, which is more than than twice the calculated net loss for the Balmer series and approximately equals the total radiation observed in the Balmer continuum. Examination of these statements reveals that much of the observed radiation in Hα and the Balmer continuum must be scattered photospheric light, which is what we would expect for radiative transitions with the source function controlled by photoionization and not by collisions.

Athay ignores helium losses, and in particular Lyα of HeII at λ304, claiming that the observed energy radiated in these lines is only about 5 percent of the observed energy radiated in hydrogen Lyα. Since the hydrogen Lyα value represents, effectively, a net loss, and since the various helium lines' observed loss must be equal to or greater than the net loss from helium, he concludes, reasonably enough, that helium losses are negligible.

Finally, Athay ignores the neutral and ionized metal lines, claiming that the former are comparatively weak while the latter have $(NCB)_{LU} << 1.0$ for a lesser optical depth than for the hydrogen lines. His conjecture for the $(NCB)_{LU}$ for the ionized metal lines is rather speculative and, for this and other reasons we shall discuss presently, we do not accept his decision to ignore the ionized metal lines.

Zirker (1960) also derived an energy-conservation equation from the equation of radiative transfer, for the purpose of estimating net radiative losses from the solar chromosphere. He obtains the radiation-field terms for spectral lines and continua at a given frequency, J_L and $\bar{J}_C$, respectively, by solving two coupled transfer equations, using the Eddington approximation. He then uses these values of J_L and $\bar{J}_C$ in the energy-conservation equation to obtain the dF/dh for those spectral regimes treated. His results include a quantitative treatment of helium, so we include them here.

He estimates net radiative energy losses from material at the center of a uniform hydrogen-helium atmosphere satisfying the following conditions: thickness = 10^3 km, total particle density = 10^{11} cm^{-3}, hydrogen-helium abundance ratio = 10, and Balmer continuum intensity fixed by a background "photosphere" which produces black-body continuum radiation with a radiation temperature of 6000°K. These conditions roughly approximate upper chromospheric conditions of the PSC-model chromosphere, as given in Chapter II, Section D.

Zirker's calculations give the net radiative loss per gram at the center of the above atmosphere as a function of electron temperature T_e for the following radiators: the Lyman and Balmer continua and Lyα for hydrogen, the resonance continua of HeI and HeII, the Balmer continuum of HeII, and Lyα of HeII. His results show the Lyman continuum of hydrogen predominant for 7500 $< T_e <$ 25000°K, Lyα predominant for 25000 $< T_e <$ 50000°K with the Lyman continuum still non-negligible and Lyα of HeII predominant for $T_e >$ 50000°K. The predominance of the Lyman continuum of hydrogen for $T_e <$ 25000°K is contrary to the observationally based conclusion of Osterbrock that the Lyman continuum is negligible. Since Zirker's study cannot completely duplicate the actual chromosphere, where net losses in the Lyman continuum and Lyα depend strongly on the actual chromospheric opacity variation for these transitions, we do not believe that the suggested predominance of the Lyman continuum for $T_e <$ 25000°K applies to the chromosphere.

A brief digression from chromospheric loss estimates is now in order, to consider the net radiative losses from the corona. We must include these losses in our discussion, as sufficient mechanical energy must be available to balance them. In particular, if this mechanical energy has its source in the turbulent motions near and above the top of the hydrogen convection zone, as we are assuming for the mechanical energy that heats the chromosphere, then enough energy must be left over after the shock waves have passed through the chromosphere to balance the coronal losses. We have already mentioned two difficulties which the accretion hypothesis (heating from an external, mechanical source) encounters when applied to the corona in Chapter II, Section F. It is very likely, therefore, that the coronal net radiative losses must be added to those of the chromosphere for an estimate of the total outer atmospheric net radiative losses to be balanced by the mechanical source in the lower photosphere.

Billings (1966) estimates net coronal energy losses from radiative, conductive, and convection mechanisms. The latter must be added, when they are non-negligible, if they represent net losses from the outer atmosphere. Billings concludes that the net radiative losses from the corona exceed net losses from convection (solar wind) and outward conduction by about one order of magnitude. He bases his net radiative-loss estimates on a review of several observational studies of the solar ultraviolet radiation. These studies treat emission lines whose intensities lie so far above the background continuum that they effectively yield net radiation losses. Lyα losses are not included in his estimate, as Billings accepts the hypothesis we have already reviewed that Lyα losses occur in the upper chromosphere. He concludes that the net radiative losses from the corona lie in the range 10^5 - 10^6 ergs cm^{-2} sec^{-1}.

There is one other important source of energy loss from the corona which, according to Billings' estimates, is also of the order of 10^6 ergs cm^{-2} sec^{-1}. This is the electron thermal conduction down to the upper chromosphere which we discussed briefly in Chapter II. As this does not constitute a net radiative loss from the corona, it is omitted from estimates of the same. In fact, one current conjecture (de Jager and Kuperus, 1961) is that the upper chromosphere is heated largely by conduction down from the corona, producing the intense Lyα emission observed. We do not include any heating of the Lyα region due to conduction, but it could be very important. Kuperus and Athay (1967) argue that thermal conduction down from the corona might even be the source of energy for the spicules.

We devote no further attention to the corona here, as we shall not carry our temperature calculations out beyond the upper chromosphere. Theoretical estimates have been made of coronal radiative energy losses, assuming an optically thin corona. Pottasch (1963, 1964) has estimated losses due to oxygen, carbon, silicon and magnesium, concluding that for $T_e \geq 25000°K$ these elements produce radiative losses exceeding those of hydrogen and helium. By neglecting dielectronic recombination (which causes a higher fraction of the net radiative loss to come out of the corona in the form of emission lines rather than free-bound continua) it is possible that Pottasch may have erred in estimating at what frequencies the corona will lose energy. For our purposes, we shall not rely on theoretical estimates of coronal radiative losses, but accept as an upper limit Billings' higher value of 10^6 ergs cm^{-2} sec^{-1}.

It is now possible for us to offer a rough estimate of the net radiative energy loss from the entire outer solar atmosphere. We do this to see if the estimates of the mechanical flux F_m given in Chapter II, Section F, provide enough energy to balance these net radiative losses. We see from an examination of the estimates of Osterbrock and Athay that there is much uncertainty regarding the lower limit of the net radiative loss from the chromosphere, because of the scattered-light problem, but that we can accept their higher estimates to provide a number that should serve well as an upper bound. Thus, the chromospheric net radiative losses should not exceed 4×10^7 ergs cm^{-2} sec^{-1}. Billings' estimate for the upper limit to the coronal net radiative losses, 10^6 ergs cm^{-2} sec^{-1}, does not alter the 4×10^7 ergs cm^{-2} sec^{-1} value when applied to the entire outer atmosphere. Thus, our criterion for accepting the proposed turbulent generation of acoustic waves is that the resulting mechanical flux F_m satisfy $F_m \gtrsim 4 \times 10^7$ ergs cm^{-2} sec^{-1}. In Chapter II, Section F, we showed that F_m is probably in the range $2.9 \times 10^8 \gtrsim F_m \gtrsim 2.7 \times 10^7$ ergs cm^{-2} sec^{-1}.

The problem we consider for the remainder of this section is the choice of spectral lines and continua to include in our final temperature calculations. We shall base this choice partly on the work of Osterbrock, Athay, and Zirker already discussed, although this work is not always adequate for our needs.

2. First-Hand Estimates

The most straightforward procedure for estimating net radiative losses in a collision-dominated line is to solve transfer Equation 6 for the case where the line source function S_ℓ is given by the general form

$$S_\ell \rightarrow B_\nu(T_{ex}) = \frac{\int J_\nu \phi_\nu' \, d\nu + \epsilon B_\nu(T_e)}{1 + s} , \tag{136}$$

where the sink term is $s = \epsilon + \eta$. This is the same as our general source function of Equation 25 except for the neglect of source term ηB^*. Temperature dependence enters primarily through the Planck function $B_\nu(T_e)$ and, to a lesser degree, through the sink term s. NETPRF and the source function series of papers by Thomas and Jefferies give numerous examples of the solution of the transfer equation with a source function of the form of Equation 136, subject to the approximations of a constant sink term s and a single exponential representation for the Planck function. Given the solution for $\int J_\nu \phi_\nu \, d\nu$, Equation 136 is then used to get S_ℓ. Finally, as in Thomas (1960), the $(NRB)_{UL}$ of Equation 39 is evaluated and the net radiative loss is obtained from

$$\frac{dF}{dh} = n_U A_{UL} (NRB)_{UL} (h\nu)_{UL} , \tag{137}$$

provided that n_U is known. Having S_ℓ for the line and the population n_L for the lower level, we can obtain n_U from the relation

$$S_\ell = B_\nu(T_{ex}) = B_\nu(n_U/n_L) .$$

So one procedure for determining the predominant energy-loss mechanism is to evaluate Equation 137 for all suspected lines and retain those lines for which dF/dh predominates in some region of the atmosphere.

The procedure we use for treating the lines and most continua here is simpler than solving the transfer equation. We rely on the Δ_j of Equation 117, derived in Chapter III; Δ_j is the fractional amount of energy that goes into the transition L → U by inelastic collisions and does not necessarily give the energy lost from the atmosphere in a corresponding U → L radiative transition. This occurs only in the restricted case of a two-level atom. Otherwise, the net radiative loss must be obtained by solving a transfer problem. For example, when we conclude that Hα is

a transition for which Δ_j should be evaluated for the low chromosphere, we must remember that the mechanical energy going into the 2 → 3 transition in hydrogen will not, in general, equal the net energy loss in Hα. In relying on Δ_j, we replace the problem of estimating net radiative loss mechanisms by the problem of estimating net collisional gain mechanisms for levels (L, U). This is the spirit of the Athay (1966) study, reviewed in the last subsection. Our only departure from this procedure is in the treatment of H^-, where the small optical thickness of the chromosphere in the H^- continuum permits a simple estimate of the net radiative losses.

We begin with the lowest part of the chromosphere, where H^- is important. We proceed along two lines. We estimate the excess of emission over absorption in the lowest region $0 \leq h \leq 500$ km, including the non-LTE effect due to the departure of the continuum source function from the Planck function. We also estimate the mechanical energy dissipated in this region, according to our assumptions about shock dissipation of acoustic waves, to see if the mechanical energy dissipated roughly equals the energy loss due to H^- and any other significant sources of radiative loss.

To estimate the excess of emission over absorption in H^-, we first calculate the b_{H^-} whose value determines the departure of the source function from the Planck function. If we assume that H^- dominates the continuum opacity and ignore the free-free absorption, it is easy to show, as in PSC, that the continuum source function is given by

$$S_c = \frac{1}{b_{H^-}} B_\nu(T_e) \ . \tag{138}$$

The dominance of the continuum opacity by H^- for $0 \leq h \leq 500$ km is justified presently. That we can neglect the free-free absorption, compared to the bound-free absorption, is apparent from the estimates of $j_{\nu fb}/j_{\nu ff}$ at $\lambda = 4700$ Å:

T_e (°K)	5040	6300
$\frac{j_{\nu fb}}{j_{\nu ff}}$	24.8	10.1

We obtain these estimates from the following equations, which PSC derives using the Planck function and the Saha equation:

$$j_{\nu fb} = 4.14 \times 10^{-16} \left(\frac{2\pi h\nu^3}{c^2}\right) n_e n_H T_e^{-3/2} e^{\chi_{H^-}} e^{-\chi_\nu} \alpha_{\nu bf} \ , \tag{139}$$

$$j_{\nu ff} = 4.14 \times 10^{-16} \left(\frac{8\pi h\nu^3}{3c^2}\right) n_e n_H T_e \, e^{-\chi_\nu} \alpha_{\nu ff} \ . \tag{140}$$

The units for $\alpha_{\nu bf}$ are cm^2; for $\alpha_{\nu ff}$, they are cm^4 $dyne^{-1}$. Using the $\alpha_{\nu ff}$ from Chandrasekhar (1958) and the $\alpha_{\nu ff}$ from Chandrasekhar and Breen (1946) gives the $j_{\nu fb}/j_{\nu ff}$ we exhibit. Newer

calculations of the $\alpha_{\nu ff}$ make our conclusions stronger. 4700 Å is a representative line-free point of the solar spectrum near the maximum observed intensity. For $\lambda_0 \gtrsim$ 16000 Å, where $\alpha_{\nu ff}$ does become large,

$$\int_0^{\nu_0} B_\nu \left(T_{eff} = 5800°\right) d\nu$$

is very small compared to

$$\int_{\nu_0}^{\infty} B_\nu \left(T_{eff}\right) d\nu \ ,$$

so our neglect of the free-free absorption is justified.

Induced emission, also, can be ignored in our further work with H^-, owing to the fact that $(h\nu) \geq 0.75$ ev, the ionization potential for H^-, and hence the factor $\exp\{-h\nu/kT_e\}$ is negligible in the chromosphere.

With these preliminaries, we can go on to calculate b_{H^-}. From the condition of a statistically steady state, we obtain

$$b_{H^-} = \frac{n_e D_{e,H^-} + n_H D_{H,H^-} b_{H_2} + 4\pi \int_{\nu_0}^{\infty} \frac{B_\nu (T_e)}{h\nu} \alpha_{\nu bf} \, d\nu}{n_e D_{e,H^-} + n_H D_{H,H^-} + 2\pi \int_{\nu_0}^{\infty} \frac{J_\nu (T_{eff})}{h\nu} \alpha_{\nu bf} \, d\nu} \ , \tag{141}$$

where we use the notation of PSC. The units for the collision rates per particle are $cm^3\ sec^{-1}$. Thomas has shown that the term for electron collisional excitation $n_e D_{e,H^-}$ is orders of magnitude less than the term for the associative detachment reaction $n_H D_{H,H^-}$ under photospheric conditions. This conclusion remains valid in the low chromosphere, when we use more recent values for the electron-negative hydrogen ion cross section (lower values) reported in Tisone (1966), or even the older, higher cross section used by Thomas in making his estimates of $n_e D_{e,H^-}$ for the photosphere. Frisch (1966) argues in her thesis that the concentration of H_2 is maintained in LTE, giving $b_{H_2} = 1$. Thus, Equation 141 becomes

$$b_{H^-} = \frac{n_H D_{H,H^-} + 4\pi \int_{\nu_0}^{\infty} \frac{B_\nu (T_e)}{h\nu} \alpha_{\nu bf} \, d\nu}{n_H D_{H,H^-} + 2\pi \int_{\nu_0}^{\infty} \frac{J_\nu (T_{eff})}{h\nu} \alpha_{\nu bf} \, d\nu} \ . \tag{142}$$

Table 13

Values for Departure Coefficients b_{H^-} in Lowest Region of the Chromosphere.

$$2\pi \int_{\nu_0}^{\infty} \left[J_\nu (T_{eff}) / h\nu \right] \alpha_{\nu bf} \, d\nu = 0.95 \times 10^6 \ sec^{-1} .$$

h (km)	n_H (cm^{-3})	$n_H D_{H,H^-}$ (sec^{-1})	T_e (°K)	$4\pi \int_{\nu_0}^{\infty} \frac{B_\nu(T_e)}{h\nu} \alpha_{\nu bf} \, d\nu$ (sec^{-1})	b_{H^-}
0	3.78 (15)	5.70 (6)	5050	1.34 (6)	1.06
100	1.60 (15)	2.08 (6)	5250	1.50 (6)	1.18
200	6.99 (14)	0.95 (6)	5460	1.66 (6)	1.37
300	3.15 (14)	0.41 (6)	5680	1.84 (6)	1.65
400	1.46 (14)	0.19 (6)	5910	2.02 (6)	1.94
500	6.95 (13)	0.09 (6)	6150	2.24 (6)	2.24

This equation gives us b_{H^-}. We exhibit the results of our calculation in Table 13 above. To derive b_{H^-}, we have used the PSC model for the low chromosphere for (n_H, T_e), the already quoted value of $D_{H,H^-} = 1.3 \times 10^{-9}$ cm^3 sec^{-1} (Dalgarno, 1967; Schmeltekopf, et al., 1967), and the value of the integral

$$4\pi \int_{\nu_0}^{\infty} \frac{B_\nu(T_e)}{h\nu} \alpha_{\nu bf} \, d\nu \simeq 1.5 \times 10^3 \, T_e \, e^{-\chi_{H^-}} , \qquad (143)$$

given in PSC, which uses the Chandrasekhar (1958) values for $\alpha_{\nu bf}$. For T_{eff}, we choose $T_{eff} = 5800°$.

Table 13 shows that at $h = 200$ km the associative detachment reaction rate $n_H D_{H,H^-}$ has decreased to become equal to the photoionization rate

$$2\pi \int_{\nu_0}^{\infty} \left[J_\nu (T_{eff}) / h\nu \right] \alpha_{\nu bf} \, d\nu .$$

Beyond 200 km, the photoionization rate dominates. These conclusions are similar to Schmeltekopf's conclusions, which we gave in Chapter II, Section F.

In the low chromosphere, we would expect a combination of the photoionization and our assumed local value of mechanical energy input to fix the local electron temperature T_e until a height is reached where H^- becomes a minor source of continuum opacity. We use this to calculate the temperature in the lowest region $0 \leq h \leq 500$ km in the next section.

With these b_{H^-}, we can now write the excess, E, of emission over absorption in H^-:

$$E = 4\pi \int_{\nu_0}^{\infty} S_\nu K_\nu \, d\nu - 4\pi \int_{\nu_0}^{\infty} J_\nu K_\nu \, d\nu \, . \tag{144}$$

If we use Equation 138 for S_ν and ignore the frequency-dependence of the nearly grey H^- bound-free absorption coefficient, Equation 144 becomes

$$E \simeq 2\sigma K^*_{H^-} \left[2T_e^4 - \left(b_{H^-}\right) T_{eff}^4 \right] \, , \tag{145}$$

where σ is again the Stefan-Boltzmann constant and $K^*_{H^-} = n^*_{H^-} \bar{\alpha}_{H^-}$ for the LTE population of n_{H^-}. We obtain $K^*_{H^-}(h)$ by noting that, at $h = 0$, H^- completely dominates the opacity and $b_{H^-} \simeq 1$, so $n_{H^-} \simeq n^*_{H^-}$. From the Bilderberg Continuum Atmosphere or the opacity tables of Cox and Stewart (1964a, b) for physical conditions at $h = 0$ in the Sun, we find $K^*_{H^-} \simeq 10^{-2}\, \rho \simeq 6.31 \times 10^{-11}$ cm^{-1}. We use the $h = 0$ value of ρ of the PSC model to obtain the latter value. In addition, the PSC model gives us values of $n^*_{H^-}(h)$. Thus we obtain

$$K^*_{H^-}(h) = K^*_{H^-}(0) \frac{n^*_{H^-}(h)}{n^*_{H^-}(0)} \tag{146}$$

The results of the calculation of excess emission E appear in Table 14.

It is interesting to compare the results of this calculation with calculated values of the shock dissipation D(h) in the same chromospheric region. Table 15 gives D(h) obtained by using $T_e(h)$ from the PSC model, $\rho(h)$ from Equation 120, η_s from Equation 84, and Equation 81 for D(h) itself. We see that $D(h) \gtrsim E(h)$ at $h = 400 - 500$ km and $D(h) \simeq E(h)$ at $h = 300$ km, all of which is consistent with the idea of H^- dominating the energy loss out to $h \simeq 500$ km—though we must point out that this is no proof, considering that every estimate upon which this coincidence is based is quite rough, particularly the estimate of D(h). Furthermore, the huge excess of E(h) over D(h) as we proceed in toward the limb is not unreasonable when we consider that the $T_e(h)$ values from the PSC model chromosphere are almost certainly too high there. We conclude that the mechanical energy input and the excess emission in H^- are roughly equal in the region $0 \leq h \leq 500$ km. The total mechanical dissipation $\int D(h)\, dh$ in this range is approximately 10^6 ergs cm^{-2} sec^{-1}. If we ignore our very large estimates of E(h) below 200 km, the $\int E(h)\, dh$ over this region yields a like value. This is roughly equal to Athay's lower estimate and is a good order of magnitude below Osterbrock's estimate. It suggests that the net radiative loss from the entire outer atmosphere may lie between 10^6 and 10^7 ergs cm^{-2} sec^{-1}, well below the oft-quoted Osterbrock value.

We must consider the other possible energy sinks for the mechanical energy in the region $0 \leq h \leq 500$ km, to check our conjecture that H^- does dominate the net radiative losses there. We must consider the hydrogen continua and the spectral lines from hydrogen and the neutral

Table 14

Values of Excess Emission E(h) in H^- from Low Chromospheric Region $0 \leq h \leq 500$ km.

h (km)	$K^*_{H^-}$ (cm^{-1})	T_e (°K)	b_{H^-}	E(ergs cm^{-3} sec^{-1})
0	6.31×10^{-11}	5050	1.06	0.714
100	1.87 (-11)	5250	1.18	0.401
200	6.66 (-12)	5460	1.37	0.173
300	2.64 (-12)	5680	1.65	0.063
400	1.09 (-12)	5910	1.94	0.031
500	4.71 (-13)	6150	2.24	0.018

Table 15

Calculated Shock Dissipation D(h) for Height Range $0 \leq h \leq 500$ km Using $D(h) = 1.025 \times 10^5 \rho T_e \eta_s^3$.

h (km)	ρ (gm cm^{-3})	T_e (°K)	η_s	D(ergs cm^{-3} sec^{-1})
0	6.3×10^{-9}	5050	0.0	0.0
100	2.9 (-9)	5250	0.22	0.0158
200	1.4 (-9)	5460	0.39	0.0452
300	6.3 (-10)	5680	0.53	0.0548
400	2.9 (-10)	5910	0.63	0.0440
500	1.3 (-10)	6150	0.71	0.0303

metals. The temperatures below 500 km are too low for any helium transitions to be important and we shall show, in our treatment of the ionized metals to follow presently, that the optical depth in the lines of the more abundant ionized metals becomes so large below 500 km that detailed balance can be expected for them there.

First, consider the hydrogen continua. It will be convenient to consider these continua for the entire low chromosphere, rather than restrict ourselves to the region $0 \leq h \leq 500$ km.

In the lower part of the low chromosphere, where $0 \leq h \leq 500$ km, the departure coefficients b_k will all lie near unity, with the extreme variation from unity given by $b_1 \simeq b_2 = 3.4$, according to the PSC model of Table 1. Actually, b_2 may be slightly greater than b_1 here, but the difference is not important for our purposes. Since the b_k for $k > 2$ all lie below this value, and since all the b_k decrease rapidly as height h decreases, we expect all the $(NCB)_{k\kappa}$ connecting the bound levels of hydrogen with the continuum to rapidly approach zero with decreasing height in this region, at least until such height is reached where $b_1 \simeq b_2$ decreases below unity.

Frisch (1966) has calculated b_1 for this low region, assuming $b_1 = b_2$ and including the contribution of H^- and the Paschen continuum to the opacity and an Osterbrock (1961) type of

mechanical dissipation term. She gives values for b_1 ranging from 0.78 to 1.00 at $h = 0$, depending on initial conditions for the model. These are minimum values for b_1 in the region $0 \leq h \leq 500$ km; the thickness of the sub-region for which $b_1 < 1$ never exceeds about 100 km in her models, except in one extreme case where it is about 200 km. These $b_k < 1$ will make the $(NCB)_{1K}$ negative for $b_K = 1$. However, these negative values seem to occur over a thin sub-region only, the very sub-region near our $h = 0$ point where we know that all our estimates—$D(h)$, $E(h)$, and $T_e(h)$—are rather unreliable. Thus, we ignore the departures of $(NCB)_{kK}$ from zero in this sub-region, and exclude the hydrogen continua from our energy balance in the lower region, $0 \leq h \leq 500$ km.

In the next region, $500 < h \leq 1250$ km, we are faced with a different situation. Here the $(NCB)_{kK}$'s for the lower levels of hydrogen are better approximated by unity than by zero. It becomes necessary to calculate the quantities $n_k C_{kK} (NCB)_{kK} (h\nu)_{kK}$, for $k = 1, 2, \cdots$ up to some value of k where this quantity becomes negligibly small. We do this for the first three hydrogen continua, using $(NCB)_{kK} = 1$, the C_{kK} from the previously referenced Henze work for $n_e = 10^{11}$, $T_e = 10^4$, Table 1 for values of n_1 and n_2, the Boltzman equation and $b_3 \simeq 0.2\, b_2$ for n_3, and the previously referenced Thomas and Pottasch study and Tables 1 and 16 for the behavior of b_1, b_2, and b_3 as functions of τ_{LyC} and of height h. Table 16 gives the results of this calculation.

Table 16

Calculated Values of $n_k C_{kK} (NCB)_{kK} (h\nu)_{kK}$ (ergs cm^{-3} sec^{-1}) for the First Three Hydrogen Continua for Selected Heights in the Range $500 < h \leq 1250$ km.

h (km)	$n_1 C_{1K} (NCB)_{1K} (h\nu)_{1K}$ (ergs cm^{-3} sec^{-1})	$n_2 C_{2K} (NCB)_{2K} (h\nu)_{2K}$ (ergs cm^{-3} sec^{-1})	$n_3 C_{3K} (NCB)_{3K} (h\nu)_{3K}$ (ergs cm^{-3} sec^{-1})
750	1.6×10^{-2}	1.1×10^{-3}	2.4×10^{-3}
1000	3.0×10^{-3}	7.3×10^{-4}	1.6×10^{-3}
1250	4.2×10^{-4}	4.9×10^{-4}	1.0×10^{-3}

Table 16 shows that the amount of mechanical energy delivered to the chromosphere in the first three hydrogen continua is not completely negligible compared to the mechanical energy input given by $\int D(h)\, dh$ over the region $500 < h \leq 1250$ km. We have already noted that this integral has a value of $\sim 10^6$ ergs cm^{-2} sec^{-1}. We readily see that the mechanical energy required by each of the first three hydrogen continua for $500 < h \leq 1250$ km is of the order of 10^5 ergs cm^{-2} sec^{-1}. We have somewhat overestimated the requirements of these three continua by using $T_e = 10^4$, making C_{kK} too large. However, this could be balanced by the additional requirements of the higher continua, which must be included until $(NCB)_{kK}$ becomes a small fraction of unity. The hydrogen continua could easily take up half of the mechanical energy $\int D(h)\, dh$ which we estimate to be available.

The Balmer continuum deserves further treatment. The observed radiation in the Balmer continuum is far from negligible, as examination of Table 12 reveals. Since Table 12 is confined to the region $500 \leq h \leq 1500$ km, we should ask if the Balmer continuum losses below 500 km are

of comparable magnitude. Athay (1966) remarks that the observed radiation in the Balmer continuum actually reaches a maximum at 400 km (below which good data were not available from the 1952 eclipse), so this observed radiation is of the order of the mechanical energy dissipated in the lower region $0 \leq h \leq 500$ km, according to Table 15 for $D(h)$. The comparatively low values of the mechanical energy estimated in Table 16 to ionize hydrogen from the second bound level suggest that much of this observed Balmer continuum radiation is scattered photospheric light. However, this still leaves the possibility of more absorption of Balmer continuum radiation than is emitted in the chromosphere, so we must assure ourselves that there is no appreciable net transfer of this energy into the thermal modes.

Thomas in PSC evaluated the net radiative (or rate) bracket for the Balmer continuum $(NRBC)_2$ for the two cases of detailed balance in the Lyman continuum and negligible Lyman continuous opacity, where the atmosphere is assumed transparent in the Balmer continuum but is locally opaque in the Lyman lines. In both cases, he finds $(NRBC)_2$ equals a negative number. Physically, this is due to the predominance of photoionization from level 2 over collisional excitation between levels 2 and 3, an effect we mentioned when discussing the source function for photoionization-dominated lines. The negative value of $(NRBC)_2$ shows that there is no net radiative loss from the atmosphere in the Balmer continuum, but rather that the atmosphere actually does absorb more radiant energy in the Balmer continuum than it emits.

We now ask if this could be an important source of thermal energy. We proceed by determining whether the net flux of photospheric radiant energy *into* the Balmer continuum is small compared to the local mechanical dissipation, and thus ignorable. We start by exhibiting several useful relations derived by Thomas in PSC. For the Balmer continuum, it is easy to show from the equations in PSC, Chapter IV, that the flux gradient under conditions of detailed balance in the Lyman lines can be approximated by

$$\frac{dF_{Balc}}{dh} \simeq 8.2 \times 10^{-7} T_e (NRBC)_2 , \tag{147}$$

where a three-level atom plus continuum approximation has been used and no transfer problem has been solved. Under the same conditions, using values of departure coefficients b_1 and b_2 for the low chromosphere taken from Pottasch and Thomas (1959), and also assuming transparency in the Balmer continuum, Thomas obtains the two expressions for $(NRBC)_2$ mentioned before. These are

$$(NRBC)_2 = -\Delta , \tag{148}$$

for detailed balance in the Lyman continuum, and

$$(NRBC)_2 = -(2 + \Delta) , \tag{149}$$

for transparency in the Lyman continuum. The quantity Δ is given by

$$\Delta \simeq 0.4 \, b_3 \, X_2 \, e^{X_3} \, (NRB)_{32} , \tag{150}$$

with all parameters defined in Chapter II, Section C.

If we take $T_e = 6000°K$ and further reduce Equation 150, we obtain

$$\Delta \simeq 49.0\, b_3\, (NRB)_{32}, \qquad T_e \simeq 6000°K . \tag{151}$$

Table 17

Height Dependence of τ_{LyC} and $\tau_{0H\alpha}$ from PSC Model Chromosphere.

h (km)	τ_{LyC}	$\tau_{0H\alpha}$
750	1×10^3	34.5
850		28.5
950		23.4
1000	2×10^2	21.7
1100	96.0	18.7
1200	35.0	17.0
1250	19.8	
1300	6.6	

Since the temperature dependence of Δ is not too strong for $5000 < T_e < 8000°K$, we need only determine b_3 and $(NRB)_{32}$ for $H\alpha$, and we can evaluate the flux gradient in the Balmer continuum in the low chromosphere with Equations 147-149, using Equation 151 for Δ.

Consider, first the lower region $0 \leq h \leq 500$ km. Here, $\tau_{0H\alpha} \gtrsim 100$, as shown in Table 17, which also shows that this lower region satisfies detailed balance in the Lyman continuum. Using the result $b_3 \leq b_2$ to obtain $b_3 \simeq 1$ for $\tau_{0H\alpha} \gtrsim 100$, and using Thomas' (1960) values for $(NRB)_{32}$ as a function of $\tau_{0H\alpha}$ ($\tau_{0H\alpha} = 100$, $(NRB)_{32} = 0.0012$), we obtain the value $\Delta \simeq 0.06$. Using this value and combining Equations 148 and 147, we obtain

$$\frac{dF_{BalC}}{dh} \simeq -3.0 \times 10^{-4} \text{ ergs cm}^{-3} \text{ sec}^{-1} , \tag{152}$$

$$0 \leq h \leq 500 \text{ km} .$$

Comparing this with the values for $E(h)$ for H^- and $D(h)$ for the local mechanical energy input (Tables 14 and 15, respectively), we see that dF_{BalC}/dh is more than two orders of magnitude below either and can surely be neglected in the region $0 \leq h \leq 500$ km.

Now consider the higher region $500 \leq h \leq 1250$ km. Repeating the type of calculation done for the lower region, we find that

$$\frac{dF_{BalC}}{dh} \simeq -10^{-2} \text{ ergs cm}^{-3} \text{ sec}^{-1} , \tag{153}$$

$$500 \leq h \leq 1250 \text{ km} ,$$

where we use intermediate values of $(NRB)_{32}$ as functions of $\tau_{0H\alpha}$ from Thomas (1960), Equation 151 with $T_e \simeq 6000°K$ for Δ, $b_3 \gtrsim 1$ from Pottasch and Thomas (1959), and either Equation 148 or 149 for $(NRBC)_2$. It does not matter much which equation, 148 or 149, is used as Equation 151 gives $\Delta \simeq -1$, so $(NRBC)_2$ is of order unity in either case. Equation 153 is uncertain to more than a factor of two anyway, as we are in the region of intermediate Lyman continuous opacity where all quantities are estimated at values between those for optically thick and thin atmospheres.

We are now faced with two problems: 1) the roughness of the above analysis, difficult to improve without solving a transfer problem, and 2) the magnitude of dF_{Balc}/dh, which says that the net flux of photospheric radiant energy into the Balmer continuum is of the same order as the mechanical energy dissipated in this region. We see the latter by noting that $\int D(h)\, dh$ for $500 \leq h \leq 1250$ yields $\sim 10^6$ ergs cm^{-2} sec^{-1}, while $\int \left(dF_{Balc}/dh\right) dh$ also gives $\sim 10^6$ ergs cm^{-2} sec^{-1} in this region.

Without going into detail on where this dF_{Balc}/dh energy flux goes, we can make one simple observation concerning energy balance. The region currently under discussion has $T_e > T_{eff}$ according to the PSC model of Table 1, and the photospheric radiation field absorbed by the chromosphere is well described by a Planck function at $T \simeq T_{eff}$ in the continuum. Thus, the energy of the Balmer continuum photons absorbed in this $T_e > T_{eff}$ region cannot heat the gas beyond T_{eff} without violating the second law of thermodynamics. As far as competing with $D(h)$ as a source of thermal energy, the Balmer continuum can be ignored in this upper region, provided that the condition $T_e > T_{eff}$ is actually satisfied there, as the PSC model suggests.

This completes our special study of the Balmer continuum. Let us consider the lower region $0 \leq h \leq 500$ km again, regarding the mechanical-energy input into bound-bound transitions of hydrogen and the neutral metals.

First consider the hydrogen transitions. The mechanical energy input into Lyα is negligible because of the great optical thickness of the lower region in the Lyman continuum, so that $b_1 \simeq b_2$, giving $(NCB)_{12} \simeq 0$. However, the Lyβ transition may take up much mechanical energy. If we use the Table 11 value for C_{13} at $n_e = 10^{11}$ and $T_e = 10^4$, and the n_1 ($h = 200$ km) from Table 1, and allow that b_1 at $h = 200$ km may be as large as 2.0 with $b_3 \simeq 1$, we see that $n_1 C_{13} (NCB)_{13} (h\nu)_{13}$ is more than an order of magnitude *larger* than the total $D(h)$ at 200 km. On the other hand, C_{13} should really be recalculated in this region, since the actual temperature is more like 5000° than 10,000°. Also, Frisch's (1966) models show that b_1 ($h \simeq 200$ km) may be as low as unity, depending on the amount of mechanical energy dissipated in the low region which is poorly known. Thus, it is quite possible that our above estimate at $h = 200$ km is several orders of magnitude too large. Below and above $h \simeq 200$ km, $n_1 C_{13} (NCB)_{13} (h\nu)_{13}$ should drop off from the value around $h = 200$ km because $b_1 \lesssim 1$ below and $n_1(h)$ decreases above. Finally, C_{14} is almost an order of magnitude less than C_{13} so the members of the Lyman series above Lyβ are comparatively unimportant mechanical-energy sinks. Unfortunately, we cannot be sure from these estimates that Lyβ is completely negligible in the region $0 \leq h \leq 500$ km.

The local net gain of mechanical energy by Hα is $n_2 C_{23} (NCB)_{23} (h\nu)_{23}$. Even for $(NCB)_{23} = 1$, which is too large for the low region, we see that $n_2 C_{23} (NCB)_{23} (h\nu)_{23} << 10^{-2}$ ergs cm^{-3} sec^{-1}, considering our use of C_{23} at $T_e = 10^4$. Thus, the Hα collisional excitations are small enough compared to $D(h)$ to be ignored. The same argument shows all of the Balmer and higher hydrogen-series transitions to be negligible compared to $D(h)$.

To estimate the mechanical-energy input into transitions of the neutral metals, we cannot assume LTE to be valid in the low chromosphere, as Zirker (1956, 1958) has shown in his analysis

of several lines of neutral metals (Na, Mg, Al, Ca, and Fe) for which he provides estimates of the height h at which $\tau_0(h)$ equals unity for each line. The necessity for some non-LTE effect arises when we compare 1) the inference from the Saha equation that the ionization of the metals should leave such a small LTE ratio of neutrals to ions (10^{-2} - 10^{-5} for $0 \leq h \leq 500$ km) that the chromosphere should be optically thin in the metal lines, with 2) Zirker's analysis which shows definite self-absorption effects for these lines. Zirker uses data from the same 1952 Khartoum eclipse that the PSC-model chromosphere is based on. Unfortunately, the data were of poor quality for $h < 500$ km, and many of his results do not directly affect the region $0 \leq h \leq 500$ km, where the neutral metals could play an important role.

The rough estimates of radiative losses by Osterbrock and Athay, giving the total observed radiative flux in the lines of all neutral and singly ionized metals as a few times 10^6 ergs cm^{-2} sec^{-1}, are not too helpful either, particularly when one considers that each is based on different assumptions, different data, and even different spectral regimes. Furthermore, the observed fluxes from the neutral metal lines are certainly not net radiative losses from the chromosphere, but arise primarily from scattered photospheric light, if we judge by their similarity to the Balmer lines, i.e., most have photoionization-dominated source terms. On the other hand, to examine the 100 strongest, or 1100 strongest such lines described by Athay, even by several "prototypes" of similar excitation potential, arising from atoms of similar fractional abundance, etc., would be extremely time-consuming. And it should be pointed out that the total observed loss from the 1100 mentioned was observed to be twice that of the strongest 100, so we cannot restrict ourselves to the few strongest when discussing these lines.

We proceed, therefore, by first noting that the total radiative flux from the chromosphere in the neutral lines is not likely to exceed 10^6 ergs cm^{-2} sec^{-1}, if we judge by the observations of Osterbrock and Athay. Then we recall that lines with photoionization-dominated source functions scatter more energy than is received from collisional excitation, as mentioned above. How much more, we could estimate by examining the predominance of the photoionization source term ηB^* over the collision source term in the line $\epsilon B_\nu(T_e)$. However, since the mechanical dissipation $D(h)$ of Table 15 yields a value for $\int D(h)\,dh$ over $0 \leq h \leq 500$ km of order 10^6 ergs cm^{-2} sec^{-1}, it follows that at least the bulk of our mechanical energy must be available for collisional excitations in other energy sinks than all the neutral metals taken together.

This concludes our consideration of the other possible mechanical-energy sinks in the region $0 \leq h \leq 500$ km. We cannot discount the possibility that the cumulative contribution of the hydrogen continua, the hydrogen series, and the neutral metals could equal $\int D(h)\,dh$ over this region. Our earlier conjecture that only H^- is an important mechanical energy sink in the lower region is weakened by the above considerations.

Nevertheless, we shall ignore the contribution of all mechanical energy sinks other than H^- in this lower region, justifying this procedure on the generally reasonable correspondence between $E(h)$ and $D(h)$ in Tables 14 and 15, at least above 200 km. However, we must keep in mind the reservations mentioned here.

This concludes our consideration of the region $0 \leq h \leq 500$ km. What about the chromosphere for $h > 500$ km? Provided that T_e does not exceed 50000°K, we can ignore helium, according to the Zirker (1960) study, so we consider the lines of neutral hydrogen and the abundant singly ionized metals.

First, consider the hydrogen lines. We have already noted that, for $T_e \lesssim 25000$°K and chromospheric conditions at $h > 500$ km, the condition of Equation 130

$$C_{23} >> \sum_{k>3} C_{2k} ,$$

holds, so in the upper region of the low chromosphere the $2 \rightarrow 3$ transition is the only Balmer collisional transition that could be a significant energy sink. The Paschen and higher hydrogen series can be ruled out because of the b_k's. For $k \geq 3$, if $b_k \simeq b_{k+1}$, $(NCB)_{k,k+1} \simeq 0$, and, if $b_k >> b_{k+j}$ $(j = 1, \cdots)$, then the number density $n_{k+j} << n_k$. In either case, $n_k C_{k,k+j} (NCB)_{k,k+j} (h\nu)_{k,k+j}$ are negligible when compared to this quantity for the Balmer case with $(k, j) = (2,1)$. To see this, we use again the table of Henze's $C_{k,k+j}$ provided by Athay (1965b), and the non-LTE Boltzmann relation (with the b_k's), and assume that the behavior of $b_k (\tau_{LyC})$ for all $k \geq 3$ mimics that of b_3 from Pottasch and Thomas (1959), subject to the condition $b_k \geq b_{k+1}$. This covers the case of hydrogen except for the Lyman series, which we now examine.

Consider once more inequality

$$C_{12} >> \sum_{k>2} C_{1k} ,$$

which says that the $1 \rightarrow 2$ collisional transition is the dominant energy sink in the Lyman series as long as $(NCB)_{12} \neq 0$. Where in the chromosphere does this mechanical energy input occur? To answer this question, we compare the quantity $n_1 C_{12} (NCB)_{12} (h\nu)_{12}$ for this transition with the analogous expression for the singly ionized metals, which are treated next. When this comparison is made for the region of $h \leq 1250$ km, we find the condition $(NCB)_{12} \simeq 0$ to hold, by examining the PSC-model low chromosphere and the Pottasch and Thomas (1959) study of departure coefficients b_1 and b_2. The PSC model gives $T_e \lesssim 8000$°K and $\tau(LyC) \gtrsim 10$ for $h \leq 1250$ km. The Pottasch and Thomas study gives $b_1 \lesssim b_2$ for $\tau(LyC) \geq 10$, $T_{r2} = 6000$°K, $n_e = 10^{11}$, $T_e = 10^4$, and detailed balance in the Lyman lines. Thus, $(NCB)_{12} \simeq 0$ should be a good assumption below 1250 km and above the H^- region. From this it follows that $n_1 C_{12} (NCB)_{12} (h\nu)_{12} \simeq 0$ below 1250 km, so we ignore this transition there.

Consider the singly ionized metals. Because of their low ionization potentials, we would expect and shall assume the more abundant metals to be singly ionized in the region $500 < h < 1250$ km. Zirker (1956) has studied this problem. From his determination of optical depths in

the resonance lines from the singly ionized metals BaII, ScII, SrII, TiII, observed in the 1952 eclipse, he calculates the neutral hydrogen density at $h = 500$ km, assuming that all these metals are in the singly ionized state above this height (ionization potentials: Ba, 5.21 ev; Sc, 6.54 ev; Sr, 5.69 ev; Ti, 6.82 ev) and that the Allen (1955) relative abundances apply everywhere. He obtains excellent agreement with the value for the neutral hydrogen density reported in Table 1 for the PSC model, which is based on continuum data. This supports the assumption that above 500 km, all metals with I.P. $\lesssim 8.0$ (Ca, Mg, Si) will be singly ionized in the region $500 < h < 1250$ km. Additional support for this assumption is provided in a study by Athay and Zirker (1962), which shows that for $n_e = 10^{11}$, $T_e = 10^4$, most of the calcium will be singly ionized, but that, by the time $T_e = 15000°K$ is reached, most of the calcium will be doubly ionized. They obtain these results by approximating the CaII ion by three bound levels (4S, 3D, 4P) and the continuum. Their results are independent of optical depth in the center of the resonance doublet. In view of the above result, when we examine the temperature structure of the PSC-model chromosphere of Chapter II we can reasonably assume that all calcium is singly ionized in the region $500 < h < 1250$ km and, for $h \geq 1500$ km, calcium is at least doubly ionized. We can make no statement for $1250 < h < 1500$ km, except that the transition from predominantly singly to doubly ionized calcium occurs there.

What transitions in the singly ionized metals should we expect to be strongest in the solar spectrum? From considerations of chemical abundance and observations of strong chromospheric lines, we conclude that the resonance transition in MgII is by far the strongest, and that the resonance transitions in CaII and SiII might also be important. This conclusion is supported by the spectra of Purcell, et al. (1963) for MgII, Dunkelman and Scolnik (1959) for CaII, and Detwiler, et al. (1961) for SiII. These three studies span the spectral range 4000Å - 500Å and show that the resonance lines of the above three ions and Lyα of hydrogen dominate the line spectrum. Also, in the extreme ultraviolet spectra down to 250Å reported by Zirin, et al. (1963) and Austin, et al. (1966), there are emission lines of highly ionized elements characteristic of the corona, but no line comparable in intensity to those just mentioned.

The disk spectra of MgII, CaII, and SiII exhibit the emission cores characteristic of the singly ionized metals and illustrated, with a central reversal, in Chapter II, Section C. The central reversal is also present. MgII has a particularly strong emission core.

In addition to assuming that all magnesium, calcium, and silicon are singly ionized in the region $500 < h < 1250$ km, we can show that it is reasonable to assume that the ground state population can be approximated by the total population of the ion. Since $T_e < 10{,}000°$ in this region, according to Table 1, we consider the most unfavorable case ($T_e = 10{,}000°$). Using partition functions from Allen (1962) and estimating the fraction of the total population lying in the ground state for each ion, we find that this fraction is greater than one-half for all three ions. Table 18 shows this. Non-LTE effects favoring the ground will enhance this result. Table 18 is derived from the relation

$$\frac{n_0}{n} = \frac{g_0}{U}, \tag{154}$$

Table 18

Ratio n_0/n of Ground State to Total Ion Populations Using Partition Functions at T_e = 10000° from Allen (1962).

Ion	Ground State	Partition Function U	n_0/n
MgII	3S	2.04	0.980
CaII	4S	3.48	0.575
SiII	3P	6.0	1.0

where g_0 and U are the statistical weight of the ground state and the partition function of the ion, respectively. Of course, $g_0 = (2S_0 + 1) \times (2L_0 + 1) = 2(2L_0 + 1)$ for the one-electron states.

Now let us consider which of the important mechanical energy sinks discussed for $500 < h < 1250$ km should be included in the final temperature calculation for this region. We shall not treat the hydrogen continua or the collisional transition for Lyβ further, even though they may absorb half the mechanical energy. Thus, an uncertainty of a factor of 2 is introduced into the amount of mechanical energy D(h) available for the other four. This uncertainty does not affect the final results to a first approximation. Table 19 contains the necessary atomic parameters for the ions we consider. The first three columns need no explanation, except that λ_0 refers to the principle line of the multiplet. $(A_{UL})_T$ in column 4 is the Einstein coefficient for spontaneous emission, calculated from

$$(A_{UL})_T = 0.667 \times 10^8 \frac{(gf)_T}{g_U \lambda_0^2}, \qquad (155)$$

Table 19

Atomic Parameters for Selected Ions. See Text for Description.
$\tau_{01} = \tau_0\,(\text{Ly}\alpha) = 10^{[3 \times 10^{-8}\,(3 \times 10^8 - h)]}$.

1	2	3	4	5	6	7	8	9	10
Ion	Transition Terms	λ_0 (Å)	$(A_{UL})_T$ (sec^{-1})	$A = \frac{g_U}{g_L} A_{UL} \lambda_0^2$	$(f_{LU})_T$	Relative Element Abundance ($\log_{10}$ scale)	a_0 (cm^2)	$\tau_0(h)$	ϵ
Hydrogen (for Hα)	$^2S - {}^2P^0$ $^2P^0 - {}^2S$ $^2P^0 - {}^2D$	6562	0.441×10^8	0.428	0.6408	12.00			
CaII	$^2S - {}^2P^0$	3933	1.51×10^8	0.700	1.05	6.22	$\frac{3.1 \times 10^{-10}}{T_e^{1/2}}$	$\tau_{01} \times 10^{-4.06}$	2.5×10^{-4}
MgII	$^2S - {}^2P^0$	2795	2.56×10^8	0.600	0.90	7.46	$\frac{1.45 \times 10^{-10}}{T_e^{1/2}}$	$\tau_{01} \times 10^{-3.15}$	9.2×10^{-5}
SiII	$^2P^0 - {}^2D$	1816	8.10×10^8	0.445	0.67	7.47	$\frac{7.5 \times 10^{-11}}{T_e^{1/2}}$	$\tau_{01} \times 10^{-3.43}$	2.5×10^{-5}

where $(gf)_T$ is the product $g_L f_{LU} = -g_U f_{UL}$ for the multiplet, g_U is the statistical weight of the upper level, and λ_0 is the wavelength in microns (Allen, 1962). Subscript T refers to the entire multiplet. The statistical weight g_k for the k-th level is given by $g_k = (2S_k + 1)(2L_k + 1)$ for the k-th level in MgII, CaII, and SiII and by $g_k = 2k^2$ for the k-th level in hydrogen. Column 5 with $A = (g_U/g_L) A_{UL} \lambda_0^2$ is self-explanatory. In column 6 f_{LU} is obtained from Allen using $f_{LU} = (gf)_T/g_L$. Column 7 follows from Table 9 of relative abundances of the elements.

Column 8 is the theoretical absorption coefficient at line center for zero radiative damping given by

$$\alpha_0 = \left(\frac{g_U}{g_L} A_{UL} \lambda_0^2\right) \frac{c}{8\pi^{3/2} \nu_0} \sqrt{\frac{M}{2kT_e}}, \tag{156}$$

where M is the mass of the absorbing ion. Equation 156 is derived in Allen (1963). It reduces further to

$$\alpha_0 = 4.06 \times 10^{16} \frac{A}{\nu_0} \sqrt{\frac{M}{T_e}}, \tag{157}$$

by our definition of $A = (g_U/g_L)(A_{UL} \lambda_0^2)$. We use α_0 to estimate the optical thickness of the chromosphere in the ionized metal lines. By assuming that the relative chemical abundance is constant with height, and recalling our assumption that all magnesium, calcium, and silicon are in the ground state of the singly ionized ion for $500 < h < 1250$ km, we can use

$$\frac{\tau_{0j}}{\tau_{0i}} = \frac{\alpha_{0j}}{\alpha_{0i}} \frac{n_{Lj}}{n_{Li}} \tag{158}$$

to estimate the ratio of optical thicknesses in different lines. Equation 158 follows immediately from the variation of τ_{0j} with $K_{0j} = \alpha_{0j} n_{Lj}$. Subscripts "i" and "j" refer to different lines. If we know $\tau_0(h)$ for one line, we can find it for the others.

If we examine Table 1 to estimate $\tau_0(h)$ for Lyα, we find that a reasonable fit to the few data points is obtained by the equation

$$\tau_0(\text{Ly}\alpha) = 10^{[3 \times 10^{-8} (3 \times 10^8 - h(\text{cm}))]}. \tag{159}$$

This is illustrated in Table 20. The fit is adequate for our purposes in the region $500 < h < 1250$ km, though we are not justified in using Equation 159 for $h > 1250$ km, where we shall actually treat Lyα itself. The scale height corresponding to Equation 159 is 145 km, the value we chose for $\rho(h)$ in the region $500 < h < 1250$ km in Section A of this chapter.

Table 20

Comparison of $\tau_{0Ly\alpha}$ vs h from PSC Model Chromosphere with Our $\tau_{0Ly\alpha}(h) = 10^{[3\times10^{-8}\ (3\times10^{8}-h)]}$ from Equation 159.

h (km)	PSC τ_0 (Lyα)	Equation 159 τ_0 (Lyα)
750	1×10^7	5.6×10^6
1000	2×10^6	1×10^6
1200	3×10^5	2.5×10^5
1250	2×10^5	1.8×10^5
1300	7×10^4	1.3×10^5

For the number density $n_{Lj}(h)$, which appears in Equation 158 for τ_{0j}, we use

$$n_{Lj}(h) = n_1(500)\,\frac{n_{Lj}}{n_H}\,e^{-(h-500)/H_2}\ ,$$

$$H_2 = 145\ \text{km}\ , \qquad (160)$$

where $n_1(500) = 8.07 \times 10^{13}$ corresponding to Equation 120 for no hydrogen ionization and mean molecular weight unity in the region $0 \le h \le 500$ km, and (n_{Lj}/n_1) is obtained from the relative abundances of Table 10.

We should mention that there is some inconsistency between our adopted scale height of 145 km for the region $500 < h < 1250$ km and Zirker's (1956) value of 200 km at a height of 500 km, slowly increasing to a value just under 300 km at a height of 1500 km. (This latter value is highly uncertain due to scatter in the data.) Zirker's results are based on his study of lines from singly ionized metals. Even if we assume that his results give $H_2 = 200$ km throughout the region $500 < h < 1250$ km, we note that this gives densities at 1250 km which are 6 times as great as those obtained with $H_2 = 145$ km in Equation 160. We use the smaller scale height for greater consistency with the PSC model of the low chromosphere, noting that our previous conclusions drawn from Zirker's work concerning single-stage ionization of the metals do not strongly depend on scale height.

In Table 19, the last column gives values of ϵ computed from

$$\epsilon \simeq 21\,\lambda_0^3\,n_e\,T_e^{-1/2}\,\bar{g}\left(1 - e^{-h\nu/kT_e}\right)\ , \qquad (161)$$

which is given in NETPRF and is derived by combining the definition of ϵ in Equation 27, C_{LU} from Equation 115, A_{LU} from Equation 155, and Equation 43 connecting C_{UL} and C_{LU} for a Maxwellian electron-velocity distribution. We use $n_e = 10^{11}$, $T_e = 10^4$, and $\bar{g} = 0.2$ to derive ϵ for singly ionized metals.

To estimate the fractional part of the mechanical energy going into the j-th energy sink (which is equivalent to estimating the quantity $\Delta_j(h)$ for the four lines we consider here), substitute Equation 160 for $n_{Lj}(h)$ into Equation 117 for $\Delta_j(h)$, use $\bar{g} = 0.2$, and approximate the net-collisional-bracket by $(NCB)_{LUj} = 1$ to derive the equation to be solved for $\Delta_j(h)$, which is

$$\Delta_j(h) = \frac{\left(\frac{n_{Lj}}{n_H}\right) f_{LUj}\, e^{-(h\nu)_{LUj}/kT_e}}{\sum_i^N \left(\frac{n_{Li}}{n_H}\right) f_{LUi}\, e^{-(h\nu)_{LUi}/kT_e}}\ , \qquad (162)$$

The $\bar{g} = 0.2$ value is very good for the three singly ionized metals and is somewhat too large for Hα, introducing a temperature-dependent error of about a factor of 2 which will give overestimation of $\Delta_j(h)$ for Hα (van Regemorter, 1962). Since the values of $\Delta_j(h)$ for Hα are less than or equal to the values for the other principle mechanical-energy sinks, this error is not serious.

Consider the assumption $(NCB)_{LU} = 1$. For Hα, this demands that $b_3 \ll b_2$. Although $b_3 < b_2$ for $500 < h < 1250$, we offer no proof that $b_3 \ll b_2$ for this region. The Pottasch and Thomas (1959) study does not apply in this region as it was done for $T_e = 10^4$. Athay (1966) reports that $(NCB)_{32} = 1$ is justified here, and offers some estimates of b_3 made by Henze which support this view. We assume that $(NCB)_{32} = 1$ in our calculation of $\Delta_j(h)$'s.

Regarding the singly ionized metals, Athay (1966) notes that the product $n_L C_{LU}$ for the MgII resonance doublet in particular may exceed the same product for Hα by as much as two orders of magnitude at $h = 500$ km. He also notes that higher opacities in singly ionized metals at a given height h should make the b_k's of the upper and lower state approach each other higher in the atmosphere, which is reasonable. Thus, allowing that $(NCB)_{LU} = 1$ where τ_0 is sufficiently small for all these lines, we would indeed expect $(NCB)_{LU}$ to approach zero (or depart from unity) higher in the atmosphere for these ionized metal lines than for Hα. How then do we justify assuming $(NCB)_{LU} = 1$ for ionized metals over $500 < h < 1250$ km without a detailed separate study of these lines, when we have every reason to believe that this may be completely wrong for the lower part of this region? We do so because our results obtained in the next section with this assumption tell us that, for any reasonable value of the mechanical-energy input obtained from the weak-shock theory, $T_e(h)$ in this region lies well below the PSC values, and that letting $(NCB)_{LU}$ approach zero midway through the region will not raise the temperature. Thus, as we shall argue presently, either more mechanical energy is being dissipated in this region than the weak shock theory gives, or the metals are not mostly ionized in this region, or severe departures from spherical symmetry are encountered in this region. Some combination of these effects might also be encountered. The point is that this conclusion is independent of how the $(NCB)_{LU}$ varies in the region $500 < h < 1250$ km.

So we perform the calculation of the Δ_j's using Equation 162 and the temperature distribution of the PSC model of Table 1, and exhibit the results in Table 21. These are interesting. The temperature dependence of the Δ_j's for CaII and MgII for the temperature range considered is rather weak, with variation of less than a factor of 2 for CaII and effectively no variation for MgII. Thus the entry of T_e into Equation 162 does not affect the grosser results of Table 21, except for the case of Hα. The two

Table 21

Values of Fractional Apportionment Coefficient Δ_j for Four Predominant Lines in the Region $500 < h < 1250$ km. $T_e(h)$ is from Table 1.

h	T_e	$\Delta_{H\alpha}$	Δ_{CaII}	Δ_{MgII}	Δ_{SiII}
500	6150	0.0154	0.4389	0.5417	0.0040
750	6650	0.0483	0.3851	0.5602	0.0064
850	6840	0.0705	0.3573	0.5652	0.0070
950	7040	0.1017	0.3311	0.5590	0.0082
1000	7150	0.1200	0.3195	0.5522	0.0083
1100	7400	0.1660	0.2861	0.5385	0.0094
1200	7700	0.2218	0.2502	0.5178	0.0102
1250	7901	0.2547	0.2420	0.4922	0.0111

dominant metal lines also greatly dominate SiII, which is not surprising at these temperatures. Finally, the lower region, where the assumption $(NCB)_{LU} = 1$ is most in error for the metal lines, is also the region where $\Delta_{H\alpha}$ is smallest, reducing the possibility that the energy delivered to the two dominant metal lines is a small fraction here.

We conclude that MgII, CaII, and Hα are important energy sinks for the region 500 < h < 1250 km. SiII may not be negligible at some height above 1250 km but it certainly is below 1250 km.

The final region where we calculate T_e is $h > 1250$ km. Here, Lyα of hydrogen is important. We showed earlier that we could exclude Lyα from the region of the singly ionized metals where the PSC model says $T_e \lesssim 8000°$ and $\tau(\text{LyC}) \gtrsim 10$ for $h \leq 1250$ km. At some higher h, where $b_1 > b_2$ so that $0 < (NCB)_{12} \lesssim 1$, the product $n_1 C_{12} (NCB)_{12} (h\nu)_{12}$ for Lyα becomes predominant. If we use $n_1 = 10^{11}$, $n_e = 10^{11}$, $T_e = 10^4$, and $C_{12} = 5 \times 10^{-2}$ from the Henze table for these conditions, we obtain $n_1 C_{12} (NCB)_{12} (h\nu)_{12} \simeq 0.08$ ergs cm^{-2} sec^{-1}, which is even larger than D(h) in this upper region, according to our weak-shock theory. However, uncertainties in our T_e, n_e, C_{12}, and $(NCB)_{12}$ in the upper region could account for this. We merely note the support given our assumption that Lyα of hydrogen should dominate the energy balance in the region immediately above, where the singly ionized metals are important.

Our further assumption that we may ignore Lyα of HeII, λ304, is supported by the calculations of Zirker (1960) already mentioned, using the admittedly questionable PSC-model upper chromosphere of Table 4 for which $T_e(h) < 50000°$. Further support is provided by the disk euv observations reported in Athay (1966) showing Lyα of HeII to be negligible. On these grounds, we include only the Lyα line of hydrogen in our temperature calculations for the upper region $h > 1250$ km. Our results support the assumption that Lyα is formed in a region for which $T_e < 50{,}000°$.

C. The Chromospheric Temperature Calculation

Our calculation of the temperature distribution is divided into three parts, corresponding to three different height regimes in the chromosphere. In what we call the "low chromosphere," we make separate calculations for two subregions: $0 \leq h \leq 500$ km, which we call the H^- region, and $500 < h < 1250$, where we calculate the temperature distribution from the MgII and CaII resonance doublets. The third region for which we calculate the temperature distribution lies at heights above 1250 km. We extend this last calculation up to small τ_0's in Lyα.

1. Temperature Distribution from H^- in $0 \leq h \leq 500$ km

This calculation employs the values of b_{H^-} obtained in the previous section (Table 13) and is therefore subject to the assumptions upon which these b_{H^-} values are based. These assumptions are 1) that we can ignore the free-free H^- opacity and induced emission; 2) $b_{H_2} \simeq 1$; 3) the PSC model chromosphere of Table 1 gives the best available representation of (n_H, T_e) for this region; 3) $D_{H,H^-} = 1.3 \times 10^{-9}$ cm^3 sec^{-1} is the best available value for the associative detachment reaction-rate constant; and 4) Equation 138, which states that $S_c = \left(b_{H^-}\right)^{-1} B_\nu(T_e)$, is a good representation of the continuum source function. We have already discussed assumptions 1, 2, and 3.

This leaves assumption 4, which is rigorously true only if H^- is the dominant source of opacity. We have already noted that this may not be true for $h \gtrsim 400$ km, because of the Paschen continuous opacity. In particular, Frisch (1967) claims that above 400 km the Paschen continuous opacity is predominant; she offers this as the reason why the Cayrel mechanism is not effective in heating the low region above 400 km, since for $b_3 = 1$ the S_c of Equation 163 (below) approaches the Planck function $B_\nu(T_e)$ as the $R_{3,fb}$ term becomes predominant.

To determine the effect of the Paschen continuum on our continuum source function S_c, we note that, with both H^- free-bound and Paschen continuous opacity considered, S_c can be written

$$S_c = B_\nu(T_e)\left[\frac{1 + R_{3,fb}}{b_{H^-} + b_3 R_{3,fb}}\right] \tag{163}$$

where $R_{3,fb} = \left(n_3^* \alpha_{3,fb}/n_{H^-}^* \alpha_{H^-,fb}\right)$. If we assume that $b_3 = 1$ for $0 \leq h \leq 500$ km, and evaluate $R_{3,fb}$ from PSC, which gives

$$R_{3,fb} \simeq \frac{4 \times 10^{15} T_e^{3/2} e^{-(\chi_{13}+\chi_{H^-})}}{n_e} , \tag{164}$$

we can evaluate the quantity $(1 + R_{3,fb})/(b_{H^-} + R_{3,fb}) = S_c/B_\nu(T_e)$ to determine the effect of the Paschen continuous opacity on the source function in this region. Using the PSC model of Table 1 for (n_e, T_e) once again, and b_{H^-} from Table 13, we compute $R_{3,fb}$ and $(1 + R_{3,fb})/(b_{H^-} + R_{3,fb})$, giving the results in Table 22. For comparison we include $(b_{H^-})^{-1}$, which equals $S_c/B_\nu(T_e)$ when $R_{3,fb}$ equals zero.

We see immediately that, for the PSC model, we can conclude that H^- continues to dominate the opacity out to 500 km, and that the continuum source function S_c is well represented by $S_c = (b_{H^-})^{-1} B_\nu(T_e)$.

Table 22

Values of $R_{3,fb}$ and Related Quantities to Illustrate S_c Dependence on Paschen Continuous Opacity.

h (km)	$10^{-11} n_e$ (cm^{-3})	T_e (°K)	$R_{3,fb}$	b_{H^-}	$\frac{1 + R_{3,fb}}{b_{H^-} + R_{3bf}}$	$(b_{H^-})^{-1}$
0	6.36	5050	3.32×10^{-4}	1.06	0.943	0.943
100	5.04	5250	1.37 (-3)	1.18	0.848	0.847
200	4.65	5460	4.72 (-3)	1.37	0.731	0.730
300	4.58	5680	1.47 (-2)	1.65	0.610	0.606
400	4.63	5910	4.29 (-2)	1.94	0.526	0.515
500	4.72	6150	0.119	2.24	0.474	0.446

We now use the $b_{H^-}(h)$ of Table 13 along with the approximation $S_c = (b_{H^-})^{-1} B_\nu(T_e)$ to calculate $T_e(h)$ in the region $0 \leq h \leq 500$ km. Our conservation equation for this region becomes

$$D(T_e) = 2\sigma K^*_{H^-} \left[2T_e^4 - (b_{H^-}) T_{eff}^4 \right] ; \tag{165}$$

Table 23

Values of T_e (h) for $0 \leq h \leq 500$ km.

h (km)	$K^*_{H^-}$ (cm^{-1})	b_{H^-}	T_e (°K)	T_e (PSC)(°K)
0	6.31×10^{-11}	1.06	4980	5050
100	1.87 (-11)	1.18	5090	5250
200	6.66 (-12)	1.37	5320	5460
300	2.64 (-12)	1.65	5655	5680
400	1.09 (-12)	1.94	5985	5910
500	4.71 (-13)	2.24	6285	6150

this is exactly like Equation 145, which we used to estimate the excess of emission over absorption in H^-, except that here we identify the left-hand side with the local mechanical-energy input. $D(T_e)$ is always given by Equation 84. Using the same $K^*_{H^-}$ and b_{H^-} as in this last section, and $T_{eff} \approx 5800°$ again, we calculate the T_e (h) given in Table 23, which includes T_e (h) from the Table 1 PSC model for comparison. Commensurate with the uncertainties in $D(T_e)$, the agreement is quite good.

This temperature calculation offers only a consistency check on the temperature distribution of the PSC model and does not prove this the best model available for the low chromosphere in the light of current observations. Nevertheless, in spite of our disbelief in a boundary temperature as high as 5000°, this is as reasonable a distribution as we know to date for $0 \leq h \leq 500$ km, and it leaves unchanged the PSC conclusion that there is an appreciable rise of the order of 1000° in the first 500 km.

2. Temperature Distribution from CaII and MgII in 500 < h < 1250 km

Here, we apply the method of Chapter III to calculate the temperature distribution in this upper portion of the lower chromosphere. We have already shown that MgII and CaII are the predominant mechanical-energy sinks among the singly ionized metals studied in Section B of this chapter. SiII was shown to absorb $\lesssim 1.0$ percent of the mechanical energy as long as $T_e \lesssim 8000°$. Hα was shown to be an important mechanical-energy sink, but because the source function for Hα is of the photoionization type discussed in Chapter II, we shall restrict the temperature calculation to the resonance doublets of MgII and CaII, for which we assume a two-level atom source function of the form of Equation 30,

$$S_\ell = \frac{\int J_\nu \phi_\nu \, d\nu + \epsilon B_\nu(T_e)}{1 + \epsilon} , \tag{30}$$

for which the solution to the transfer equation is particularly simple.

Table 24

Calculated Values of Mechanical Dissipation Term $(2/A_j)(D_j/n_{Lj})$ for CaII and MgII with Local Values of Selected Representations $C_j\, e^{-\beta_j \tau_{0j}}$ from Equations 166 and 167.

h (km)	$\left[\frac{2}{A_j}\frac{D_j}{n_{Lj}}\right]_{CaII}$	$\left[Ce^{-\beta\tau_0}\right]_{CaII}$	$\left[\frac{2}{A_j}\frac{D_j}{n_{Lj}}\right]_{MgII}$	$\left[Ce^{-\beta\tau_0}\right]_{MgII}$
500	0.000	1.71×10^{-12}	0.000	7.50×10^{-15}
750	1.91×10^{-10}	1.57×10^{-10}	1.86×10^{-11}	1.16×10^{-11}
850	2.55×10^{-10}	2.56×10^{-10}	2.70×10^{-11}	2.57×10^{-11}
950	3.17×10^{-10}	3.28×10^{-10}	3.59×10^{-11}	3.83×10^{-11}
1000	3.40×10^{-10}	3.53×10^{-10}	3.94×10^{-11}	4.29×10^{-11}
1100	3.71×10^{-10}	3.85×10^{-10}	4.68×10^{-11}	4.94×10^{-11}
1200	3.83×10^{-10}	4.01×10^{-10}	5.30×10^{-11}	5.30×10^{-11}
1250	4.19×10^{-10}	4.07×10^{-10}	5.70×10^{-11}	5.42×10^{-11}

As a preliminary to the calculations, we substantiate the claim, made in Chapter III, that we can represent the line source function S_ℓ in the form

$$S_\ell = \int J_\nu \phi_\nu \, d\nu + Ce^{-\beta\tau_0} , \tag{100}$$

for both the MgII and CaII resonance doublets. In terms of the parameters of Section B of this chapter, this means that Equation 99,

$$C_j\, e^{-\beta_j \tau_{0j}} \simeq \left(\frac{2}{A_j}\right)\frac{D_j}{n_{Lj}} , \tag{99}$$

must be fulfilled, where the "j" refers to a particular line. We can easily show that this representation is possible. Table 24 compares $(2/A_j)(D_j/n_{Lj})$ with $C_j \exp\{-\beta_j \tau_{0j}\}$ for MgII and CaII. The A_j are obtained from Table 19. The D_j are obtained from Equation 81 and the Δ_j of Table 21. Finally, the n_{Lj} are obtained from the assumptions of constant chemical composition with height, using the relative chemical abundances by number in Table 9, and a density scale height of 145 km, where we assume all hydrogen to be neutral at $h = 500$ km and all magnesium and calcium to be in the ground state of the first ionization stage throughout $500 < h < 1250$ km, to obtain absolute values of n_{Lj}. The values of C_j and β_j used for the CaII and MgII resonance doublets, respectively, are

	For CaII	For MgII
C_j	4.2×10^{-10}	5.7×10^{-11}
β_j	$10^{-2.7}$	$10^{-3.4}$

Substituted in $Ce^{-\beta\tau_0}$, these give

$$\left[Ce^{-\beta\tau_0}\right]_{CaII} = 4.2 \times 10^{-10}\, e^{-(10^{-2.7})\tau_0(CaII)} , \tag{166}$$

and

$$\left[Ce^{-\beta\tau_0}\right]_{MgII} = 5.7 \times 10^{-11}\, e^{-(10^{-3.4})\tau_0(MgII)} . \tag{167}$$

Table 24 amply justifies our choice of (C_j, β_j) for each line. Equations 166 and 167 are now used to calculate the temperature distribution.

First we solve the transfer equation for each line in the manner outlined in Chapter III, to derive

$$\int J_\nu \phi_\nu \, d\nu \simeq \sum_i^3 \alpha_i J_i$$

for each line. We use Equations 166 and 167 in the source function, which is of the form 100 in the transfer equation. We shall also solve the transfer equation for a second set of $C_j\, e^{-\beta_j \tau_{0j}}$ for each line, for reasons that appear soon. This second set is

$$\left[Ce^{-\beta\tau_0}\right]_{CaII} = 4.2 \times 10^{-9}\, e^{-(10^{-2.7})\tau_0(CaII)} , \tag{168}$$

and

$$\left[Ce^{-\beta\tau_0}\right]_{MgII} = 5.7 \times 10^{-10}\, e^{-(10^{-3.4})\tau_0(MgII)} . \tag{169}$$

The actual solution of the transfer equation follows the method outlined in Chapter III and developed in detail in Appendix C. The results are

$$\sum_i^3 \alpha_i J_i = 2.497 \times 10^{-6} - 1.822 \times 10^{-8-.286\tau_0} + \cdots$$

$$- 2.830 \times 10^{-7-.0195\tau_0} - 0.8772 \times 10^{-6-.000868\tau_0}$$

$$- 1.2929 \times 10^{-6-.000041\tau_0} \text{ for CaII, corresponding to Equation 166 ;} \tag{170}$$

$$\sum_i^3 \alpha_i J_i = 2.513 \times 10^{-7} - 7.895 \times 10^{-9-.286\tau_0} + \cdots$$

$$- 1.187 \times 10^{-7-.0195\tau_0} - 3.3529 \times 10^{-6-.000174\tau_0}$$

$$+ 3.2396 \times 10^{-6-.000041\tau_0} \text{ for MgII, corresponding to Equation 167 ;} \qquad (171)$$

$$\sum_i^3 \alpha_i J_i = 2.497 \times 10^{-6} - 1.660 \times 10^{-7-.286\tau_0} + \cdots$$

$$- 2.586 \times 10^{-6-.0195\tau_0} - 8.772 \times 10^{-6-.000868\tau_0}$$

$$+ 9.263 \times 10^{-6-.000041\tau_0} \text{ for CaII, corresponding to Equation 168 ;} \qquad (172)$$

and

$$\sum_i^3 \alpha_i J_i = 2.513 \times 10^{-7} - 8.098 \times 10^{-8-.286\tau_0} + \cdots$$

$$- 1.164 \times 10^{-6-.0195\tau_0} - 3.3530 \times 10^{-5-.000174\tau_0}$$

$$+ 3.4629 \times 10^{-5-.000041\tau_0} \text{ for MgII, corresponding to Equation 169 .} \qquad (173)$$

To obtain a temperature distribution from these solutions, rewrite Equation 119

$$B_\nu(T_e) = \frac{1+s}{\epsilon} Ce^{-\beta\tau_0} + \frac{s}{\epsilon}\int J_\nu \phi_\nu \, d\nu \ ,$$

where the sink term $s = \epsilon + \eta$ becomes $s \simeq \epsilon$ for the CaII and MgII resonance doublets. To obtain $T_e(h)$, we use the $\tau_0(h)$ relations for these doublets derived in Section B and given in Table 19. The results of the temperature calculation are given in Table 25.

To interpret Table 25, note that $T_{e_{CaII}}(1)$ and $T_{e_{MgII}}(1)$ both correspond to the set of parameters represented by Equations 166 and 167, i.e., the initial set obtained from all the assumptions and estimates made so far. On the other hand, the $T_{e_{CaII}}(2)$ and $T_{e_{MgII}}(2)$ correspond to the set of parameters represented by Equations 168 and 169, which differ from the first set in that the coefficient C has been increased by one order of magnitude.

Table 25

Results of T_e (h) Calculation for 500 < h < 1250 km Based on CaII and MgII Resonance Doublets. $T_{e_{CaII}}$ (1) and $T_{e_{MgII}}$ (1) Correspond to Equations 170 and 171. $T_{e_{CaII}}$ (2) and $T_{e_{MgII}}$ (2) Correspond to Equations 172 and 173.

h (km)	$\tau_{0_{CaII}}$	$T_{e_{CaII}}$ (1)	$T_{e_{CaII}}$ (2)	$\tau_{0_{MgII}}$	$T_{e_{MgII}}$ (1)	$T_{e_{MgII}}$ (2)
600	1.38×10^3	4360	5783	1.12×10^4	5412	7029
750	4.91×10^2	4413	6024	3.99×10^3	5624	7476
1000	87.3	4512	6279	7.10×10^2	5364	7038
1250	15.5	4501	6271	1.78×10^2	5187	6745

We first note that the temperatures obtained from the first set of parameters are too low, particularly for CaII. Even if our value of 6285° at 500 km, obtained from the H^- calculations, is somewhat high, it is not reasonable, in the light of everything we have done so far, for T_e at that height to be much below 6000°K. Retaining our spherically symmetric model for the moment, we see three possibilities: 1) The parameter ϵ may have been overestimated. Equation 119 with $s = \epsilon << 1$, shows that, if ϵ were smaller, the term $\left[(1+\epsilon)/\epsilon\right] \cdot C \exp\{-\beta\tau_0\}$ would be increased without change of parameter C. 2) We may have underestimated the local mechanical dissipation, owing perhaps to a breakdown of the weak-shock theory. 3) Our assumption that all magnesium and calcium atoms are singly ionized in this region may be wrong. Both alternatives 2 and 3 would require that the parameter C be increased. To verify this, see Equation 99. We consider these possibilities in turn.

Since the values of $(n_e, T_e) = (10^{11}, 10^4)$, which we used to estimate the values of ϵ for these lines, give slightly smaller values than would be obtained from any combination of (n_e, T_e) taken from the PSC model of Table 1, this would at least partially compensate for any errors in Equation 161, used to obtain ϵ. Also, if we look at Equation 170, which is our

$$\sum_i^3 \alpha_i J_i$$

for CaII for the first set of parameters (C,β), we note that there is a monotonic outward decrease of the radiation field, which does not appear in the other solutions, Equations 171-173, until some distance out in the atmosphere has been reached. This lack of an increase in

$$\sum_i^3 \alpha_i J_i$$

is not compatible with the observed emission core in the line profile of the H and K lines seen on disk spectra. Increasing ϵ will not change this, but a sufficient increase in the parameter C will, as illustrated by the solution, Equation 172, for these lines, where only C has changed among all the parameters.

On these grounds, we reject the possibility that an error in ϵ is responsible for our low $T_e(h)$ values obtained with the first set of parameters.

Table 26

Values of Local Mechanical Dissipation D(h) for the Region 500 < h < 1250 km.

h (km)	D(ergs cm^{-3} sec^{-1})	h	D
500	0.030	1000	0.0024
750	0.010	1100	0.0013
850	0.0058	1200	0.00074
950	0.0033	1250	0.00055

We must now consider which of our alternatives, 2) or 3), offers the more likely explanation for the increase in parameter C needed to raise the temperature. To determine this, it is useful to obtain the mechanical energy input $D(h)$ and $\int D(h)dh$ for this region. $D(h)$ from Equation 81 is given in Table 26 for the PSC model chromosphere in the region 500 < h < 1250 km. Table 26 shows that $\int D(h)dh$ for the entire region yields approximately 5×10^5 ergs cm^{-2} sec^{-1}. From this estimate and the contribution from the lower H^- region, we find that the total mechanical energy dissipated below 1250 km is only about 1.5×10^6 ergs cm^{-2} sec^{-1}. The fact that our estimates of the total efflux of mechanical energy from the photosphere give more than an order of magnitude more mechanical energy than this value shows that there might be enough mechanical energy available to substantially increase the amount of chromospheric heating by shock dissipation. Also, the fact that the shock strength parameter η_s becomes a significant fraction of unity in the region 500 < h < 1250 km (which makes the weak-shock theory of doubtful validity) indicates that $D(h)$ might be substantially larger than the initial values we have computed. Finally, we recall the arguments of Zirker in favor of single ionization for these metals in this region. From these considerations, we conclude that present evidence favors an increase in local mechanical-energy dissipation over a decrease in the ionization of the metals in this region. In any event, either or both of these effects will increase the parameter C, and this in turn will increase $T_e(h)$, as we readily see from $T_{e_{CaII}}(2)$ and $T_{e_{MgII}}(2)$ in Table 25.

The manner in which $T_e(h)$ varies with h presents a further problem. For CaII, $T_e(h)$ increases with h at least out to 1000 km, though the increase is slow. But for MgII, $T_e(h)$ begins to drop somewhere between 750 and 1000 km. This is not a realistic temperature distribution, at least not in the outer part of the region. Possibly our single exponential representation of the mechanical dissipation in Equation 100 is inadequate, and an additional exponential term or terms may be required to account for an increase in mechanical dissipation in the smaller τ_0 region. An increase in β would place the mechanical dissipation relatively farther out and change the shape of the temperature distribution. Such an increase in β for the MgII doublet is reasonable, since it is doubtful that the assumption $(NCB)_{LU} = 1$ is valid for this doublet in the lower part of the region in question owing to the large optical thickness, and beginning to decrease $(NCB)_{LU}$ at a higher point in the atmosphere has the effect of increasing β.

Also, we do not obtain the same distribution $T_e(h)$ from MgII and CaII with either set of parameters (C,β). This means that our original conservation Equation 94 is not strictly satisfied. We could develop an iterative program to obtain a convergent temperature distribution in this two-line region. This should be done when we have more confidence in the mechanical-heating term $D(h)$ and good estimates for $(NCB)_{LU}$ as a function of τ_0 for the lines. Under present circumstances, this would be an unrewarding numerical exercise.

What can we conclude about $T_e(h)$ in this region from these calculations? Obviously, we must set bounds to the temperature in the region $500 < h < 1250$ km. We cannot find the temperature gradient without a better knowledge of the $(NCB)_{LU}$'s. As a lower limit, we would choose 6000°, in the light of our H^- study. As an upper limit, we would select 7500°, on the grounds that this value, calculated for the MgII doublet, is the peak temperature reached anywhere in the region. On the other hand, the fact that our analysis does not adequately cover the outer, low τ_0 region does not eliminate the possibility that T_e may reach higher values. These limiting values, along with all our calculated values, are plotted in Figure 4 at the end of this section.

A "plateau effect" appears in the T_e distribution for CaII, but since this depends ultimately on our choice of $D(h)$, which is poorly known, this might be accidental. Such an effect is barely discernable in the MgII distribution of $T_e(h)$.

3. Temperature Distribution from Hydrogen Lyα for h > 1250 km

We do not extend the calculations for the region of the singly ionized metals beyond $h = 1250$ km, because we have no reason to believe that the homogeneous low chromosphere extends beyond this height. Indeed, we have already noted the evidence of House (1961) which suggests that spicules may originate as low as 700 km, so some of our previous calculations for an assumed homogeneous region between 700 and 1250 km may be subject to modification on this account. We showed at the end of Section B of this chapter why we should expect Lyα to become the dominant energy sink above the region of the singly ionized metals. We now proceed to calculate $T_e(\tau_0)$ from Lyα.

The results we now give for $T_e(\tau_0)$ from Lyα pertain to heights above 1250 km. We do not attempt to relate τ_0 to h because our knowledge of this upper chromospheric region is too poor. We shall refer briefly to the PSC model of the upper chromosphere for estimating parameters for the Lyα temperature calculation.

We start the Lyα calculation with a study of the Lyα source function. Using Equation 161 for ϵ, with the mean Gaunt factor $\bar{g}$ given by 0.034 for $T_e = 10^4$ and 0.124 for $T_e = 10^5$ from the van Regemorter (1962) study, we obtain for ϵ:

$$\left.\begin{aligned} n_e &= 10^{10},\ 10^{11} \\ T_e &= 10^4 \end{aligned}\right\} \epsilon = 1.28 \times 10^{-7},\ 1.28 \times 10^{-6}\ , \qquad (174)$$

$$\left.\begin{array}{l} n_e = 10^{10},\ 10^{11} \\ \\ T_e = 10^5 \end{array}\right\} \epsilon = 1.48 \times 10^{-7},\ 1.48 \times 10^{-6} . \qquad (175)$$

We make the temperature calculation for both $\epsilon \simeq 10^{-6}$ and 10^{-7}. The value 10^{-6} corresponds more closely to the upper chromospheric model of PSC.

Evaluating parameter η from Equation 33 gives $\eta = 4.3 \times 10^{-5}$, where $T_{r1} = 6900°K$, $T_{r2} = 6000°K$, and the dilution factor W_{K1} equals 1/2. Thus, we conclude that, even for $n_e = 10^{11}$ and $\epsilon = 10^{-6}$, $\eta >> \epsilon$ is a good approximation.

So far, we have reproduced the results of Morton and Widing (1961). The approximation $\epsilon B_\nu(T_e) >> \eta B^*$ is more marginal for our purposes than in their case, because they overlooked the possibility that T_e may be as low as 10^4 at the base of the Lyα region, and considered only $T_e \geq 2 \times 10^4$ for which $\epsilon B_\nu(T_e) >> \eta B^*$ is liberally fulfilled. Using $T_{r1} = 6900°$ again, we obtain ηB^* as $0.1574 \cdot \exp(-Y_1)/Y_1$ using Equations 33 and 34 and evaluating the atomic constants. This yields $\eta B^* = 8.06 \times 10^{-13}$. The worst possible case for $\epsilon B_\nu(T_e)$ corresponds to $(n_e, T_e) = (10^{11},\ 10^4)$, since $n_e \gtrsim 10^{11}$, $T_e \gtrsim 10^4$ at the base of our Lyα region. For these values, $\epsilon B_\nu\ T_e = 2.04 \times 10^{-12}$. Thus, at worst, $\epsilon B_\nu(T_e) \gtrsim 2.4 \eta B^*$. Indeed, for $T_e = 1.2 \times 10^4$, we already have $\epsilon B_\nu(T_e) \gtrsim 14.0\, \eta B^*$. Therefore, we adopt the approximation $\epsilon B_\nu(T_e) >> \eta B^*$, and our results show that this is reasonable. The source function for Lyα is indeed of the form given by Morton and Widing and discussed in Chapter II, namely,

$$S_\ell = \frac{\int J_\nu \phi_\nu\, d\nu + \epsilon B_\nu(T_e)}{1 + \eta} . \qquad (35)$$

When the expression for S_ℓ of Equation 35 and the form in Equation 100 are equated, we again obtain the equation for T_e in the form of Equation 119, only now the approximation $s = \eta$ is used for the sink term.

Proceeding exactly as with MgII and CaII, we first obtain (C, β) from $C_j \exp\{-\beta_j T_0\} \simeq (2/A_j) D_j / n_{Lj}$, where "j" now refers to Lyα. For Lyα, $A_j = 0.059$. We obtain D_j from Equation 81, where we assume that $D_j = D$ in this upper region. To calculate D, we need the density scale height for $h > 1250$ km. We approximate this by the emission scale height for Paα of HeII at $\lambda 4686$, reported in PSC as 2.22×10^8 cm. We also need $\rho(h = 1250\ \text{km})$, so that we can use

$$\rho(h) = \rho(1250)\, e^{-(h-1250)/H_3}, \qquad H_3 = 2220\ \text{km} , \qquad (176)$$

to obtain the absolute value of $\rho(h)$ at a given height. For $\rho(1250)$, we use Equation 131 which estimates $\rho(h)$ for the low chromosphere above 500 km. We obtain $\rho(1250) = 8.0 \times 10^{-13}$ gm cm^{-3}.

Table 27

Estimates of Neutral Hydrogen Densities for the Upper Chromosphere.

h (km)	T_e (Table 4)	n_{L1}^*		b_1	n_{L1} (estimate)
		$n_e = 10^{11}$	$n_e = 10^{10}$		
1500	23440	9.5×10^2	9.5	10^3-10^4	10^5-10^7
2000	36550	43	0.43	10^4-10^5	10^5-10^7
3000	42130	20	0.20	10^6	10^6-10^7

Corresponding roughly to the two values of the shock strength $\eta_s = 0.5, 1$, there are two different values for the mechanical energy input D, one an order of magnitude higher than the other.

To derive n_{L1}, we solve the Saha equation for $n_1^* \simeq [n\ (\text{neutral})]^*$. Then we estimate values for the departure coefficient b_1 in the upper chromosphere (using the Table 4 model of the upper chromosphere) and, from these, estimate n_{L1}. The Saha equation for hydrogen can be written

$$n_1^* = 4.11 \times 10^{-16} \frac{n_e n_p}{T_e^{3/2}} e^{157,000/T_e} . \tag{177}$$

If we solve for n_1^*, we obtain the results tabulated in Table 27, assuming $n_p = n_e$ for the calculation. There we also give our estimates of b_1 obtained from the early Thomas (1948b) and the previously mentioned Thomas and Pottasch (1959) studies of b_1. From Table 27, we conclude that n_{L1} lies in the range 10^5 - 10^7 in the upper chromosphere.

There is considerable uncertainty in the values of the parameters (C, β) to be used to represent the term $(2/A_j) D_j / n_{Lj}$ for Lyα. These uncertainties arise from the high approximate values we must use for the mass density $\rho(h)$, the neutral hydrogen particle density n_{L1}, and the shock strength parameter η_s. One way to assure a reasonable estimate is to demand that the mechanical

Table 28

Temperature Distribution as a Function of τ_0 (Lyα).

τ_0 (Ly-α)	$n_e = 10^{11}$ (cm^{-3})		$n_e = 10^{10}$ (cm^{-3})	
	$C_1 = 10^{-11}$	$C_2 = 10^{-10}$	$C_1 = 10^{-11}$	$C_2 = 10^{-10}$
$10^{4.5}$	9,865	12,205	12,205	16,000
10^3	12,225	16,035	16,035	23,368
10^2	11,995	15,640	15,640	22,480
10	11,928	15,527	15,527	22,151
0	11,851	15,397	15,397	21,970

energy input corresponding to the chosen values of (C,β) must equal the net radiative loss inferred from the observed Lyα line profile. The net flux per c.p.s. and steradian is given by $\int C \exp\{-\beta\tau_0\, d\tau_0\}$ between limits 0 and ∞. Multiplying by $4\pi|\Delta\nu| = 4\pi c|\Delta\lambda|/\lambda^2$, where $|\Delta\lambda|$ is the line width at half maximum, gives an estimate of the net flux in ergs cm^{-2} sec^{-1}.

If we represent the expression $C \exp\{-\beta\tau_0\}$ for Lyα by

$$\left[C\, e^{-\beta\tau_0}\right]_{Ly\alpha(1)} = 10^{-11}\, e^{-(10^{-2.7})\tau_0}\,, \tag{178}$$

$$\left[C\, e^{-\beta\tau_0}\right]_{Ly\alpha(2)} = 10^{-10}\, e^{-(10^{-2.7})\tau_0}\,, \tag{179}$$

we can estimate the net flux for each set (C,β) in the manner just prescribed. For $(C,\beta) = (10^{-11}, 10^{-2.7})$ of Equation 178, we obtain 1.28×10^5 ergs cm^{-2} sec^{-1}. For $(C,\beta) = (10^{-10}, 10^{-2.7})$ of Equation 179, we obtain 1.28×10^6 ergs cm^{-2} sec^{-1}. In both cases, we have used $|\Delta\lambda| = 10^{-8}$ cm = 1Å. The Hinteregger (1964) observed flux in Lyα of 3×10^5 ergs cm^{-2} sec^{-1} is spanned by the above values. Since these values also agree in order of magnitude with estimates of $(2/A_j)D_j/n_{Lj}$, based on the values of $\rho(h)$, n_{L1}, and η_s already considered, we accept Equations 178 and 179 for the temperature calculation.

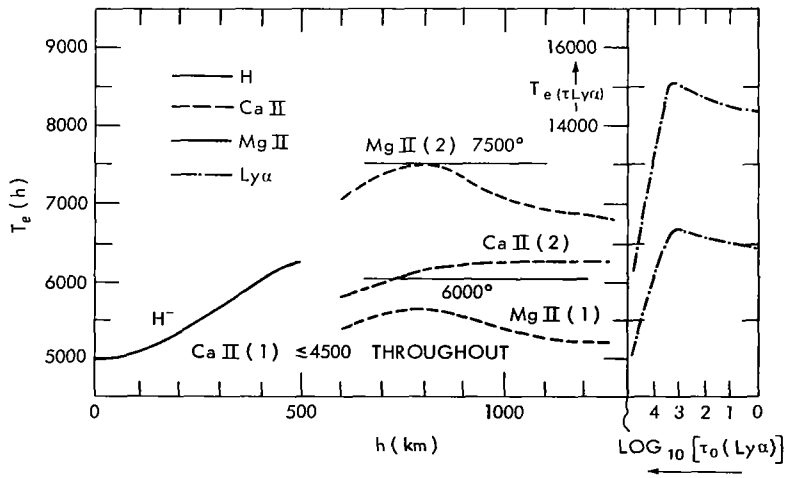

Figure 4—Graph of T_e (h) obtained from H, CaII, (1,2), MgII (1,2), and $T_e(T_0)$ from Lyα.

The temperature calculation proceeds exactly as before for MgII and CaII. The results are given in Table 28 and exhibited graphically in Figure 4. A discussion of all results, including these for Lyα, is now in order.

Chapter V

CONCLUSIONS

In the lowest region $0 \leq h \leq 500$ km, we have calculated the temperature distribution taking into account both the shock dissipation of acoustic waves and the departure of the continuum source function from the Planck function. The contribution of this latter, non-LTE effect is determined by the departure from unity of the coefficient $b_{H^-}(h)$, whose values we have calculated for the PSC-model chromosphere.

Can the departure of b_{H^-} from unity cause the temperature rise in the low chromosphere without any mechanical dissipation, i.e., in radiative equilibrium? This is the question raised by Cayrel (1963), who concluded that it is possible in the low chromosphere. In the strictest sense this situation does not seem to be met, because of the incompatibility of radiative equilibrium and departures from LTE in the H^- ionization; this is demonstrated below.

The statistical equilibrium condition for the bound level of H^-, expressed by Equation 141, can also be written in the form

$$4\pi \left[n^*_{H^-} \int_{\nu_0}^{\infty} \frac{B_\nu (T_e)}{h\nu} \alpha_{\nu H^-} \, d\nu - n_{H^-} \int_{\nu_0}^{\infty} \frac{J_\nu}{(h\nu)} \alpha_{\nu H^-} \, d\nu \right]$$

$$= n_e n_{H^-} D_{e,H^-} \left(1 - \frac{1}{b_{H^-}} \right) + n_H D_{H^-} D_{H,H^-} \left(1 - \frac{b_{H_2}}{b_{H^-}} \right) , \qquad (180)$$

The energy-balance equation for H^- ionization can be written

$$4\pi \left[n^*_{H^-} \int_{\nu_0}^{\infty} B_\nu (T_e) \alpha_{\nu H^-} \, d\nu - n_{H^-} \int_{\nu_0}^{\infty} J_\nu \alpha_{\nu H^-} \, d\nu \right]$$

$$= n_e n_{H^-} \left[\overline{D_{e,H^-} (h\nu)} \right] \left(1 - \frac{1}{b_{H^-}} \right) + n_H n_{H^-} \left[\overline{D_{H,H^-} (h\nu)} \right] \left(1 - \frac{b_{H_2}}{b_{H^-}} \right), \qquad (181)$$

where the bars over the brackets mean the enclosed quantities are suitably averaged over energies from $(h\nu_0)$ to ∞. Cayrel, in effect, equated the left-hand sides of these two equations to zero, which

corresponds to radiative equilibrium, as Equation 181 shows. He then solved the resulting equations for b_{H^-} and the temperature in the chromosphere corresponding to a suitable dilution factor for the photospheric background radiation field. The b_{H^-} enters the equations through $b_{H^-} = n_{H^-}/n^*_{H^-}$, after which n_{H^-} cancels out of both of the equations Cayrel used.

However, Frisch (1966) concluded that $b_{H_2} = 1$ for the low chromospheric region under discussion. When $b_{H_2} = 1$, the only time Cayrel's equations are valid is for $b_{H^-} = 1$, as indicated by either or both of Equations 180 and 181. Thus, Cayrel's procedure, which yields $b_{H^-} > 1$ ($\sim$1.3), is invalid in the low chromosphere if $b_{H_2} = 1$. It does not seem possible (*is* not possible if $b_{H_2} = 1$) for departures from LTE in the H^- ionization to exist in the low chromosphere in radiative equilibrium. Therefore, the temperature rise cannot be produced solely by non-LTE ionization of H^- in radiative equilibrium.

It is interesting to consider the relative contribution of the radiation field and mechanical-energy input in determining the temperature distribution in the light of these conclusions. Recalling that we have used the symbol D, without subscripts, to represent the mechanical energy input in ergs cm^{-3} sec^{-1}, we can write

$$D = \left[\left\{n_e \left[\overline{D_{e,H^-}(h\nu)}\right]\right\} + \left\{n_H \left[\overline{D_{H,H^-}(h\nu)}\right]\right\}\right] \cdot \left[n_{H^-}\left(1 - \frac{1}{b_{H^-}}\right)\right] , \qquad (182)$$

for the mechanical input, where $b_{H_2} = 1$ has been assumed. It follows directly from Equation 182 that, as b_{H^-} increases ($b_{H^-} \geq 1$), D increases, and vice versa. So in that part of the low chromosphere where H^- dominates the continuum opacity, the non-LTE effect corresponding to a departure of b_{H^-} from unity and the mechanical heating of the gas go hand in hand. This is exactly what we would expect on physical grounds. We can envision a cycle of collisional and radiative ionization (with the associative detachment reaction $H + H^- \rightarrow H_2 + e$ dominating the collisional ionization) followed by collisional and radiative recombination, where the collisional ionizations minus the collisional recombinations, representing the increase in mechanical energy, are just balanced by the excess radiative emission, obtained from the radiative recombinations minus the radiative ionizations.

A comment on the Frisch (1967) model of the low chromosphere is now in order. We have already noted her claim that the Paschen continuum opacity predominates over the H^- bound-free opacity for $h \gtrsim 400$ km. As she assumes $b_3 = 1$ for the Paschen continuum, the departure of the continuum source function from the Planck function is less under these conditions than in our calculations.

We have estimated the ratio $R_{3,fb}$ of the Paschen continuum opacity to the H^- bound-free opacity in Table 22, for the PSC model chromosphere, and the results show that this ratio reaches a maximum of 0.119 at $h = 500$ km. Why is there such a discrepancy between Frisch's and our results?

It is not easy to answer this question, but we can make the following observations. Frisch states that, above 400 km, the Paschen continuum opacity predominates, but she does not say how she

arrives at this. She arrives at her final models by solving a system of rate-process and energy-balance equations plus an equation of state. If we use the (P_e, T_e) values from her final models, compute $n_e(P_e, T_e)$ and take Equation 164 to compute $R_{3,fb}$, we derive for her models I, II, and III, respectively: ($n_e = 3.98 \times 10^{10}$, $R_{3,fb} = 0.0045$), ($n_e = 2.67 \times 10^{11}$, $R_{3,fb} = 0.142$), and ($n_e = 9.6 \times 10^{10}$, $R_{3,fb} = 0.269$) at those heights nearest to 400 km among her tabulated values. Ignoring the first set (which is for her zero mechanical dissipation case), we conclude that her statement on the Paschen continuum opacity still does not seem consistent with her results, which predict conditions similar to those of the PSC model. This conclusion is true even though her $n_e(h)$ lie below the $n_e(h)$ of PSC in Table 1, and we see from Equation 164 that $R_{3,fb}$ varies inversely with n_e. Her results and Equation 164 support the conclusion that the H^- bound-free opacity dominates the lower region $0 \leq h \leq 500$ km. Thus, we retain the conclusion that the H^- bound-free opacity is dominant.

The reasonable conformity between our calculated temperature distribution and that of the PSC model of Table 1 tends to confirm the conclusion that T_e rises at least 1000° from $h = 0$ to $h = 500$ km. This suggests a lower limit of $T_e \simeq 6000$°K at $h = 500$ km, a value lying somewhat below our calculated value and that of Table 1 (6150° and 6285°, respectively). We should note, however, that we have established only that the PSC model offers a reasonable description of the H^- region in view of our results. We have not, in any sense, proved that the PSC model is correct. Nor have we considered the possibility that the type of consistency test we applied to the H^- region of the PSC model might not apply equally well to another model. So the possibility that the temperature at $h = 500$ km may lie below 6000°K does exist, though this higher value seems more probable.

The results of the temperature calculation in the next higher region above 500 km present several problems. The numerical problem of convergence of the two temperature profiles obtained from MgII and CaII is easy to solve, with convergence assured in the two-line case, but the solution would offer no useful information until a more detailed study of the $(NCB)_{LU}$'s has been completed. So we shall consider this problem no further here. This leaves the following problems:

I. In that portion of the chromospheric gas found in the region $500 < h \leq 1250$ km (and as long as we retain the assumption of spherical symmetry there, this means all the gas in the region), we concluded that either 1) an order of magitude more energy ($\sim 5 \times 10^6$ ergs cm^{-2} sec^{-1}) is needed to satisfy T_e (min) $\simeq 6000$°K at $h = 500$ km for the two lines treated than is provided by rough estimates of the available mechanical energy given by the weak-shock theory, or 2) the magnesium and calcium are predominately neutral in this region, in conflict with Zirker's conclusions reported in Section B of this chapter.

II. The net radiative loss from the MgII doublet corresponding to the first set of the heating parameters (C,β) agrees to within a factor of 2 with Osterbrock's (1961) estimate of 2.5×10^5 ergs cm^{-2} sec^{-1}, thus placing it about an order of magnitude above the observationally based Osterbrock value for the second set of (C,β), which represent more heating.

III. The net radiative loss from the CaII doublet is significantly larger in calculated than in observed values, even for the lower values of the heating parameters (C,β). The flux in H and K is estimated in the Osterbrock study as $\gtrsim 10^4$ ergs cm^{-2} sec^{-1}, while the lower values for (C,β) correspond to $> 10^5$ ergs cm^{-2} sec.

IV. The temperature gradients obtained from the line calculations are wrong—at least in the outer part of the region.

V. Possible departures from spherical symmetry have so far been ignored. Fredga's (1966) spectroheliograms of the Sun in MgII λ2802.7 confirm the idea that most of this emission comes from essentially the same regions as the CaK_2 emission. Thus, severe departures from spherical symmetry, apparently associated with the magnetic-field structure, are virtually assured.

Let us consider these problems in turn. We have already mentioned the possibility that the weak-shock theory, valid only for values of the shock-strength parameter $\eta_s < 1$ (how much less is difficult to establish), might break down for values of η_s approaching unity in this region. If this happens, we have underestimated the mechanical heating, and the correct value would be in the right direction to produce the higher temperatures.

Zirker's (1956) conclusion that the metals should be singly ionized in this region seems well founded, the chief source of error in his study being the data from the 1952 eclipse. Of the two alternatives, 1) mechanical dissipation in the regions producing emission from the singly ionized metals significantly exceeds 10^6 ergs cm^{-2} sec^{-1} or, 2) those metals are predominately neutral there, the former seems more probable.

Consider the problems posed by the apparent discrepancy between the calculated and observed net radiative losses from MgII and CaII. Let us examine the procedure for estimating net radiative losses from the observed emission cores, as outlined by Clearman (1953). It is this work to which Osterbrock and Athay ultimately refer in discussing MgII. The procedure is to estimate an equivalent width for the emission core as high as the adjacent continuum and multiply this by the blackbody emission at a temperature characteristics of this continuum. Clearman used $T_r = 5000°$. If he had used $T_r = 5800°$, this would have increased the predicted flux by more than 4 times in the MgII resonance doublet. So in the MgII case, at least, the flux estimate is sufficiently uncertain to raise doubts about the reliability of the quoted numbers, though it is unlikely that the observations could give a flux value of greater than 10^6 ergs cm^{-2} sec^{-1} for the average value over the solar surface. In the CaII case, no errors of the type just described could possibly explain the vast discrepancy between the calculated and observed fluxes. Here we must examine the possibility that the region producing the H and K emission may be optically thin compared with our estimates (Zirker, 1968), or that our two-level atom model has failed.

We could at least partially remove these discrepancies by forcing $(NCB)_{LU}$ to approach zero higher in the atmosphere, corresponding to a more realistic treatment of the relevant departure coefficients b_k. Such an approach, which would force the mechanical heating farther out for the line in question (requiring a change in the mechanical-energy input distribution or a different distribution of the other mechanical-energy sinks), would also raise the temperature in the outer layers. Thus, we might also be able to reduce or change the unrealistic, negative temperature gradient in those layers.

Finally, the probable departures from spherical symmetry indicate a higher local value for the mechanical heating, where the MgII and CaII emission is strong. If 10 percent of the gas in

this region emits most of the observed flux, the higher temperatures obtained from the second set of heating parameters (C, β) are obtained there, and the total mechanical heating will not significantly exceed the quoted fluxes from MgII, though the CaII emission will still be too large to agree with observations. Unfortunately, the behavior of the other 90 percent of the gas is still unknown.

To conclude the discussion of the MgII and CaII doublets and the temperature distribution calculated from them, let us ask: what model for the region $500 < h \leq 1250$ km is roughly consistent with the results of our calculations? The preceding remarks demand a two-component model for this region, with one component (producing most of the emission) covering about 10 percent of the surface. In this component, shock dissipation, greatly influenced by the stronger magnetic fields in the spicules (which we identify with this component), could produce the necessary mechanical energy to balance the observed emission. The temperature T_e in this component should be 7000° ± 1000°K. Nothing can be said about conditions in the other component—a serious problem.

Several changes occur in the chromosphere where the transition to the Lyα emitting region takes place: 1) The temperature will begin to rise rapidly above the 6000° - 8000°K values characteristic of the singly ionized metals region. Such a rapid rise begins in the PSC-model low chromosphere around 1250 km. 2) Associated with this rapid rise, τ_0 (Lyα) will decrease rapidly owing to hydrogen ionization. Thus, the condition of detailed balance in Lyα, valid in the singly ionized metals region, becomes invalid, and net radiative losses in Lyα become large. 3) The dominance of Lyα is furthered by second-stage ionization of the metals MgII and CaII when T_e exceeds 10,000°. 4) Helium emission should be observed above 1250 km. Significant helium emission in HeI and λ4686 of HeII (whose resonance line λ304 cannot be observed below the ozone layer of our atmosphere) are observed at and below 1250 km, as shown by the Khartoum data reported in PSC. 5) There is direct evidence, already discussed, for departures from spherical symmetry above 1500 km, in addition to the strong possibility of a departure below this height.

The results of the Lyα calculation support this picture, even to the extent of fully justifying the neglect of the contribution of helium emission to the energy balance in the region producing strong Lyα emission. We recall that a temperature of 50,000°K was required (Zirker, 1960) for helium emission to predominate. Even the effect of strong departures from spherical symmetry in the Lyα emission (which could concentrate the mechanical heating of our spherically symmetric study by more than an order of magnitude) could not raise the temperature to this value, in view of the result showing an increase of ~6000° corresponding to an order-of-magnitude increase in mechanical heating. The greatest uncertainty in the Lyα calculation, other than that caused by ignoring departures from spherical symmetry, is the estimate of the mechanical heating. The final temperature values should be considered as "ballpark" figures only, offered to illustrate the effects of varying the mechanical heating and the electron densities.

What is the stability of the temperature gradients obtained from these calculations? We have already noted that the negative dT_e/dh found at small τ_0 for all the calculations above $h = 500$ km (quite pronounced for MgII) conflicts with the expectation that, when one radiator becomes an ineffective loss mechanism, the temperature should rise to a higher value at which a new radiator can become effective, provided that we maintain a mechanical input per unit mass of material that

is approximately constant. The quantity $D(h)/\rho(h)$ actually increases slightly in the ionized metal's region, so we certainly do not believe in the negative dT_e/dh.

Ignoring this aspect of the results and considering MgII and CaII to represent a single temperature plateau (or perhaps two temperature plateaus), we ask if the results for these ionized metals and the other radiators are reasonable as regards general stability. The general-stability criterion, given in Chapter II, Section D, is

$$\frac{dE_{out}}{dT_e} > \frac{dE_{in}}{dT_e} \quad , \tag{45}$$

where it is convenient to express E in units of ergs gm^{-1} sec^{-1}.

Starting the stability study with the H^- region, $0 \leq h \leq 500$ km, we find that $E_{in} = D(h)/\rho(h)$ increases rapidly with height h and hence with increasing T_e, as the shock strength parameter η_s increases rapidly in this region and $D(h) \propto [\eta_s(h)]^3$. What can we say about E_{out}? For the free-bound continuum transitions of the H^- ion,

$$E_{out} = \int_{\nu_L}^{\infty} n_e n_i A_{kL} (NRB)_{kL} (h\nu)_{kL} dk/\rho(h) \quad , \tag{183}$$

in the notation of Chapter II, Section C. We could numerically solve equation 183 for E_{out} directly, or we could use the estimates of the excess of emission over absorption in H^- from Table 14. The latter procedure is more direct. Noting that the results of Table 14 are expressed in units of ergs cm^{-3} sec^{-1}, requiring that we divide them by $\rho(h)$ to get the net radiative loss per unit mass, and recalling that, for $0 \leq h \leq 200$ km, the values of Table 14 are greatly overestimated, we see that $dE_{out}/dT_e > 0$ is certainly satisfied for the assumed density-scale height of 130 km. Since the big jump in η_s (hence $D(h)/\rho(h) = E_{in}$) occurs for the range in h where there are many uncertainties in all the estimates, the possibility that condition 45 will be violated there is not too disturbing. Beyond $h \simeq 200$ km, dE_{in}/dT_e does not increase rapidly and with $dE_{out}/dT_e > 0$, condition 45 can probably be fulfilled. Since the estimate of the variation of η_s with h is rough (as is the estimate of excess emission) it would hardly be worth a more quantitative study at this point.

Then there is the question of the MgII and CaII region. Again, we shall not attempt to calculate exactly where we expect this region to begin. We simply note that beyond $h = 500$ km, the Paschen-continuum opacity becomes increasingly important. This means that at some height above 500 km, according to our estimates, H^- will cease to dominate the continuum source function and the temperature determined thereby. Also, at some such height, the $(NCB)_{LU}$'s for CaII and MgII will begin to depart from unity.

If the region $500 < h \leq 1250$ km is a region of singly ionized magnesium and calcium, then the form of E_{out} we must use is

$$E_{out} = n_U A_{UL} (NRB)_{UL} (h\nu)_{UL}/\rho(h) \quad . \tag{184}$$

Since A_{UL} and $(h\nu)_{UL}$ are constants for each line, the variation of E_{out} over $500 < h \leq 1250$ km is determined by the variation of n_U, ρ, and $(NRB)_{UL}$. Qualitatively, we may state that $(NRB)_{UL}$ increases from zero to unity through the region, and that n_U decreases faster with increasing height h than n_L as $(NCB)_{LU}$ $(1 - b_U/b_L)$ increases. Thus, since n_L and $\rho(h)$ have the same scale height if the metals are singly ionized, the ratio $n_U/\rho(h)$ decreases with height, somewhat offsetting the effect of the increasing $(NRB)_{UL}$. However, E_{in} does not increase rapidly through this region. From the variation in η_s over the region, $E_{in} = D(h)/\rho(h)$ only increases by about a factor of 2. Thus, only a small increase in E_{out} is necessary to satisfy condition 45. Again, without making a quantitative study, we note that condition 45 is probably satisfied by MgII and CaII.

Could Lyα possibly play a significant role at some height below 1250 km, where we expect it to predominate? We argued that Lyα should be negligible below 1250 km on the grounds that the optical depth τ_0(Lyα) is greater than 10^5 below this height, according to the PSC-model chromosphere of Table 1. For such optical depths, we noted that detailed balance is expected for Lyα. Unless this conclusion is in error, or unless the PSC model for τ_0 (Lyα) is in error so that the upper part of the region below 1250 km loses Lyα radiation, we can stand by the conclusion that Lyα losses and the associated higher temperatures are confined to the region above 1250 km.

Finally: is the calculated Lyα region thermally stable? According to Table 27, where $n_H(h)$ is given for three heights (in a highly questionable upper-chromosphere model), $n_H(h)$ appears to be almost constant with height h after the bulk of the hydrogen has been ionized. With $\rho(h)$ almost constant in the Lyα region (scale height chosen = 2200 km), and $(NCB)_{LU} = 1$ (a good approximation for the outer part where hydrogen is largely ionized), the variation in E_{out} from Equation 184 is determined largely by the variation in n_U. To obtain this, knowing $n_L \simeq n_H$, would require a more detailed knowledge of the variation of b_1 and b_2 through the Lyα region than we have. We merely note that, since here E_{in} is roughly constant with height (η_s is assumed constant.), it may be possible for $dE_{out}/dT_e > 0$ to be fulfilled, thus satisfying condition 45.

It is too early to appraise the method offered here for calculating the chromospheric temperature distribution, as compared with the standard approach, namely: assuming a distribution of electron densities and temperatures for various chromospheric models and computing line profiles from the resulting source functions as outlined in NETPRF, after which a comparison of the calculated with observed profiles is made to select the best model. Our approach has been to make a reasonable guess of the mechanical energy input (which still depends on temperature), and construct a source function from this to solve the transfer equation. From the solution a temperature distribution can be calculated.

The former, standard approach has recently been applied to the MgII and CaII doublets by Athay and Skumanich (1968). Since their results are also based on a two-level atom, but were obtained after a much more thorough series of numerical calculations, it will be interesting to compare their results with those we hope to obtain from a more detailed calculation. In addition, the results of the new calculation should yield profiles good enough to compare with observed profiles. Only then will it be possible to offer a reasonable estimate of the utility of calculating the temperature as described in this report.

ACKNOWLEDGMENTS

This report represents an exposition of the general problem of the structure of the solar chromosphere and offers an approximate method for calculating the temperature distribution there. The method was developed as part of a Ph.D. dissertation under the supervision of Dr. Richard N. Thomas of the Joint Institute for Laboratory Astrophysics at the University of Colorado. I am deeply grateful for his advice and encouragement. The actual calculations reported here were done at Goddard Space Flight Center, though in some cases this involved only a reproduction and check of the thesis work. The treatment of the lowest chromospheric subregion differs markedly from the thesis, however.

Goddard Space Flight Center
National Aeronautics and Space Administration
Greenbelt, Maryland, June 1969
188-38-01-04-51

REFERENCES

Abbot, C. G., Fowle, F. E., and Aldrich, L. B., Annals of the Astrophysical Observatory, 4, Smithsonian Institute, 1922.

Allen, C. W., "Astrophysical Quantities," 1st ed., London: Athlone Press, 1955.

Allen, C. W., "Astrophysical Quantities," 2nd ed., London: Athlone Press, 1962.

Aller, L. H., "Astrophysics, The Atmospheres of the Sun and Stars," 2nd ed., New York: Ronald Press, 1963.

Athay, R. G., "The Number of Spicules in the Middle Chromosphere," *Astrophys. J.* 129(1):164-171, January 1959.

Athay, R. G., and Zirker, J. B., "Ionization and Excitation Equilibrium of CaII in the Solar Atmosphere," *Astrophys. J.* 136(1):242-249, July 1962.

Athay, R. G., "Theoretical Line Intensities. 1. Strong Emission Lines," *Astrophys. J.* 142(2):724-731, August 1965a.

Athay, R. G., "Theoretical Line Intensities. II, Excitation of Chromospheric HeII and Hydrogen," *Astrophys. J.* 142(2):732-754, August 1965b.

Athay, R. G., "Radiative Energy Loss from the Solar Chromosphere and Corona," *Astrophys. J.* 146(1):223-240, October 1966.

Athay, R. G., and Skumanich, A., "Emission Cores in H and K Lines. I. The Optically Thick Chromosphere," *Solar Physics*, 3(1):181-203, January 1968.

Austin, W. E., Purcell, J. D., Tousey, R., and Widing, K. G., "Coronal Emission - Line Intensities in the Extreme Ultraviolet," *Astrophys. J.* 145(2):373-379, August 1966.

Avrett, E. H., and Hummer, D. G., "Noncoherent Scattering II. Line Formation with a Frequency Independent Source Function," JILA, Boulder, Colo., JILA Report No. 16, 1964.

Babcock, H. W., and Babcock, H. D., "The Sun's Magnetic Field, 1952-1954," *Astrophys. J.* 121(2): 349-366, March 1955.

Bahng, J., and Schwarzschild, M., "Lifetime of Solar Granules," *Astrophys. J.* 134(2):312-322, September 1961.

Bazer, J., and Ericson, W. B., "Hydromagnetic Shocks," *Astrophys. J.* 129(3):758-785, May 1959.

Beckers, J. M., "Solar Spicules," *Solar Physics*, 3(3):367-433, March 1968.

Bhatnagar, P. L., Krook, M., Menzel, D. H., and Thomas, R. N., "'Turbulence,' Kinetic Temperature, and Electron Temperature in Stellar Atmospheres," in "Vistas in Astromony," vol. 1, ed. by A. Beer, New York: Pergamon, 1960.

Biermann, L., "Zur Deutung der chromosphärischen Turbulenz und des Exzesses der UV - Strahlung der Sonne," *Naturwiss.* 33(4):118-119, August 30 1946.

Biermann, L., "Über die Ursache der Chromosphärischen Turbulenz und des UV - Exzesses der Sonnenstrahlung," *Z. Astrophys.* 25(1-2):161-177, July 1948.

Biermann, L., Kippenhahn, R., Lüst, R., and Temesváry, St., "Beiträge zur Theorie der Sonnengranulation," *Z. Astrophys.* 48(3):172-188, October 1959.

Billings, D. E., "A Guide to the Solar Corona," New York: Academic Press, 1966.

Bird, G. A., "The Behavior of Shock Waves in a Gravitational Atmosphere," *Astrophys. J.* 139(2): 675-683, February 1964a.

Bird, G. A., "A Gas-Dynamic Model of the Outer Solar Atmosphere," *Astrophys. J.* 139(2):684-689, February 1964b.

Bird, G. A., "The Propagation of Acoustic Waves Through the Solar Chromosphere," *Astrophys. J.* 140(1):288-291, July 1964c.

Böhm, K. H., "Stromungsformen verschiedener vertikaler Wellenlängen in der Solaren Wasserstoffkonvektionszone," *Z. Astrophys.* 57(4):265-277, July 1963.

Böhm-Vitense, E., "Über die Wasserstoffkonvektionszone in Sternen verchiedener Effektivtemperaturen und Leuchtkräfte," *Z. Astrophys.* 46(2):108-143, October 1958.

Branscomb, L. M., and Smith, S. J., "Experimental Cross Section for Photodetachment of Electrons from H^- and D^-," *Phys. Rev.* 98(4):1028-1034, May 15, 1955.

Cayrel, R., "Sur une cause purement radiative de remontée de température dans une atmosphère stellaire aux densitiés chromosphériques," *Comp. Rend. Acad. Sc.* Paris, 257:3309-3312, November 1963.

Chandrasekhar, S., and Breen, F. H., "On the Continuous Absorption Coefficient of the Negative Hydrogen Ion. III.," *Astrophys. J.* 104(3):430-445, November 1946.

Chandrasekhar, S., and Elbert, D. D., "On the Continuous Absorption Coefficient of the Negative Hydrogen Ion. V.," *Astrophys. J.* 128(3):633-635, November 1958.

Chandrasekhar, S., "Radiative Transfer," New York: Dover, 1960.

Clearman, H. E., "The Solar Spectrum from λ2285 to λ3000A," *Astrophys. J.* 117(1):29-40, January 1953.

Courant, R., and Friedricks, K. O., "Supersonic Flow and Shock Waves," New York: Interscience, 1948.

Cox, A. N., Stewart, J. N., and Eilers, D. D., "Effects of Bound-Bound Absorption on Stellar Opacities, *Astrophys. J. Supp.* 11(94):1-21, January 1965a.

Cox, A. N., and Stewart, J. N., "Radiative and Conductive Opacities for Eleven Astrophysical Mixtures," *Astrophys. J. Supp.* 11:(94):22-46, January 1965b.

Curtis, G. W., "Interference of the Line Source Function for Sodium D Lines," in Smith. Inst. Ap. Obs. Report 174, Cambridge, Mass., 1965.

Dalgarno, A., and Browne, J. C., "The Associative Detachment of H and H^-," *Astrophys. J.* 149(1): 231-232, July 1967.

Detwiler, C. R., Purcell, J. D., Tousey, R., "The Extreme Ultraviolet Spectrum of the Sun," *Mem. Soc. Roy. Liege,* 4:253-263, 1961.

Doughty, N. A., Fraser, P. A., and McEachran, R. P., Monthly Notices R.A.S., 132:255, 1966a.

Doughty, N. A., and Fraser, P. A., Monthly Notices R.A.S., 132:267, 1966b.

Dunkelman, L., and Scolnik, R., "Solar Spectral Irradiance & Vertical Atmospheric Attentuation in the Visible & Ultraviolet," *J. Opt. Soc. Am.* 49:356-367, 1959.

Dunn, R. B., "A multiple-image camera for chromosphere photometry," *Astron. J.* 61(1):3, February 1956 (abstract).

Dunn, R. B., "Solar Limb Darkening Near λ6563 from 0.9 to 1.00 R," *Astrophys. J.* 130(3):972-984, November 1959.

Edlén, B., "Die Deutung der Emissionslinien im Spektrum der Sonnenkorona," *Z. Astrophys.* 22(1): 30-64, November 1942.

Edmonds, F. N., Jr., "The Coefficients of Viscosity and Thermal Conductivity in the Hydrogen Convection Zone," *Astrophys. J.* 125(2):535-549, March 1957.

Edmonds, F. N., Jr., "A Statistical Photometric Analysis of Granulation Across the Solar Disk," *Astrophys. J. Supp.* 6(60):357-406, February 1962.

Evans, J. W., and Michard, R., "Observational Study of Macroscopic Inhomogeneities in the Solar Atmosphere. I. Velocity Displacements of Fraunhofer Lines as a Function of Line Strength and Position on Disk," *Astrophys. J.* 135(3):812-821, May 1962a.

Evans, J. W., and Michard, R., "Observational Study of Macroscopic Inhomogeneities in the Solar Atmosphere. II. Brightness Fluctuations in Fraunhofer Lines and the Continuum," *Astrophys. J.* 136(2):487-492, September 1962b.

Evans, J. W., and Michard, R., "Observational Study of Macroscopic Inhomogeneities in the Solar Atmosphere. III. Vertical Oscillatory Motions in the Solar Photosphere," *Astrophys. J.* 136(2): 493-506, September 1962c.

Ferraro, V. C. A., and Plumpton, C, "Hydromagnetic Waves in a Horizontally Stratified Atmosphere," *Astrophys. J.* 127(2):459-476, March 1958.

Fredga, K., "Monochromatic Pictures of the Sun in the Mg II Line at 2802.7 Å," *Astrophys. J.* 144(2): 854-856, May 1966.

Frisch, H., "Non-LTE in the Solar Atmosphere Thesis," University of Paris, 1966.

Frisch, H., "Influence of the Dissipation of Mechanical Energy on the Temperature of the Low Chromosphere," New York: Columbia University Report, 1967.

Gingerich, O., and de Jager, C., "The Bilderberg Model of the Photosphere and Low Chromosphere," *Solar Physics,* 3(1):5-25, January 1968.

Heintze, J. R. W., Hubenet, H., and de Jager, C., "A Reference Model of the Solar Photosphere & Low Chromosphere," *Bull. Astr. Inst. Neth.* 17:442-445, 1964.

Heintze, J. R. W., "The Extreme Limb of the Sun," Dordrecht, Holland: Reidel, 1965.

Henze, W., "Eclipse Observations of the Solar Atmosphere," Ph. D. Thesis, University of Colorado, Boulder, Colo., 1966.

Hiei, E., "Model of the Coronal Condensation," *J. Phys. Soc. Jap.* 17:227-231, 1962.

Hinteregger, H. E., Hall, L. A., and Schweizer, W., "Solar XUV-Spectrum from 310 Å to 55 Å," *Astrophys. J.* 140(1):319-327, July 1964.

Holweger, H., "Ein empirisches Modell der Sonnenatmosphäre mit lokalem thermodynamischem Gleichgewicht," *Z. Astrophys.* 65(5):365-417, March 1967.

House, L. L., "Departures from Thermodynamic Equilibrium in Chromospheric Magnesium I, Calcium I, & Oxygen I," High Altitude Observatory, Boulder, Colo., HAO Technical Report, 1962.

Hoyle, F., "Some Recent Researches in Solar Physics," London: Cambridge University Press, 1949.

Huang, S. S., and Struve, O., "Stellar Rotation and Atmospheric Turbulence," in "Stellar Atmospheres," ed. by J. L. Greenstein, Chicago: University of Chicago Press, 1960.

Hulst, H. C. van de, "Problems of Cosmical Aerodynamics," Chapter 6, Dayton: Central Air Documents Office, 1951.

Hulst, H. C. van de, "The Chromosphere and the Corona," in "The Sun," ed. by G. P. Kuiper, Chicago: University of Chicago Press, 1953.

Jager, C. de, and Kuperus, M., "The Acoustic Energy Flux of the Sun and the Formation of the Corona," *Bull. Astr. Inst. Neth.*, 16:71-82, 1961.

Jefferies, J. T., and Thomas, R. N., "Source Function in a Non-Equilibrium Atmosphere. III. The Influence of a Chromosphere," *Astrophys. J.* 129(2):401-407, March 1959.

Jefferies, J. T., and Thomas, R. N., "The Source Function in a Non-Equilibrium Atmosphere. V. Character of the Self-Reversed Emission Cores of Ca^+ H and K," *Astrophys. J.* 131(3):695-704, May 1960.

Jordan, S. D., "Why the Temperature Rise Does Not Occur in Radiative Equilibrium in Stellar Chromospheres of Dominant H^- Opacity," *Astrophys. J.* July 1969.

Kourganoff, V., "Basic Methods in Transfer Problems; Radiative Equilibrium and Neutron Diffusion," New York: Dover, 1963.

Krook, M., "On the Solution of Equations of Transfer. I," *Astrophys. J.* 122(3):488-497, November 1955.

Kulsrud, R. M., "Effect of Magnetic Fields on Generation of Noise by Isotropic Turbulence," *Astrophys. J.* 121(2):461-480, March 1955.

Kuperus, M., "The Transfer of Mechanical Energy in the Sun and the Heating of the Corona," Dordrecht, Holland: Reidel, 1965.

Kuperus, M., and Athay, R. G., "On the Origin of Spicules in the Chromosphere—Corona Transition Region," *Solar Physics* 1(3):361-370, June 1967.

Lehnert, B., "Plasma Physics on Cosmical and Laboratory Scale," *Nuovo Cimento Supp.* 13:59-110, 1959.

Leighton, R. B., Noyes, R. W., and Simon, G. W., "Velocity Fields in the Solar Atmosphere. I. Preliminary Report," *Astrophys. J.* 135(2):474-499, March 1962.

Lighthill, M. J., "On Sound Generated Aerodynamically. I. General Theory," *Proc. Roy. Soc. London*, A211:564-587, March 20, 1952.

Lighthill, M. J., "On Sound Generated Aerodynamically II. Turbulence as a Source of Sound," *Proc. Roy. Soc. London,* A222:1-32, February 23, 1954.

Lighthill, M. J., "Velocity Field . . . in a Layer Overlying a Convectively Unstable Atmospheric Region," in "Fifth Symposium on Cosmical Gas Dynamics," ed. by R. N. Thomas, London: Academic Press, 1967.

Livshits, M. A., "Energy Balance in the Transition Region Between the Chromosphere and Corona," *Soviet Astronomy,* 8(3):376-383, Nov.-Dec. 1964.

Menzel, D. H., "Physical Processes in Gaseous Nebulae. I. Absorption and Emission of Radiation," *Astrophys. J.* 85(4):330-339, May 1937.

Minnaert, M., "The Photosphere," in *The Sun, ed. by G. P. Kuiper,* Chicago: University of Chicago Press.

Moore, D. W., and Spiegel, E. A., "The Generation and Propagation of Waves in a Compressible Atmosphere," *Astrophys. J.* 139(1):48-71, January 1964.

Moore, D. W., "Velocity Field . . . and Generalized Turbulence in . . . Atmospheric Region," in "Fifth Symposium on Cosmical Gas Dynamics," ed. by R. N. Thomas, London: Academic Press, 1967.

Morton, D. C., and Widing, K. G., "The Solar Lyman-Alpha Emission Line," *Astrophys. J.* 133(2): 596-605, March 1961.

Noyes, R. W., and Leighton, R. B., "Velocity Fields in the Solar Atmosphere II. The Oscillatory Field," *Astrophys. J.* 138(3):631-647, October 1963.

Osterbrock, D. E., "The Electrical Conductivity in the Solar Atmosphere," *Phys. Rev.* 87(3):468-470, August 1, 1952.

Osterbrock, D. E., "The Heating of the Solar Chromosphere, Plages, and Corona by Magnetohydrodynamic Waves," *Astrophys. J.* 134(2):347-388, September 1961.

Pagel, B. E. J., "The Role of H^- in the Solar Photosphere and Chromosphere," Proc. Uccle Conference, 28, 1959.

Parker, E. N., "Instability of Thermal Fields," *Astrophys. J.* 117(3):431-436, May 1953.

Peyturaux, R., "Sur la répartition spectrale de l'énergie au centre du disque Solaire entre 6700 et 23000 Å," *Compt. Rend. Acad. Sci., Paris,* 232:931-932, March 5, 1951.

Piddington, J. H., "Solar Atmosphere Heating by Hydromagnetic Waves," Monthly Notices R.A.S., 116:314-323, 1956.

Pierce, A. K., "Relative Solar Energy Distribution in the Spectral Region 10,000-25,000 Å," *Astrophys. J.* 119(2):312-327, March 1954.

Pierce, A. K., and Waddell, J. H., "Analysis of Limb Darkening Observations," *Mem. Roy. Astro. Soc.* 68:89-112, 1961.

Pikel'ner, S. B., and Livshits, M. A., "Theory of Heating of the Active and Undisturbed Chromosphere," *Soviet Astronomy,* 8(6):808-818, May-June 1965.

Pottasch, S. R., and Thomas, R. N., "Departures from the SAHA Equation Under Varying Conditions of Lyman Continuous Opacity," *Astrophys. J.* 130(3):941-953, November 1959.

Pottasch, S. R., "The Lower Solar Corona: Interpretation of the Ultraviolet Spectrum," *Astrophys. J.* 137(3):945-966, April 1963.

Pottasch, S. R., "On the Interpretation of the Solar Ultraviolet Emission Line Spectrum," *Space Sci. Rev.* 3:816-855, 1964.

Proudman, I., "The Generation of Noise by Isotropic Turbulence," *Proc. Roy. Soc. London,* A214: 119-132, August 7, 1952.

Purcell, J. D., Garrett, D. L., Tousey, R., "Solar Spectra from 3500 to 2200 Å at 30 mÅ Resolution," COSPAR 3rd Int. Space Science Sym., Washington, D. C., 1963.

Regemorter, H. van, "Rate of Collisional Excitation in Stellar Atmospheres," *Astrophys. J.* 136(3): 906-915, November 1962.

Seaton, M. J., "The Impact Parameter Method for Electron Excitation of Optically Allowed Atomic Transitions," *Proc. Phys. Soc.,* 79(6):1105-1117, June 1, 1962.

Schmeltekopf, A. L., Fehsenfeld, F. C., and Ferguson, E. E., "Laboratory Measurement of the Rate Constant for $H^- + H \rightarrow H_2 + e$," *Astrophys. J. Letters* 148:L155-L156, June 1967.

Schwarzschild, M., "On Noise Arising from the Solar Granulation," *Astrophys. J.* 107(1):1-5, January 1948.

Schwarzschild, M., "Photographs of the Solar Granulation Taken from the Stratosphere," *Astrophys. J.* 130(2):345-363, September 1959.

Souffrin, P., "Hydrodynamique d'une Atmospherè Perturbeé par une Zone Convective Turbulente Sous-Jacente," *Ann. d'Astrophys.* 29(2):55-101, March-April 1966.

Spitzer, L., Jr., "Physics of Fully Ionized Gases," New York: Interscience, 1956.

Thomas, R. N., "Superthermic Phenomena in Stellar Atmospheres I. Spicules and the Solar Chromosphere," *Astrophys. J.* 108(1):130-141, July 1948a.

Thomas, R. N., "Superthermic Phenomena in Stellar Atmospheres II. Departure from Thermodynamic Equilibrium in an Idealized Chromosphere," *Astrophys. J.* 108(1):142-152, July 1948b.

Thomas, R. N., "The Source Function in a Non-Equilibrium Atmosphere I. The Resonance Lines," *Astrophys. J.* 125(1):260-274, January 1957.

Thomas, R. N., "The Source Function in a Non-Equilibrium Atmosphere IV. Evaluation and Application of the Net Radiative Bracket," *Astrophys. J.* 131(2):429-437, March 1960.

Thomas, R. N., and Athay, R. G., "Physics of the Solar Chromosphere," (PSC), New York: Interscience, 1961.

Thomas, R. N., "Non-Equilibrium Thermodynamics in the Presence of a Radiation Field" (NETPRF), Boulder, Colo.: University of Colorado Press, 1965.

Tisone, G. C., JILA, Boulder, Colo.: JILA Report No. 73, 1966.

Trumpler, R. J., and Weaver, H. F., "Statistical Astronomy," Berkeley: University of California Press, 1953.

Uchida, Y., "Resonant Responses of the Solar Atmosphere to the Gravitational-Hydrodynamic Waves," *Astrophys. J.* 147(1):181-192, January 1967.

Unno, W., and Kato, S., "On the Generation of Acoustic Noise from the Turbulent Atmosphere," *J. Astro. Soc. Jap.* 14:417-430, 1962.

Unno, W., "Generation of Acoustic Noise in Convective Zones," *Transact. I.A.U. Joint Disc. D,* Hamburg, 1964, pp. 555-558.

Unsold, A., "Physik der Sternatmosphären II," Berlin: Springer, 1955.

Vitense, E., "Die Wasserstoffkonvektionszone der Sonne," *Z. Astrophys.* 32(3):135-164, 1953.

Waddell, J. H., "Analysis of the Center-to-Limb Observations of the Sodium D Lines," *Astrophys. J.* 136(1):231-241, July 1962.

Weymann, R., "Heating of Stellar Chromospheres by Shock Waves," *Astrophys. J.* 132(2):452-460, September 1960.

Whitaker, W. A., "Heating of the Solar Corona by Gravity Waves," *Astrophys. J.* 137(3):914-930, April 1963.

Whitney, C. A., "Thermal Response of the Solar Atmosphere," *Astrophys. J.* 138(2):537-551, August 1963.

Wildt, R., "Electron Affinity in Astrophysics," *Astrophys. J.* 89(2):295-301, March 1939.

Zirin, H., Hall, L. A., and Hinteregger, H. E., "Analysis of the Solar Emission Spectrum from 1300 to 250 Å as Observed in August, 1961," *Space Research* 3:760-771, 1963.

Zirin, H., and Dietz, R. D., "The Structure of the Solar Chromosphere. I. A Picture Based on Extreme Ultraviolet, Millimeter, and λ10830 Data," *Astrophys. J.* 138(3):664-679, October 1963.

Zirin, H., "The Solar Atmosphere," Waltham, Mass.: Blaisdell, 1966.

Zirin, H., and Howard, R., "The Structure of the Solar Chromosphere. II. Spectroheliograms in λ10830 Å and Their Interpretation," *Astrophys. J.* 146(2):367-371, November 1966.

Zirker, J. B., "Departures from Non-LTE in the Solar Chromosphere from Eclipse Observations," HAO, Boulder, Colo.: HAO Technical Report 10, 1956.

Zirker, J. B., "The Metallic Chromosphere at the Khartoum Eclipse," *Astrophys. J.* 127(3):680-713, May 1958.

Zirker, J. B., "The Energy Balance of Opaque Atmospheres," *Astrophys. J.* 131(3):684-689, May 1960.

Zirker, J. B., "The Solar H and K Lines of Ionized Calcium," *Solar Physics* 3(1):164-180, January 1968.

Appendix A

The General Line Source Function

In this appendix we derive, in detail, the line source function of Equation 25, Chapter II, Section C. We begin by applying the very general condition of a statistically steady state expressed by Equation 16

$$\frac{dn_k}{dt} = 0 , \qquad \underline{SSS} , \qquad (16), (A-1)$$

where, of course, n_k is the number density of the k-th energy level. (We shall use a double reference number for equations that appear in the body of the report.) From Chapter II, Section C, we also have the following completely general expression for the line source function S_ν, which is

$$S_\nu = \frac{j_\nu}{\phi_\nu} \cdot B_\nu (T_{ex}) , \qquad (18), (A-2)$$

where j_ν and ϕ_ν are the profile coefficients for spontaneous emission and absorption, respectively, and

$$B_\nu (T_{ex}) = \frac{2h\nu^3}{c^2} \left(\frac{g_U n_L}{g_L n_U} - 1 \right)^{-1} , \qquad (19), (A-3)$$

with the same notation used throughout the report. Since, for reasons given in Chapter II, Section C, the profile coefficients j_ν and ϕ_ν vary in a similar way across the Doppler core of resonance lines, we restrict our treatment here to determining the detailed form for $B_\nu (T_{ex})$. For a detailed treatment of the profile coefficients, see Chapter III, Part 1 of NETPRF or the first paper in the Source Function Series (Thomas, 1957). These references also outline the derivation of a general expression for $B_\nu (T_{ex})$, so this appendix is intended to fill in some details for readers unversed in non-LTE spectral line theory.

The object of this derivation is to find a general expression for the ratio n_L/n_U in Equation A-3. This expression must include the general collisional and radiation field dependence of n_L/n_U. We obtain such a ratio by applying the SSS condition A-1 to both levels (U, L) of the spectral line.

This gives

$$\sum_{\ell>U} n_\ell A_{\ell U} (NRB)_{\ell U} + \sum_{\substack{j<U \\ j\neq\ell}} n_j C_{jU} (NCB)_{jU} + \cdots$$

$$\cdots + n_L C_{LU} (NCB)_{LU} + \int_{\nu_U}^{\infty} A_{\kappa U} n_i n_e (NRB)_{\kappa U} d\kappa$$

$$= n_U \left[\sum_{\substack{j<U \\ j\neq L}} A_{Uj} (NRB)_{Uj} + A_{UL} + \sum_{\ell>U} C_{U\ell} (NCB)_{U\ell} \right] \qquad \text{(A-4)}$$

for the upper level U, and

$$\sum_{\substack{\ell>L \\ \ell\neq U}} n_\ell A_{\ell L} (NRB)_{\ell L} + n_U A_{UL} (NRB)_{UL} + \cdots$$

$$\cdots + \sum_{j<L} n_j C_{jL} (NCB)_{jL} + \int_{\nu_L}^{\infty} A_{\kappa L} n_i n_e (NRB)_{\kappa L} d\kappa$$

$$= n_L \left[\sum_{j<L} A_{Lj} (NRB)_{Lj} + \sum_{\substack{\ell>L \\ \ell\neq U}} C_{L\ell} (NCB)_{L\ell} + C_{LU} (NCB)_{LU} \right] \qquad \text{(A-5)}$$

for the lower level L. All quantities appearing in Equations A-4 and A-5 are defined in Chapter II, Section C. In particular, the net radiative brackets (NRB) are given by Equation 39, the net collisional brackets (NCB) by Equation 44, and C_{LU} (any L and U where L < U) by Equation 23. Note that Equations A-4 and A-5 are equivalent to Equation 24 where k becomes equal to U and L, respectively. We retain the convention of including collisional processes that have an upper level in the continuum in the middle term on the right-hand sides of Equations A-4 and A-5.

It is useful to introduce several new quantities at this point. Though this appears to complicate matters at first, these quantities have physical significance, and their introduction greatly facilitates our derivation and the subsequent physical interpretation. First, we replace the

radiation terms involving the continuum by

$$\int_{\nu_U}^{\infty} A_{\kappa U}\, n_i\, n_e\, (NRB)_{\kappa U}\, d\kappa \;=\; R_{CU} - n_U J_{UC}\,, \tag{A-6}$$

$$\int_{\nu_L}^{\infty} A_{\kappa L}\, n_i\, n_e\, (NRB)_{\kappa L}\, d\kappa \;=\; R_{CL} - n_L J_{LC}\,, \tag{A-7}$$

noting that $R_{Ck} - n_k J_{kC}$ is simply used to represent $P(\text{rad}; C, k) - R(\text{rad}; k, C)$ in the notation of Equation 21. Next, we introduce four quantities which couple U and L to levels other than L and U, respectively. These are

$$\delta_1 \;=\; \sum_{\substack{\ell > L \\ \ell \neq U}} C_{L\ell}\, (NCB)_{L\ell} \;+\; \sum_{j<L} A_{Lj}\, (NRB)_{Lj} \;+\; J_{LC}\,, \tag{A-8}$$

$$\delta_2 \;=\; \sum_{\substack{\ell > L \\ \ell \neq U}} n_\ell\, A_{\ell L}\, (NRB)_{\ell L} \;+\; \sum_{j<L} n_j\, C_{jL}\, (NCB)_{jL}\,, \tag{A-9}$$

$$\delta_3 \;=\; \sum_{\substack{j<U \\ j \neq L}} A_{Uj}\, (NRB)_{Uj} \;+\; \sum_{\ell > U} C_{U\ell}\, (NCB)_{U\ell} \;+\; J_{UC}\,, \tag{A-10}$$

$$\delta_4 \;=\; \sum_{\substack{j<U \\ j \neq L}} n_j\, C_{jU}\, (NCB)_{jU} \;+\; \sum_{\ell > U} n_\ell\, A_{\ell U}\, (NRB)_{\ell U}\,, \tag{A-11}$$

where δ_1 and δ_3 represent terms that depopulate levels L and U, respectively, and δ_2 and δ_4 represent terms that populate L and U, respectively. These "indirect" processes (not coupling U and L directly) represent a complete set of all indirect processes except for R_{CU} and R_{CL}, which we introduced in equations A-6 and A-7. To include these also, we define

$$F_U \;=\; R_{CU} + \delta_4\,, \tag{A-12}$$

$$F_L \;=\; R_{CL} + \delta_2\,, \tag{A-13}$$

following the notation of NETPRF. Now we have included all indirect processes in δ_1, δ_3, F_U, and F_L. We introduce no more new quantities.

If we combine Equations A-4, A-6, A-10, A-11, and A-12, we can write

$$F_U = n_U \left[\delta_3 + A_{UL} (NRB)_{UL}\right] - n_L C_{LU} (NCB)_{LU} . \tag{A-14}$$

In a like manner, combining Equations A-5, A-7, A-8, A-9, and A-13 gives

$$F_L = n_L \left[\delta_1 + C_{LU} (NCB)_{LU}\right] - n_U A_{UL} (NRB)_{UL} . \tag{A-15}$$

We express A-14 and A-15 in a slightly different form by noting that

$$n_U A_{UL} (NRB)_{UL} = n_U A_{UL} + n_U B_{UL} \int J_\nu \phi_\nu \, d\nu - n_L B_{LU} \int J_\nu \phi_\nu \, d\nu \tag{A-16}$$

for $\psi_\nu = \phi_\nu$, which we assume throughout, and

$$n_L C_{LU} (NCB)_{LU} = n_L C_{LU} - n_U C_{UL} . \tag{A-17}$$

Equation A-16 follows from Equations 21 and 36. Equation A-17 follows from Equations 22 and 40. Substituting Equations A-16 and A-17 in Equations A-14 and A-15 gives the equations to solve for n_U and n_L:

$$n_U \left[\delta_3 + A_{UL} + B_{UL} \int J_\nu \phi_\nu \, d\nu + C_{UL}\right] - n_L \left[B_{LU} \int J_\nu \phi_\nu \, d\nu + C_{LU}\right] = F_U , \tag{A-18}$$

$$- n_U \left[A_{UL} + B_{UL} \int J_\nu \phi_\nu \, d\nu + C_{UL}\right] + n_L \left[\delta_1 + B_{LU} \int J_\nu \phi_\nu \, d\nu + C_{LU}\right] = F_L . \tag{A-19}$$

These two equations express only direct processes between levels U and L except for the terms δ_1, δ_3, F_U, and F_L. In addition, the net brackets for the direct processes no longer appear. We solve

for n_U and n_L by determinants. This gives, for the ratio n_L/n_U:

$$\frac{n_L}{n_U} = \frac{B_{UL}\int J_\nu \phi_\nu \, d\nu (F_L + F_U) + A_{UL}(F_L + F_U) + C_{UL}(F_L + F_U) + \delta_3 F_L}{B_{LU}\int J_\nu \phi_\nu \, d\nu (F_U + F_L) + C_{LU}(F_U + F_L) + \delta_1 F_U} . \qquad \text{(A-20)}$$

We obtain a long expression for $B_\nu(T_{ex})$ by substituting Equation A-20 in Equation A-3. Now recall the relations among the three Einstein coefficients A_{UL}, B_{UL}, and B_{LU} expressed by Equations 38 and reproduced here:

$$\frac{A_{UL}}{B_{UL}} = \frac{2h\nu^3}{c^2}, \qquad g_L B_{LU} = g_U B_{UL} . \qquad \text{(38), (A-21)}$$

Also recall that, for a Maxwellian electron-velocity distribution, we have shown that

$$C_{LU} = C_{UL}\frac{g_U}{g_L} e^{-\chi_{LU}}, \qquad \chi_{LU} = \frac{h\nu}{kT_e} . \qquad \text{(43), (A-22)}$$

Using Equations A-21 and A-22 in the expression obtained for $B_\nu(T_{ex})$ by substituting Equation A-3, we arrive at

$$B_\nu(T_{ex}) = \frac{\left\{\int J_\nu \phi_\nu \, d\nu + \frac{C_{UL}}{A_{UL}}\left(1 - e^{-\chi_{LU}}\right)B_\nu(T_e) + \frac{2h\nu^3}{c^2}\frac{g_L}{g_U}\frac{\delta_1}{A_{UL}}\frac{F_U}{F_L + F_U}\right\}}{\left\{1 + \frac{C_{UL}}{A_{UL}}\left(1 - e^{-\chi_{LU}}\right) + \left(\frac{\delta_3}{A_{UL}}\frac{F_L}{F_L + F_U} - \frac{g_L}{g_U}\frac{\delta_1}{A_{UL}}\frac{F_U}{F_L + F_U}\right)\right\}} . \qquad \text{(A-23)}$$

We need only consider the third term in the denominator.

First, note that

$$\frac{\delta_3}{A_{UL}}\frac{F_L}{F_L + F_U} = \frac{F_L}{F_U}\frac{g_U}{g_L}\frac{\delta_3}{\delta_1}\left(\frac{g_L}{g_U}\frac{\delta_1}{A_{UL}}\frac{F_U}{F_L + F_U}\right), \qquad \text{(A-24)}$$

where the term in parentheses is identical, except for a sign change, to the second part of the third term in the denominator. Thus,

$$\left(\frac{\delta_3}{A_{UL}}\frac{F_L}{F_L+F_U} - \frac{g_L}{g_U}\frac{\delta_1}{A_{UL}}\frac{F_U}{F_L+F_U}\right) = \cdots$$

$$\cdots = \frac{g_L}{g_U}\frac{\delta_1}{A_{UL}}\frac{F_U}{F_U+F_L}\left(\frac{F_L}{F_U}\frac{g_U}{g_L}\frac{\delta_3}{\delta_1} - 1\right) . \qquad \text{(A-25)}$$

Now consider the defined quantities we introduced in Equations 27 - 29 in Chapter II, Section C. We reproduce them here:

$$\epsilon = \frac{C_{UL}}{A_{UL}}\left(1 - e^{-\chi_{LU}}\right) , \qquad \text{(27), (A-26)}$$

$$\eta = \frac{g_L}{g_U}\frac{\delta_1}{A_{UL}}\frac{F_U}{F_L+F_U}\left(\frac{F_L}{F_U}\frac{g_U}{g_L}\frac{\delta_3}{\delta_1} - 1\right) , \qquad \text{(28), (A-27)}$$

$$\eta B^* = \frac{2h\nu^3}{c^2}\frac{g_L}{g_U}\frac{\delta_1}{A_{UL}}\frac{F_U}{F_L+F_U} \qquad \text{(29), (A-28)}$$

Using these definitions and Equation A-25, we can write Equation A-23 for $B_\nu(T_{ex})$ in the desired form:

$$B_\nu(T_{ex}) = \frac{\int J_\nu \phi_\nu \, d\nu + \epsilon B_\nu(T_e) + \eta B^*}{1 + \epsilon + \eta} . \qquad \text{(25), (A-29)}$$

The derivation is completed.

A brief discussion of the physical significance of the terms appearing in Equation A-29 has been given in Chapter II, Section C. For a more complete discussion of the physical interpretation of Equation 29, see Chapter III of NETPRF.

Appendix B

Special Solutions to the Transfer Equation

In Chapter III, where we derived the method for making the calculations, we deferred to this appendix the details of deriving and solving the basic differential equation of the problem, Equation 105. We do this now, starting with the transfer equation in the form

$$\nu \frac{dI_\nu}{d\tau_\nu} = I_\nu - S_\nu \ . \qquad (6), (B\text{-}1)$$

Operating on both sides of Equation B-1 with $\int \cdots d\mu$, we obtain

$$\frac{1}{4\pi} \frac{dF_\nu}{d\tau_\nu} = J_\nu - S_\nu \ , \qquad (B\text{-}2)$$

provided that S_ν is not a function of $\mu = \cos\theta$. Now we introduce a new auxiliary quantity K_ν, defined by

$$K_\nu \equiv \frac{1}{2} \int_{-1}^{1} I_\nu (\mu) \mu^2 \, d\mu \ . \qquad (B\text{-}3)$$

With this definition, Equation B-3, we can operate on Equation B-1 with $\int \mu \cdots d\mu$ to obtain

$$\frac{dK_\nu}{d\tau_\nu} = \frac{1}{4\pi} F_\nu \ , \qquad (B\text{-}4)$$

where, again, we assume that S_ν is not a function of μ.

Now we introduce the Eddington approximation we use here, by replacing the μ^2 in the integral of Equation B-3 by its mean value, namely 1/3. This immediately gives

$$J_\nu \simeq 3K_\nu \ . \qquad (B\text{-}5)$$

This approximation ignores the anisotropy of the radiation field near the boundary where $\tau_\nu \to 0$. Since we have applied the subsequent equation to strong spectral lines whose behavior at $\tau_0 \gtrsim 1$ is

our primary concern, this approximation is adequate for the calculations we have performed. Combining Equations B-2, B-4, and B-5, we obtain

$$\frac{1}{3}\frac{d^2 J_\nu}{d\tau_\nu^2} = J_\nu - S_\nu \ . \qquad \text{(B-6)}$$

with $d\tau_\nu = 3^{-1/2} x_\nu d\tau_0$, Equation B-6 becomes

$$\frac{d^2 J_\nu}{d\tau_0^2} = x_\nu^2 \left(J_\nu - S_\nu\right) , \qquad \text{(102), (B-7)}$$

which is the equation that we solve. The form of the source function S_ν is given in Chapter III by combining the general source function for the line and continuum of Equation 8 with detailed expressions for the individual line and continuum source functions of Equations 100 and 101, respectively. For reference, we write

$$S_\nu = \frac{S_\ell + r_\nu S_c}{1 + r_\nu} , \qquad \text{(8), (B-8)}$$

$$S_\ell = \int J_\nu \phi_\nu \, d\nu + Ce^{-\beta\tau_0} , \qquad \text{(100), (B-9)}$$

$$S_c = S_1 \left(1 + Ae^{-c\tau_0}\right) , \qquad \text{(101), (B-10)}$$

where $r_\nu = d\tau_c/d\tau_\ell$ and we assume that only a single line is important at frequency ν. If we define $\delta_\nu \equiv (1 + r_\nu)^{-1}$, as in Equation 104, and replace all frequency points ν by quadrature points "i", we obtain

$$\frac{d^2 J_i}{d\tau_0^2} = x_i^2 \left[J_i - \delta_i \sum_j^n \alpha_j J_j - \delta_i Ce^{-\beta\tau_0} - \delta_i r_i S_1 \left(1 + Ae^{-c\tau_0}\right)\right] \qquad \text{(105), (B-11)}$$

for an n-point quadrature. In Chapter III, we gave physical arguments for dropping the last term $\delta_i r_i S_1 Ae^{-c\tau_0}$. This gives the equation we solve:

$$\frac{d^2 J_i}{d\tau_0^2} = x_i^2 \left[J_i - \delta_i \sum_j^n \alpha_j J_j - \delta_i Ce^{-\beta\tau_0} - \delta_i r_i S_1\right] . \qquad \text{(109), (B-12)}$$

To solve Equation B-12, a second-order linear differential equation, we obtain the general solution to the homogeneous equation and add a particular solution to the complete inhomogeneous equation, thus giving the general solution to the inhomogeneous equation. We then apply the boundary conditions of our problem to obtain the solution used for our calculations. The homogeneous equation corresponding to Equation B-12 is

$$\frac{d^2 J_i}{d\tau_0^2} = x_i^2 \left[J_i - \delta_i \sum_j^n \alpha_j J_j \right] . \tag{B-13}$$

If we assume a solution of the form

$$J_{ih} = S_1 \left(\sum_j^n A_{ij} e^{-k_j \tau_0} + \sum_j^n B_{ij} e^{k_j \tau_0} \right) , \tag{B-14}$$

where

$$A_{ij} \equiv \delta_i \left({}_+L_j \right) \left(1 - \frac{k_j^2}{x_i^2} \right)^{-1} , \tag{B-15}$$

and

$$B_{ij} \equiv \delta_i \left({}_-L_j \right) \left(1 - \frac{k_j^2}{x_i^2} \right)^{-1} , \tag{B-16}$$

and substitute Equation B-14 in Equation B-13, we obtain the following equation for the k_j's:

$$\sum_i^n \delta_i \alpha_i \left(1 - \frac{k_j^2}{x_i^2} \right)^{-1} = 1 . \tag{111), (B-17}$$

Now we need a particular solution to the inhomogeneous equation. Assume for this that

$$J_{ip} = S_1 \left[P_i + \left(\frac{Q_i}{S_1} \right) e^{-\beta \tau_0} \right] . \tag{B-18}$$

Substituting Equation B-18 into Equation B-12 yields the following two relations:

$$P_i - \delta_i \sum_j^n \alpha_j P_j - \delta_i r_i = 0 , \tag{B-19}$$

$$Q_i = \frac{\delta_i \sum_j^n \alpha_j Q_j + \delta_i C}{\left(1 - \frac{\beta^2}{x_i^2}\right)} . \qquad \text{(B-20)}$$

The solution to C-19 is $P_i = 1$; this is evident if we recall that $\delta_i \equiv (1 + r_i)^{-1}$ and

$$\sum_i^n \alpha_i = 1 .$$

We can obtain an explicit expression for Q_i from Equation B-20. Summing $\alpha_i Q_i$ over "i", and noting that the summation index is arbitrary, we can write

$$\sum_j^n \alpha_j Q_j = \frac{C \sum_j^n \delta_j \alpha_j \left(1 - \frac{\beta^2}{x_j^2}\right)^{-1}}{1 - \sum_j^n \delta_j \alpha_j \left(1 - \frac{\beta^2}{x_j^2}\right)^{-1}} . \qquad \text{(B-21)}$$

Finally, substituting Equation B-21 in Equation B-20, we obtain

$$Q_i = \delta_i C \left(1 - \frac{\beta^2}{x_i^2}\right)^{-1} \left[1 - \sum_j^n \delta_j \alpha_j \left(1 - \frac{\beta^2}{x_j^2}\right)^{-1}\right]^{-1} . \qquad \text{(112), (B-22)}$$

Thus, the general solution to the inhomogeneous Equation C-12 is the sum of J_{ih} and J_{ip}, and is given by

$$J_i = S_1 \left[1 + \delta_i \sum_j^n {}_+L_j \left(1 - \frac{k_j^2}{x_i^2}\right)^{-1} e^{-k_j \tau_0} + \cdots \right.$$

$$\left. \cdots + \delta_i \sum_j^n {}_-L_j \left(1 - \frac{k_j^2}{x_i^2}\right)^{-1} e^{k_j \tau_0} + \left(\frac{Q_i}{S_1}\right) e^{-\beta \tau_0} \right] . \qquad \text{(B-23)}$$

The ${}_+L_j$ and ${}_-L_j$ are determined by the boundary conditions.

So far, we have not introduced any restriction on the extent of the atmosphere. We do this now by recalling that, for all the spectral lines for which we actually solve Equation B-12, we showed that the chromosphere could be treated as a "semi-infinite" atmosphere. The boundary conditions

for such an atmosphere can be stated: $J_i \rightarrow S_1$ as $\tau_0 \rightarrow \infty$. Thus $_-L_j = 0$ in Equation B-23. The $_+L_j$ are then obtained from the boundary condition at $\tau_0 = 0$. Krook (1955) has provided the outer boundary condition we use. This is

$$J_i = x_i^{-1} \frac{dJ_i}{d\tau_0}, \qquad \tau_0 = 0 . \tag{B-24}$$

Applying condition Equation B-24, to the solution, Equation B-23, with $_-L_j = 0$ gives for the $_+L_j$:

$$\sum_j^n {}_+L_j \left(1 - \frac{k_j}{x_i}\right)^{-1} + \delta_i^{-1} \left[1 + \left(\frac{Q_i}{S_1}\right)\left(1 + \frac{\beta}{x_i}\right)\right] = 0 . \tag{113), (B-25}$$

The solution of Equation B-12 becomes

$$J_i = S_1 \left[1 + \delta_i \sum_j^n {}_+L_j \left(1 - \frac{k_j^2}{x_i^2}\right)^{-1} e^{-k_j \tau_0} + \left(\frac{Q_i}{S_1}\right) e^{-\beta \tau_0}\right] \tag{109), (B-26}$$

for a semi-infinite atmosphere, where everything has now been determined.